SC-CO₂ Processing: Extraction, Scale-up and Impregnation of Essential Oil from *Mentha × piperita*

by

Yuan Meng

A thesis submitted in partial fulfillment of the requirements for the degree of

Master of Science

in

Bioresource and Food Engineering

Department of Agricultural, Food and Nutritional Science
University of Alberta

ABSTRACT

Mentha × piperita is an important aromatic plant in the Lamiaceae family with great industrial potential. In the first study, the research aimed to explore the potential of supercritical carbon dioxide (SC-CO_2) to extract essential oil from peppermint leaves as well as evaluate the scale-up of the extraction process. A systematic investigation of processing parameters such as pressure (100-400 bar), temperature (45-55 °C), CO_2 flow rate (0.5 and 3 mL/min), time (15-180 min), and co-solvent type (ethanol, acetone, and isopropyl acetate) was undertaken to maximize extraction yield. Gas chromatography was employed to analyze the essential oil extracts, focusing on quantifying menthol and menthone contents. The DPPH and FRAP methods were also used to determine the antioxidant properties of extracts obtained. The highest extraction yield (1.97%) was achieved at 400 bar and 50 °C for 120 min with a flow rate of 3 mL/min. However, superior essential oil quality, with the highest menthol content (47.50%) and menthone content (2.29%) was obtained at 110 bar and 50 °C for 120 min with a flow rate of 3 mL/min. Co-solvents enhanced the extraction yield, though they influenced the menthol and menthone contents in the extracts. Scale-up experiments resulted in yields of 0.94%, 0.79%, and 0.77% for 3-fold, 5-fold, and 10-fold increases in peppermint powder loading, respectively, at 110 bar and 50 °C. In addition, these scale-up processes resulted in menthol contents of 49.81%, 48.186%, and 47.362% and menthone contents of 1.90%, 2.00%, and 2.13% in the extracts, respectively. Furthermore, peppermint essential oil exhibited antioxidant activity, displaying its most significant scavenging activity of 77.9% and a ferric reducing power equivalent to approximately 82.253 µM ascorbic acid equivalent at a concentration of 500 mg/mL. In the second study, the solubility of menthol in SC-CO_2 was evaluated to further impregnate menthol on cotton gauze using SC-CO_2. Solubility of menthol in SC-CO_2 was carried out at various temperature (45-55 °C) and pressure (100-300 bar)

conditions, with SC-CO$_2$ density varying from 337.2 to 890.3 kg/m^3. Overall, the best solubility of menthol was 1.25×10^{-2} mole fraction obtained at 120 bar and 45 °C. Then, the impregnation of menthol onto cotton gauze was accomplished using SC-CO$_2$ at 120 bar and 45 °C, and a depressurization rate of 6 bar/min or 60 bar/min and a time of 30 min or 300 min. High impregnation yields ranging from 6% to 30.65% were achieved with the long impregnation time of 300 min and the lower depressurization rate of 6 bar/min. The impregnation process demonstrated the successful dissolution of menthol and penetration into the cotton gauze matrix. The FT-IR, SEM, and TGA analyses confirmed the effective impregnation of menthol without significant alterations in the cotton's structural integrity. Overall, this study provides significant insights into peppermint essential oil extraction by SC-CO$_2$, particularly relevant to the food and pharmaceutical sectors.

Keywords: Supercritical carbon dioxide processing; Extraction; Scale up; Mentha × piperita; Menthol; Solubility; Impregnation.

PREFACE

The research reported in this MSc thesis was led by Prof. Marleny D. Aranda Saldaña as the PI. This thesis contains original research work performed by Yuan Meng under the supervision of Prof. Marleny D. Aranda Saldaña conducted in accordance with the guidelines outlined by the Faculty of Graduate Studies and Research at the University of Alberta. The research concept for this thesis originated from my supervisor, Dr. Marleny D. Aranda Saldaña. This thesis is comprised of five chapters. Chapter 1 presents the introduction and objectives, followed by Chapter 2, which provides a comprehensive literature review.

A version of Chapter 3 has been submitted as supercritical CO_2 + co-solvent extraction of essential oil from *Mentha × piperita* and scale up to VI Iberoamerican Conference on supercritical fluids 2023 to be held in Argentina. For this chapter, I was responsible for the investigation, data collection, result interpretation, and manuscript writing. Dr. Saldaña was responsible for the conceptualization, supervision, reviewing and editing, and fund acquisition.

In Chapter 4, the solubility of menthol in supercritical carbon dioxide and its impregnation on cotton gauze were investigated. Dr. Saldaña was responsible for the conceptualization, supervision, discussion, reviewing and editing, and fund acquisition. I was responsible for the investigation, methodology, data collection, analysis and writing.

Chapter 5 provides overall conclusions and recommendations for future research.

ACKNOWLEDGEMENTS

Lastly, I would like to express my gratitude to all of those who have supported me in big and small ways throughout my academic journey. Your encouragement and assistance have played a significant role in my personal and professional growth.

TABLE OF CONTENTS

LIST OF TABLES

LIST OF FIGURES

Page

ABBREVIATIONS

AAE: Ascorbic acid equivalent

ANOVA: Analysis of variance

ATR-IR: Attenuated total reflection infrared spectroscopy

CAGR: Compound annual growth rate

DPPH: 2,2-diphenyl-1-picrylhydrazyl

EO: Essential oil

FDA: Food and drug administration

FRAP: Ferric reducing antioxidant power

FT-IR: Fourier transform infrared spectroscopy

GC: Gas chromatography

GC-MS: Gas chromatography-mass spectrometer

GRAS: Generally recognized as safe

HPLC: High-performance liquid chromatography

LDPE: Low-desnity polyethylene

NRV: One-way valve

PG: Pressure gauge

PGSS: Particle from gas-saturated solutions

PLA: Polylactic acid

PV: Poly (vinyl alcohol)

PVP: Poly (vinylpyrrolidone)

RV: Relief valve

SAS: Supercritical antisolvent

SC-CO$_2$: Supercritical carbon dioxide

SEM: Scanning electron microscope

TEAC: Trolox equivalent antioxidant capacity

TGA: Thermo gravimetric analysis

TI: Temperature indicator

TIC: Temperature indicator controller

USD: United States dollar

V: Valve

Chapter 1: Introduction

1.1. Rationale

The Lamiaceae family is one of the largest herbal plant families, which is grown worldwide except in the Antarctic and Arctic region (Ansari and Goodarznia, 2012). The most important genus in the Lamiaceae family is *Mentha* or *Menthe*, because it has essential oils with high economic value. These essential oils can be extracted from *Mentha*, including corn mint (*Mentha arvensis*, the source of natural menthol), peppermint (*Mentha × piperita)*, scotch spearmint (*Mentha × gracilis*), and native spearmint (*Mentha spicata)* (Lawrence, 2016). Currently, the cultivation and harvesting of peppermint yield an annual output of about 4,000 metric tons of peppermint oil, with over 80% of this production attributed to the United States.

Canada produces only a small amount of mint, mainly importing $3-8 millions of mint essential oil from the United States annually. While mint is grown throughout most of Canada, large-scale field peppermint production is concentrated in the prairie provinces including Alberta. In addition, peppermint can be grown in greenhouses for the fresh-cut herb market (Wees, 2013). Peppermint has therefore established itself as an economically important crop, particularly for the production of essential oils. Peppermint oil, native spearmint oil, and scotch spearmint oil is produced in North America, whereas China and India produce mainly corn mint oil and natural menthol (Lawrence, 2016).

According to the FoodData Central (2019), fresh peppermint contains 78.6% of moisture, 1.76% of ash, 8% of fiber, 0.94% of lipids, 3.75% of proteins and 14.9% of carbohydrates.

To obtain essential oils, extraction is commonly used. According to the proximate composition of peppermint, the oil accounts for 0.94%. Therefore, it is important to find an effective method to extract essential oil from peppermint (*Mentha × piperita*). The extraction processes used to isolate

essential oils are steam distillation, supercritical carbon dioxide (SC-CO$_2$) extraction and subcritical water extraction.

Steam distillation, also known as hydrodistillation, is a method used to extract essential oils from plant materials such as leaves, flowers, and stems. This process involves the use of steam to remove the aromatic compounds from the plant material into a condenser, where the steam is cooled, and the essential oil is collected. In steam distillation, the plant material is placed in a distillation flask and heated with steam. As the steam passes through the plant material, it extracts the volatile compounds, including the essential oil. The steam and essential oil vapour are then passed through a condenser, which cools the vapour and causes it to condense back into a liquid form. The essential oil separated from the water used to generate the steam is collected in a separate container (Kant and Kumar, 2022).

On the other hand, SC-CO$_2$ extraction is a method used to extract essential oils, flavors, and other compounds from plant material. This process uses CO$_2$ at the supercritical state - a state in which the CO$_2$ is heated and pressurized beyond its critical point (73.8 bar and 31.1 °C), where it exhibits properties of both a gas and a liquid. In SC-CO$_2$ extraction, the plant material is placed in a high-pressure vessel, and SC-CO$_2$ is used as a solvent to extract the desired compounds. The SC-CO$_2$ dissolves the essential oils and other compounds from the plant material, and the CO$_2$ is easily separated from the mixture by lowering the temperature and pressure (Saldaña et al., 1999).

Subcritical water extraction, also known as pressurized liquid extraction (PLE) is a method used to extract compounds from plant materials, and food products. It involves the use of water at subcritical temperature and pressure as a solvent to extract the desired compounds. In subcritical water extraction, the sample is placed in a high-pressure vessel, and water is added to the vessel. The temperature and pressure of the water are controlled to maintain subcritical conditions,

allowing it to extract compounds from the sample. The extracted compounds are then separated from the water using various techniques such as solvent extraction, solid phase extraction, or filtration (Zakaria and Kamal, 2016).

As stated above, traditional hydrodistillation involves boiling the plant material in water to produce steam, which is then condensed to obtain the essential oil. The high temperature and prolonged exposure to water can cause some essential oils to degrade, leading to a loss of quality and quantity of the extracted compounds. Moreover, the hydrodistillation method requires a significant amount of energy and time to heat the water and maintain the boiling temperature for a prolonged period, making it a relatively inefficient and costly process (Ansari and Goodarznia, 2012).

Earlier, Barton et al. (1992) extracted essential oils from peppermint and spearmint using SC-CO_2 at 24- 43°C, 60-180 bar, and 4-9 h with CO_2 mass from 6-30 g/g dry peppermint. They obtained yields of 0.8-3.9% where the SC-CO_2 extracted essential oil had more menthofuran (4.78-11.05%) than the essential oil extracted by steam distillation (4.01%). Goto et al. (1993) also investigated the extraction of peppermint essential oil by SC-CO_2 with ethanol at 40-80 °C, 88.3-196 bar with a CO_2 flow rate of 1.98-7.8 mL/min where the best yield was 0.45%. They used a semi-batch-flow extraction apparatus, which may not accurately reflect industrial-scale extraction processes. Reverchon et al. (1994) reported that the optimum SC-CO_2 extraction condition was 90 bar and 50°C with a yield of 1.76%. Roy et al. (1996) used SC-CO_2 to extract essential oil and cuticular waxes from peppermint leaves and evaluated the effect of CO_2 flow rate (4.1-9.8×10^{-5} kg/s) and pressure (100-300 bar) on the yield. All these past studies focused on SC-CO_2 extraction of essential oil from peppermint, which had limitations in terms of scale. Some potential issues that still need to be addressed include optimizing extraction conditions for maximum yield and purity of essential oil, including time, pressure, and temperature. Enhancing these conditions could

improve the efficiency and cost-effectiveness of the process, as well as the evaluation of the impact of co-solvents (ethanol, acetone, isopropyl acetate) on extraction yield and essential oil components.

Industries have a high demand for essential oils, and therefore, any improvement in the extraction method or optimal extraction conditions could have a significant impact on the production cost and availability of these oils. Moreover, the main components of mint essential oils, menthol and menthone, have a wide range of medicinal and therapeutic applications. Hence, finding the best extraction method and optimal extraction conditions for peppermint essential oil is crucial to improve its yield for further utilization in various fields.

Peppermint oil has been widely applied in the food, cosmetics, and pharmaceutical industries. The essential oils isolated from mint leaves are composed of many valuable compounds. In peppermint, the two most abundant compounds are menthone (45%) and menthol (25.4%) (Reverchon et al., 1994). Menthone and menthol, as the main constituents of peppermint, have been proven effective in providing protection to the gastrointestinal, liver, kidney, skin, respiratory, brain and nervous systems and have effects on hypoglycemic and hypolipidemic conditions (Zhao et al., 2022). In addition, menthol offers various benefits such as analgesic effect, reducing the threshold for cold and mechanical pain (Binder et al., 2011). It also exhibits cytotoxic activity against several types of cancer cells (Kim et al., 2012) and possesses anti-inflammatory properties by suppressing the production of inflammation mediators (Juergens and Stöber, 1998).

Solubility plays a crucial role in determining the efficacy of various SC-CO_2 processes, which can greatly influence their success and outcomes. In the case of impregnation, high solubility of the compound in SC-CO_2 is typically required. Impregnation involves the dissolution of a desired compound into the supercritical fluid, allowing it to penetrate and impregnate a substrate or

material. The high solubility of the compound in SC-CO₂ ensures efficient and effective impregnation, as it allows for a greater amount of compound to be dissolved and distributed within the substrate. The solubility of menthol in SC-CO₂ has been investigated by Sovova and Jez (1994) and Galushko et al. (2006). Sovova and Jez (1994) employed a dynamic method to measure the solubility of menthol in SC-CO₂ at pressures of 67-116 bar and temperatures of 35-55 °C. The solubility values obtained in their study ranged from 6.7×10^{-4} to 9.13×10^{-3}. Similarly, Galushko et al. (2006) used a dynamic method to measure the solubility of menthol in SC-CO₂ at pressures of 66-144 bar and temperatures of 30- 60 °C. The solubility values reported in their study ranged from 3.5×10^{-4} to 3.98×10^{-2}. However, none of the two studies measured the solubility of menthol at high pressures exceeding 200 bar.

Menthol can be impregnated onto cotton gauze using SC-CO₂ as a solvent. This innovative approach holds significant potential for a range of applications, including burn care and the alleviation of muscle and joint pain. Earlier, Milovanovic et al. (2013) impregnated thymol on the cotton gauze using SC-CO₂ with a yield of 19.6%, and all impregnated cotton showed strong antimicrobial activity. Later, Ivanović et al. (2014) also impregnated thyme extract on cotton gauze using SC-CO₂ with a yield of 8.99%. To date, there is no study that has impregnated menthol on cotton gauze using SC-CO₂. Therefore, in this thesis, menthol as the main component of peppermint essential oil was impregnated on cotton gauze as a possible wound care for burn and sports injuries.

1.2. Hypothesis

The use of SC-CO₂ optimal conditions being a combination of pressure, temperature, time, CO₂ flow rate, and co-solvent will enhance the extraction yield of peppermint essential oil from *Mentha × piperita* leaves. The addition of co-solvents will further improve the extraction efficiency and

alter the chemical profile of the extracted essential oil, depending on the type of co-solvent used. Moreover, the analysis of the extracted essential oil by gas chromatography will provide valuable information on the composition and relative abundance of menthol and menthone. Menthol will be effectively impregnated onto cotton gauze by optimizing the impregnation time and depressurization rate.

1.3. Objectives

The main objective of this study was to extract essential oil from peppermint leaves to obtain valuable compounds, including menthone and menthol, for further impregnation of menthol on cotton gauze using SC-CO_2. To achieve this main objective, some specific objectives were:

- To evaluate the effectiveness of SC-CO_2 technology in extracting essential oil from peppermint leaves by investigating the impact of different extraction parameters, including pressure, temperature, CO_2 flow rate, time, and co-solvent type, on the yield and composition of the extracted essential oil, and antioxidant property of extracts by DPPH and FRAP.

- To investigate the scalability of the essential oil extraction process from *Mentha × piperita* leaves.

- To determine the solubility of menthol in SC-CO_2 at various temperatures and pressures using a dynamic method.

- To examine the impact of impregnation time and depressurization rate on the menthol entrapment efficiency and analyze the thermal stability, colour and microstructure of both original cotton gauze and menthol-incorporated cotton gauze.

6

Chapter 2: Literature Review

2.1. Mint

For thousands of years, mint has been featured prominently in the food industry worldwide. The global demand for mint essential oil was at US$ 178 million in 2018 and is expected to grow at a rate of 9.2% annually (Industry Report, 2018). As a result, mint essential oil is one of the most economically important essential oils (Lawrence, 2006).

2.1.1. Mint Classification and uses

The Lamiaceae family is one of the most diverse and widely distributed plant families, which is grown worldwide, excluding the Antarctic and northern regions. Besides the Lamiaceae being one of the largest families of dicotyledonous plants, the presence of external glandular structure makes many species in this family highly aromatic, which produces volatile oils (Giuliani and Maleci, 2008).

Mentha genus is a member of the Lamiaceae family. According to the chromosome numbers, phylogenetic analysis of morphology and main essential oil components, the genus *Mentha* is refined to 18 species and 11 named hybrids (Lawrence, 2016). Some of the most important species of this genus are *Mentha × piperita*, *Mentha gracilis*, and *Mentha spicata*, all of which are grown worldwide. Scotch spearmint (*Mentha gracilis*) is a hybrid mint between native spearmint (*Mentha spicata*) and wild mint (*Mentha arvensis*), while peppermint (*Mentha × piperita*) is a hybrid between native spearmint (*Mentha spicata*) and water mint (*Mentha aquatica*) (Ansari and Goodarznia, 2012).

Both scotch spearmint and peppermint have many benefits and economical value, which are important in the food, pharmaceutical, flavouring, fragrance, and cosmetic industries as shown in Table 2.1.

Table 2.1. Applications of Scotch spearmint and peppermint.

Mint plant	Application
Scotch spearmint (***Mentha gracilis***)	• Leaves used as flavouring in salads or cooked meal, also in mint sauce (Venkateshappa and Sreenath, 2013). • Essential oils from leaves used in the food and beverage industry, fragrance, and oral hygiene products (Lis-Balchin, 2006). • Essential oils from leaves prevent the growth of bacteria, yeast, fungi, and bacteriophage (Chao et al., 2000). • The stems can be macerated and used as a poultice on bruises (Venkateshappa and Sreenath, 2013). • Safe to directly use the essential oils on skin with no toxicity, but it may cause irritation on mucous membrane (Tisserand and Balacs, 1996).
Peppermint (***Mentha × piperita***)	• Most popular flavour used in sugar confectioneries, chewing gums, toothpaste, chocolate fillings, pharmaceuticals and liqueurs (Roy et al., 1996). • Essential oils from peppermint have many health benefits, including ulcer healing, anti-spasmodic effects, anti-bloat effects, anti-lipid peroxidation, anti-obesity, anti-cancer, anti-diabetic activity, immunomodulation, reducing irritable bowel syndrome, reducing symptoms of non-ulcer dyspepsia, anti-headache and reducing gastrointestinal complications (Masomeh et al., 2017). • Essential oils have the effect on prevention of growth of bacteria, yeast, fungi, and bacteriophage (Chao et al., 2000).

2.1.2. Essential oils market

Essential oils are combinations of volatile compounds predominantly found in aromatic plants, mainly formed by terpenes (Dhifi et al., 2016). Plant essential oils are mostly used in cosmetics and personal care, food and beverage industries, home care, and aromatherapy (Persistence Market

Research, 2023). In 2008, orange oil, cornmint oil, and lemon oil were the top three plant essential oils in the world, with outputs of 51,000, 32,000, and 9,200 metric tons, respectively. The world production of peppermint oil was 3,300 metric tons, where the United States, India and China produced the highest amounts of peppermint oil in the world. Regarding the production of spearmint essential oil, the United States and China were the main spearmint oil producers with 1,800 metric tons in 2008 (Schmidt, 2020).

Since 1990, essential oil production has tripled (45,000 tonnes) (Barbieri and Borsotto, 2018). Fig. 2.1 shows the estimated global production of essential oils in 2017 that was more than 150,000 tonnes valued at approximately $6 billion USD.
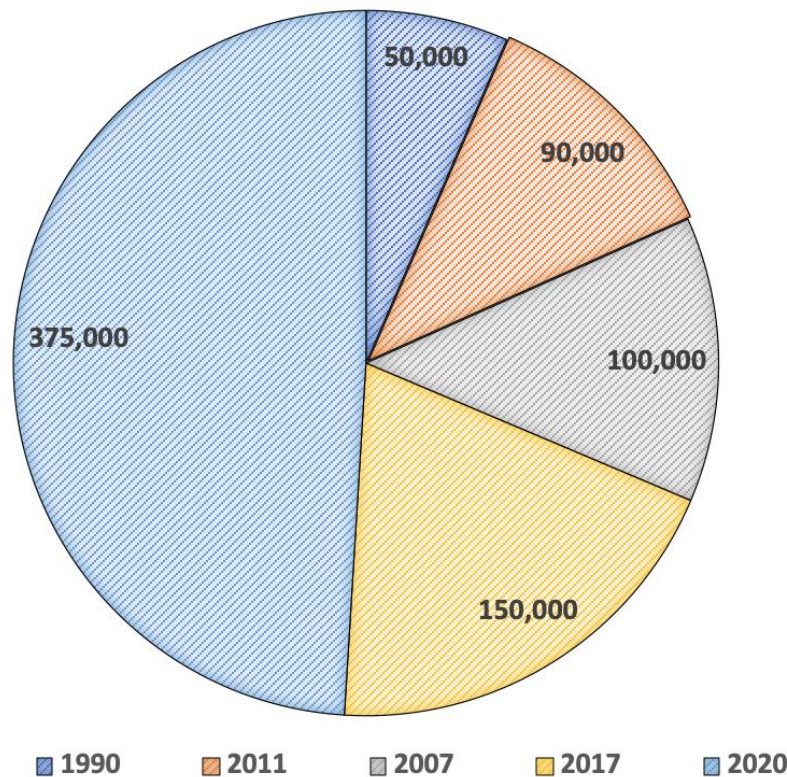
Fig. 2.1. World production of essential oils in tonnes from 1990 to 2020 (Adapted from Barbieri and Borsotto, 2018).

In Canada, several essential oils are produced. Lavender oil is produced in British Columbia, Ontario and Quebec, peppermint oil is mainly produced in British Columbia and Quebec, and tea tree oil is produced in British Columbia, Ontario and Quebec. In 2020, Canada exported $63.3 million and imported $119 million in essential oils (Essential oils in Canada, 2020).
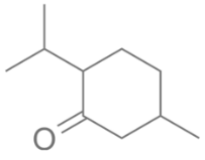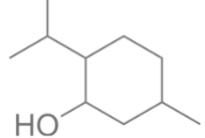
Peppermint oil production reached a milestone in 2020, totaling 48,000 metric tons. This significant figure marks more than tenfold increase compared to its production in 2007. These values underscore the diverse and widespread cultivation of essential oils across different countries, reflecting the continued demand for these aromatic and versatile natural extracts. In 2022, worldwide consumption of essential oil was 497,959 metric tons valued at USD 18.66 billion. The global essential oil market is projected to grow at a compound annual growth rate (CAGR) of 7.7% to be valued at USD 39.1 billion by 2032 (Persistence Market Research, 2023).

2.2. Chemical composition and structure of peppermint essential oil

Table 2.2 shows some components of peppermint extract (cuticular wax and essential oil) (Reverchon et al., 1994). They analyzed and identified the compounds with retention times shorter than 65 min by GC. Generally, cuticular waxes have longer retention times (> 90 min). The percentage composition of peppermint oils indicated that the most abundant compounds are menthone (45.0%) and menthol (25.4%).

Table 2.2. Percentage composition (%) of peppermint (*Mentha × piperita*) essential oils and cuticular waxes isolated by supercritical CO_2 extraction at 90 bar and 50 °C (Adapted from Barton et al., 1992 and Reverchon et al., 1994).

Compound	Percentage (%)
Essential oil	
α-Pinene	0.4
β-Pinene	0.7
β-Myrcene	0.2
1,8-Cineole	5.3
cis-β-Ocimene	0.3
Menth-2-en-1-ol	0.2
trans-Menthone	45.0
cis-Menthone	7.3
trans-Menthol	25.4
cis-Menthol	0.5
Pulegone	0.2
Piperitone	0.4
Neomenthyl acetate	0.2
trans-Menthyl acetate	9.0
β-Bourbonene	0.3
β-Elemene	0.4
β-Caryophyllene	1.8
γ-Cadinene	1.6
Cuticular wax	
n-Heptacosane	3.7
n-Octacosane	1.3
n-Nonacosane	15.5
n-Triacontane	3.6
Ethyloctacosane	1.4
n-Hentriacontane	37.7
Methyltriacontane	1.4
n-Dotriacontane	6.7
Ethyltriacontane	2.4
n-Tritriacontane	24.3

Compound	Structure	Molecular weight (g/mole)	Boiling point (°C)	Solubility* (mg/L)		
				Water	Ethanol	Dimethyl sulfoxide
Menthone $C_{10}H_{18}O$		154.25	210	688	-	-
Menthol $C_{10}H_{20}O$		156.27	212	420	30000	10000

*Solubility reported at 25 °C. Data sources: Milliporesigma, https://www.sigmaaldrich.com/CA/en and U.S. National Library of Medicine, PubChem (2023), https://pubchem.ncbi.nlm.nih.gov.

2.2.1. Menthol and biological activity

Natural menthol, obtained by extraction of peppermint leaves, is an important flavour additive and fragrance compound with its unique cooling characteristic. Studies have shown that menthol possesses the ability to scavenge free radicals and mitigate oxidative stress within biological systems (Zhang et al., 2023). Its antioxidant potential can contribute to the protection of cells and tissues from damage caused by reactive oxygen species, thus potentially reducing the risk of various chronic diseases (Bastaki et al., 2018). Binder et al. (2011) reported the analgesic effect of menthol, and they found that menthol decreased the thresholds of cold pain and mechanical pain and increased mechanical pain sensitivity. Besides, menthol was tested against the growth of *Fusarium verticillioides* at 200 ppm, reducing 75% of *F. verticillioides* (Dambolena et al., 2008). Menthol also exhibits cytotoxic activity against several types of cancer cells by affecting the gene expression of cancer cells (Kim et al., 2012). Juergens and Stöber (1998) investigated the anti-inflammatory activity of menthol, and the results showed that menthol suppressed the production of inflammation mediators by monocytes. In addition, menthol can be used as a vehicle for

transdermal drug delivery, working as a penetration enhancer. It can permeate the epidermis and increase the accessibility of other drug molecules (Patel et al., 2007).

2.2.2. Menthone and biological activity

Menthone has multiple applications, including its known antibacterial, antioxidant, anti-inflammatory, and antiviral properties (Chen et al., 2022; Dambolena et al., 2008).

2.3. Chemical composition and structure of spearmint

Table 2.3 reveals that the extracted oil from spearmint consists of 45.96% carvone and 12.81% limonene (Shahsavarpour et al., 2017). Meanwhile, Table 2.4 provides information on the structure, molecular weight, boiling point, and solubility in water and ethanol for the components found in spearmint.

2.3.1. Limonene and its biological activity

Limonene is one of the most common terpenes found in nature and an ingredient in many citrus essential oils. Limonene is a colourless liquid in the form of two optical isomers and racemic mixtures called d- or L-limonene. Limonene is listed in the Code of Federal Regulation as Generally Recognized as Safe (GRAS) (Sun, 2007). It has a pleasant lemon-like odour and is used as a flavour additive, fragrance, and various beauty products (Vieira et al., 2018). Besides, limonene has various biological effects, including anti-inflammatory activity (Kummer et al., 2013), antioxidant activity (Roberto et al., 2010), anticancer activity (Zhang et al., 2014), antidiabetic activity (Joglekar et al., 2013), treatment of metabolic syndrome (Santiago et al., 2012), and effects in the respiratory tract (Hansen et al., 2013). All of these effects have been proven by the authors by in *vitro* and in *vivo* assays.

Table 2.3. Chemical composition (%) of spearmint (*Mentha spicata)* essential oil (Adapted from Barton et al., 1992 and Shahsavarpour et al., 2017).

No	Compound	Percentage (%)
1	α - Thujene	0.609
2	Camphene	0.156
3	Sabinene	0.605
4	β - Pinene	0.912
5	Myrcene	0.586
6	Limonene	12.807
7	1,8 - Cineole	7.777
8	(Z) - β - Ocimene	0.153
9	(E) - β - Ocimene	0.073
10	Cis – Sabinene hydrate	0.082
11	Borneol	0.924
12	Isopulegone	0.785
13	α - Terpineol	0.251
14	Dihydro Carvone	3.440
15	Pulegone	13.893
16	Carvone	45.964
17	Piperitenone	1.841
18	β - Bourbonene	1.263
19	β - Caryophyllene	5.515
20	α - Humulene	0.725
21	Germacrene D	1.241
22	Bicyclogermacrene	0.408
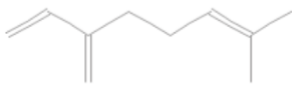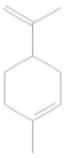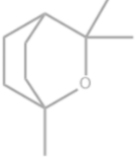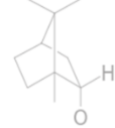
2.3.2. Carvone and its biological activity

Carvone is a monoterpene ketone and exists in two forms: (+)-carvone and (-)-carvone, which have the same chemical and physical properties but differ in their rotary power. Carvone has a sweet spearmint odour and is found in many plant species like *Origanum* spp., *Rosmarinus* spp., among others (Bouyahya et al., 2021). To date, many studies have proven that carvone has many promising biological properties. Carvone has antiparasitic effects, anti-arthritic effects, anti-convulsant effects, immunomodulatory effects, neurological effects, anti-cancer effects, anti-

inflammatory effects, antidiabetic effects, antifungal activity and antibacterial activity (Bouyahya et al., 2021).

In general, carvone is produced by extraction and purification of essential oils from caraway, dill and spearmint, and also by chemical and biotechnological synthesis (De Carvalho and Da Fonseca, 2006).

Table 2.4. Properties of essential oils in spearmint.

Name of Compound	Structure	Molecular weight (g/mole)	Boiling point (°C)	Solubility* (mg/L)	
				Water	Ethanol
Sabinene $C_{10}H_{16}$		136.23	164	2.494	330
β - Pinene $C_{10}H_{16}$		136.23	166	6.95	20000
Myrcene $C_{10}H_{16}$		136.23	167	5.60	-
Limonene $C_{10}H_{16}$		136.23	176	7.57	330
1,8 – Cineole $C_{10}H_{18}O$		154.25	176	3500	-
Borneol $C_{10}H_{18}O$		154.25	212	738	-

Table 2.4 Continued.

Name of Compound	Structure	Molecular weight (g/mole)	Boiling point (°C)	Solubility* (mg/L)	
				Water	Ethanol
α - Terpineol $C_{10}H_{18}O$		154.25	219	7100	-
Dihydro Carvone $C_{10}H_{16}O$		152.23	87-88	560	-
Carvone $C_{10}H_{14}O$		150.22	230-231	367	-
Piperitenone $C_{10}H_{14}O$		150.22	106-107	165	-
β - Caryophyllene $C_{15}H_{24}$		204.35	264-266	0.05	250
α - Humulene $C_{15}H_{24}$		204.35	99-100	0.01	-

*Solubility reported at 25 °C. Data sources: Milliporesigma, https://www.sigmaaldrich.com/CA/en and U.S. National Library of Medicine, PubChem (2023), https://pubchem.ncbi.nlm.nih.gov.

2.4. Solubility of a compound in supercritical carbon dioxide

The efficacy of various SC-CO_2 processes is heavily influenced by solubility, making it a crucial parameter. Table 2.5 shows selected published solubility data of different compounds in SC-CO_2. Different processes may require either high solubility or extremely low solubility, depending on the specific objectives. For instance, the supercritical fluid extraction process requires high solubility, whereas the particle formation process, particularly the supercritical antisolvent (SAS)

process, requires low solubility. Solubility plays a significant role in determining the yield, cost, as well as size and morphology of the final product (Gupta and Shim, 2007).

During the extraction, the solubility of essential oil constituents like menthol, limonene, and citral in $SC-CO_2$ can significantly impact the extraction yield and composition. Researchers can manipulate pressure and temperature conditions to enhance the solubility of specific compounds, leading to optimized extraction results. Consequently, understanding the solubility behavior of different constituents within $SC-CO_2$ provides valuable insights to achieve desired product compositions and qualities.

On the other hand, the utilization of SAS technology enables the simultaneous precipitation and microencapsulation of substances using $SC-CO_2$ (Santos et al., 2020). In the SAS process, the desired material is dissolved in a conventional solvent and then atomized alongside $SC-CO_2$ at a moderate temperature and pressure through a nozzle. By acting as an antisolvent, the high-pressure carbon dioxide reduces the solubility of the solute in the mixture, leading to supersaturation that initiates nucleation and facilitates the formation of nano- or microparticles (Rosa et al., 2020). In precipitation processes, supersaturation of solute relies on solubility, which greatly influences nucleation and subsequently affects precipitation kinetics (Gupta and Kompella, 2009). For example, Park et al. (2014) produced sub-micron particles of tadalafil solid dispersion. They observed that the solubility of tadalafil in ethanol and methylene (volume ratio: 1:1) was 25 mg/mL. Consequently, when the concentration of tadalafil surpassed the 25 mg/mL threshold, recrystallization occurred, resulting in the formation of a cotton-like suspension. Rossmann et al. (2013) employed SAS technique to produce acetaminophen particles and determined that the level of supersaturation can be controlled by adjusting the concentration and pressure parameters. Specifically, increasing the concentration above the solubility of acetaminophen in $SC-CO_2$ and/or

reducing the pressure (resulting in low solubility) led to a higher degree of supersaturation, while the opposite trend was observed when the concentration was decreased, or the pressure was increased. Therefore, the low solubility of compounds in SC-CO_2 facilitated the attainment of supersaturation and promoted the formation of particles.

In addition, the solubility of a compound in SC-CO_2 plays a crucial role in the impregnation process. When impregnating a compound onto a material using SC-CO_2, the solubility of the compound determines its ability to dissolve and disperse within the SC-CO_2 medium, which is important to achieve uniform and efficient impregnation of the compound onto the material.

In a study conducted by Milovanovic et al. (2013), the solubility of thymol in SC-CO_2 was investigated using a static method, where temperatures of 35, 40, and 50 °C were evaluated along with pressures ranging from 78 to 250 bar. The results indicated that at a temperature of 35 °C and a pressure of 155 bar, the solubility of thymol in SC-CO_2 was 1.1×10^{-2} mole fraction. Based on the solubility data, the impregnation of thymol on cotton gauze was carried out at 35 °C and 155 bar for 2 h. The impregnation yield achieved under these conditions was 11%. Similarly, Sanchez-Sanchez (2017) impregnated mango leaf extract, known for its antioxidant and antibacterial properties, into a polyester textile using SC-CO_2. To enhance the solubility of the mango leaf extract in SC-CO_2, 50% ethanol was utilized as a co-solvent. Under this condition, the impregnated textiles exhibited the highest antioxidant capacity, as evidenced by the 2,2-diphenyl-1-picrylhydrazyl radical (DPPH) assay, with a value of 4.04 µg DPPH/µg extract.

Table 2.5. Selected solubility data of different compounds in SC-CO_2.

Compound	Method	Temperature (°C)	Pressure (bar)	Solubility	Reference
Essential oil					
Thymol	Static	35-50	75-250	$0.9 \times 10^{-3} - 1.47 \times 10^{-2}$ mole fraction	Milovanovic et al. (2013)
Citral	dynamic	35-50	30-110	$0.3 \times 10^{-4} - 2.23 \times 10^{-2}$ mole fraction	Di Giacomo et al. (1989)
Limonene	dynamic	35-50	30-100	$0.2 \times 10^{-3} - 24.4 \times 10^{-2}$ mole fraction	
Others					
Alendronate	Dynamic	35-65	120-300	$0.1 \times 10^{-4} - 1.5 \times 10^{-4}$ mole fraction	Abourehab et al. (2022)
Caffeine	Dynamic	40, 50, 70	140-240	$200 - 2047.6$ mg/kg CO_2	Saldaña et al. (1999)
Cetirizine	Static	35-65	150-400	$1.05 \times 10^{-5} - 4.92 \times 10^{-3}$ mole fraction	Hezave et al. (2011)
Clemastine fumarate	Static	35-65	120-280	$1.61 \times 10^{-6} - 9.41 \times 10^{-6}$ mole fraction	Sodeifian et al. (2021)
Glibenclamide	Static	35-65	120-300	$0.8 \times 10^{-6} - 8.03 \times 10^{-5}$ mole fraction	Esfandiari and Sajadian (2022)
Lenalidomide	Static	35-65	120-300	$0.02 \times 10^{-4} - 1.08 \times 10^{-4}$ mole fraction	Sajadian et al. (2022)
Lansoprazole	Static	35-65	120-270	$1.15 \times 10^{-5} - 7.36 \times 10^{-4}$ mole fraction	Sodeifian et al. (2020)
Loxoprofen	Static	35-65	120-400	$1.04 \times 10^{-5} - 1.28 \times 10^{-3}$ mole fraction	Zabihi et al. (2020)
Paeonol	Static	40-60	80-150	$3.10 \times 10^{-3} - 1.32 \times 10^{-2}$ mole fraction	Jiao et al. (2019)

2.4.1. Methods to measure the solubility of a compound in SC-CO$_2$

Solubility is typically defined as the mole fraction of a solute in the SC-CO$_2$. Commonly, there are two methods to measure solubility, static, and dynamic, which are discussed below.

2.4.1.1. Static method

The static method involves allowing the solute to remain in static contact with the SC-CO$_2$ at the desired pressure and temperature for an extended period of time to achieve equilibrium as shown in Fig. 2.2.
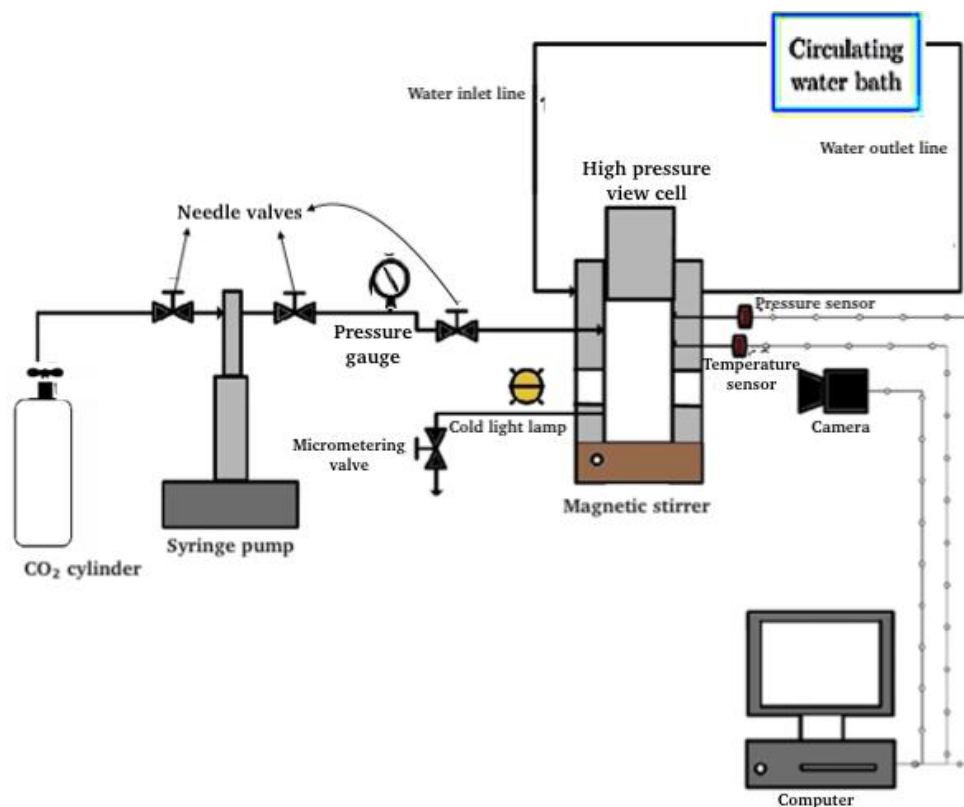
Fig. 2.2. Schematic representation of the SC-CO$_2$ static system. (Adapted from Ciftci and Saldaña, 2015 and Ciftci and Temelli, 2014).

In this method, a known amount of compound is placed in a high-pressure vessel along with CO$_2$. The vessel is closed, and the system is allowed to reach equilibrium by keeping it at a constant temperature and pressure for a specific period of time. During this time, the solute and the SC-CO$_2$

interact, and solubilization occurs. After equilibrium is achieved, a sample of the SC-CO₂ phase is collected and analyzed to determine the solute concentration using analytical techniques such as chromatography (HPLC or GC) or spectroscopy. The solubility of the compound in SC-CO₂ can then be calculated based on the measured concentration using eq 2.1.

$$Solubility \ = \frac{mole \ of \ compound}{mole \ of \ CO_2 + mole \ of \ compound} \tag{2.1}$$

2.4.1.2. Dynamic method

The dynamic method is an alternative approach used to measure the solubility of a compound in SC-CO₂. In this method, a continuous flow of SC-CO₂ is directed over a fixed quantity of the compound within a temperature- and pressure-controlled high-pressure vessel at a low CO₂ flow rate (Saldaña et al., 1999). The setup typically involves a high-pressure pump that delivers the CO₂ to the reactor as shown in Fig. 2.3.
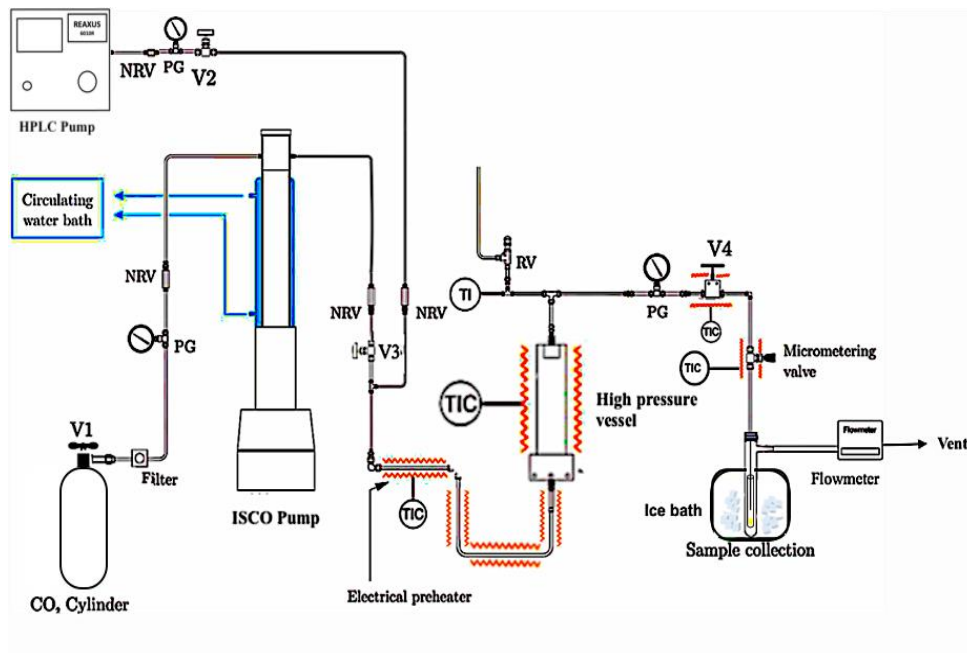
Fig. 2.3. Schematic representation of the Supercritical CO₂ Dynamic System. PG: pressure gauge, V1-4: valves, TI: temperature indicator, TIC: temperature indicator controller, NRV: one-way valve, and RV: relief valve.

21

To initiate the process, the compound is loaded into the high-pressure vessel. When the desired pressure and temperature are reached, the flow of SC-CO2 is initiated. As the SC-CO2 passes through the reactor, it comes into contact with the compound, leading to the dissolution of the solute in the SC-CO2. The resulting solution, containing the dissolved solute, continues to flow through the system. To determine the solubility of the compound in SC-CO2, the concentration of the solute within the SC-CO2 stream is analyzed using various techniques such as chromatography, spectroscopy, or gravity measurements.

2.5. Extraction of essential oils from mint

2.5.1. Conventional extraction method

There are some conventional techniques used to extract essential oils from plants such as hydro distillation, steam distillation and organic solvent extraction. The hydrodistillation process involves immersing the plant material (*Mentha* species) in water and boiling them repeatedly to condense the oil and separate it from the mixture of steam and oil as shown in Fig. 2.4.
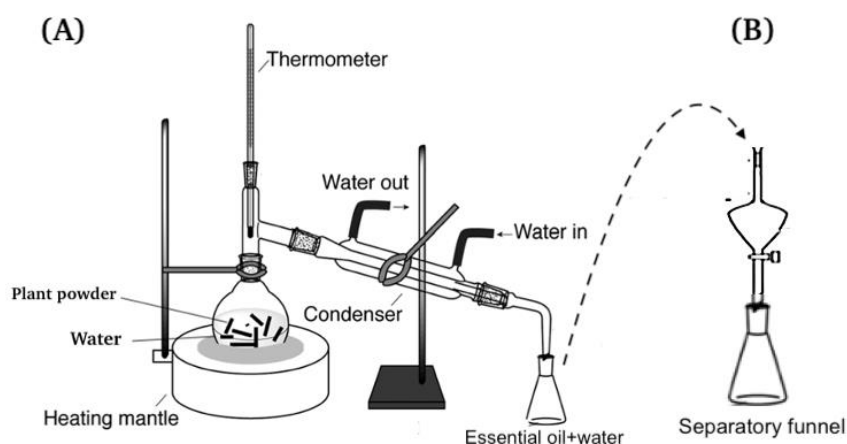
Fig. 2.4. (A) Hydrodistillation setup for the extraction (B) essential oil separation (Adapted from Dangkulwanich and Charaslertrangsi, 2020 and Sahraoui and Boutekedjiret, 2015).

This method is useful for the separation of high boiling-point organic compounds from the plant (Dangkulwanich and Charaslertrangsi, 2020).

Steam distillation occurs when water is boiled in a vessel and mint leaves are placed on a grid above the boiling water to allow the wet steam to release the essential oil as steam, which condenses and separates by a funnel as shown in Fig. 2.5. The extraction ends when there is no more essential oil left to extract (Lawrence, 2016; Sahraoui and Boutekedjiret, 2015).
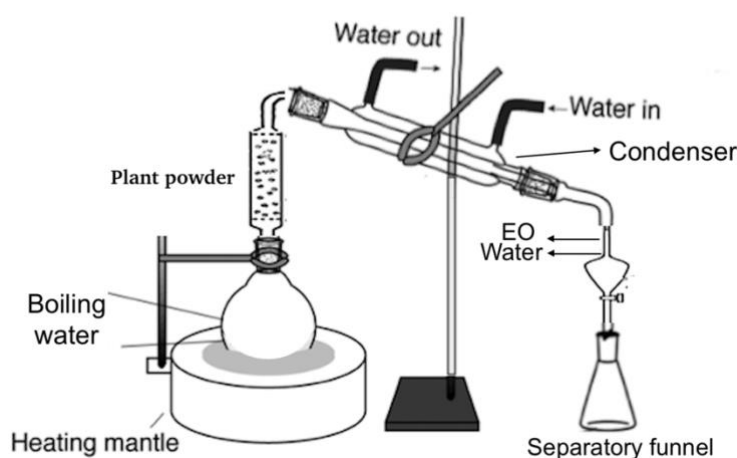
Fig. 2.5. Steam distillation setup for the extraction of essential oil (Adapted from Dangkulwanich and Charaslertrangsi, 2020 and Sahraoui and Boutekedjiret, 2015). EO: essential oil.

Conde-Hernández et al. (2017) compared SC-CO_2, hydro distillation and steam distillation for the extraction of essential oil from rosemary. They found the highest yield with the SC-CO_2 process (2.53%).

In general, the conventional extraction methods take several hours and consume many chemical solvents and energy. Also, the high temperature used in the distillation method is not suitable for the extraction of valuable thermoliable compounds, as it can result in the reduction or loss of the final product (Ansari and Goodarznia, 2012).

2.5.2. Supercritical CO_2 extraction

The supercritical state is a state in which gases and liquids are compressible but have liquid density. CO_2 has a low critical temperature (31.3 °C) and moderate critical pressure (73.8 bar). SC-CO_2 is a good solvent, because the gas-type state has low viscosity and high diffusion coefficient, and the liquid-type state has high solvating power. In addition, carbon dioxide is the most commonly used solvent since it is environmentally non-toxic, inexpensive, and easily removable from the extract due to its gaseous state at room temperature (Saldaña et al., 1999). Fig. 2.6 presents the number of scientific publications on SC-CO_2 extraction of essential oils from 2000 to 2022 with an increasing trend based on the ScienceDirect database using the keywords "supercritical carbon dioxide extraction" and "essential oil". The number of publications in this field has experienced a remarkable exponential growth, escalating from approximately 50 publications in 2000 to around 950 publications in 2022. Notably, until the year 2010, only 100 publications were recorded, indicating a remarkable tenfold increase in twelve years, highlighting the escalating interest and expanding research landscape in this area.
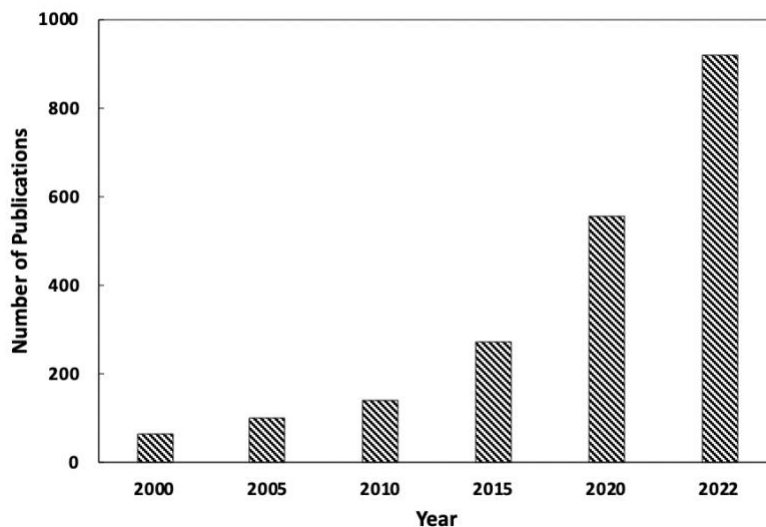
Fig. 2.6. Scientific publications on SC-CO_2 extraction of essential oils from 2000 to 2022 based on the ScienceDirect database using the keywords "supercritical carbon dioxide extraction" and "essential oil".

From the literature in Tables 2.6 and 2.7, pressure, temperature, mean particle size of the sample, $SC\text{-}CO_2$ flow rate and co-solvent are the five processing factors that influence $SC\text{-}CO_2$ extraction yield. Also, an increase in the extraction time led to a considerable increase in the extraction yield at the same temperature and pressure using the same particle size and constant CO_2 flow rate. This trend was reported by Shahsavarpour et al. (2017) for the extraction of essential oil from spearmint, *Mentha spicata.* Their analysis revealed that the yield in each fraction of 20 min was 0.036%, and after 120 min of extraction, the yield was 0.188 % at 50 °C and 120 bar with a flow rate of 0.059 g/min and particle size of 2 mm.

Also, there is a direct relationship between the extraction pressure and yield, where the yield increases when the pressure increases. However, the extraction yield of spearmint essential oil from leaves with $SC\text{-}CO_2$ has a complex relationship with the temperature and pressure. At the constant pressure of 85 bar, the increase in the temperature from 38 to 50 °C reduced the extraction yield from 0.207 to 0.156 with the particle size of 2 mm and extraction time of 120 min. However, for extraction pressures of 100 and 120 bar, an increase in temperature from 38 to 45 °C led to an increase in extraction yields, but with a further increase in the temperature from 45 to 50 °C, the extraction yield decreased (Shahsavarpour et al., 2017). At pressures above 150 bar, the yield increased as the temperature increased (Goto et al., 1993). The reason being that the increase in extraction temperature reduced the density of $SC\text{-}CO_2$ and reduced the solvating power, whereas the high extraction temperature improved the vapour pressure of the essential oils. Therefore, the yield depended on these two competing factors.

Also, Shahsavarpour et al. (2017) examined the effect of CO_2 flow rate on extraction efficiency. The increase in the flow rate from 0.059 g/min to 0.177 g/min resulted in an increase in the

extraction yield for all particle sizes used (0.177, 0.5 and 2 mm), while with a further increase in flow rate at the outlet from 0.177 to 0.354 g/min, the extraction yield decreased.

Regarding particle size, the small particle size led to a high extraction yield, especially at 50 °C. At 120 bar, small particles resulted in a higher yield, but at the low extraction pressure (85 bar), an inverse trend was observed (Shahsavarpour et al., 2017).

The most common co-solvent used with SC-CO_2 to extract essential oils from mint was ethanol. According to Goto et al. (1993), the use of 2 wt% ethanol in SC-CO_2 increased the extraction yield by three-fold, especially the extraction of l-menthol, but the further increase in ethanol concentration led to a decrease in the extraction rate.

SC-CO_2 can also be used to fractionate essential oils. According to the research of Gañán and Brignole (2011), they divided peppermint oil composition into two fractions: a more volatile fraction (20.27%) including menthofuran, 1,8-cineol and menthone, and a less volatile fraction (79.23%) including L-menthol, methyl acetate and their isomers. However, it was difficult to separate these two fractions at temperatures of 40-50°C and pressures of 80-100 bar, as menthone and L-menthol had relatively similar vapour pressures of 0.00021 and 0.00009 mbar at 25°C.

Gañán et al. (2015) used SC-CO_2 to fractionate peppermint oil with low menthol content for the recovery of piperitenone (a flavouring agent, US$36/mg, Cayman Chemical). They reported that the operation temperature and solvent density influenced fractionation selectivity and oil solubility. An increase in temperature from 40 to 50 °C at constant CO_2 density led to an increase in essential oil solubility from 6 to 8.5 g/kg and a decrease in selectivity from 4.8 to 3.4. The fractionation selectivity is calculated by the volatility of fraction 1 (a more volatile fraction) with respect to fraction 2 (a less volatile fraction). For the continuous countercurrent fractionation, they found that

the optimal operating conditions were 40 °C, 90 bar and a solvent-to-feed ratio of 98 kg/kg with approximately 91% piperitenone recovered.

Table 2.6. Extraction of essential oils from mint and other plant sources by supercritical carbon dioxide.

Essential oil	Sample matrix	Sample loaded (g)	Particle size (mm)	Processing Condition				Yield (%)	Reference
				Pressure (bar)	Temperature (°C)	Flow rate (mL/min)	Time (min)		
Mint									
Spearmint oil	*Mentha spicata* (Iran)	15	0.50	90	45	300	120	2[a]	Ansari et al. (2012)
Spearmint oil	Spearmint (USA)	NR	NR	100	33	-	252	3.9	Barton et al. (1992)
Spearmint oil	Mint leaves (Turkey)	125	0.84-2	110	40	4.9	240	80[b]	Özer et al. (1996)
Spearmint oil	Spearmint leaves (Iran)	30	0.18	120	45	96.7	120	0.5[a]	Shahsavarpour et al. (2017)
Peppermint oil	Peppermint leaves (Italy)	110	0.3	90	50	30.5 g/min	160	NR	Reverchon et al. (1994)
Peppermint oil	Peppermint leaves (Japan)	2	NR	88-196	20-80	2.0-7.8[c]	40	NR	Goto et al. (1993)
Peppermint oil	Peppermint leaves (Japan)	23-24	NR	100-300	40	2.8-6.6	0-550	0-3.2	Roy et al. (1996)
Other plant sources									
Essential oil	*Rosmarinus officinalis*	25	0.6	172	40	126.2	180	2.5[a]	Conde-Hernández et al. (2017b)
Essential oil	*Persian black cumin*	590	NR	83	12	NR	720	27.5[b]	Zarrinpashne and Gorji Kandi (2019)

Table 2.6. Continued.

Essential oil	Sample matrix	Sample loaded (g)	Particle size (mm)	Pressure (bar)	Temperature (°C)	Flow rate (mL/min)	Time (min)	Yield (%)	Reference
Other plant sources									
Essential oil	*Piper auritum*	25	NR	172	50	126.2	180	3.1[a]	Conde-Hernández et al. (2017a)
Essential oil	Clove leaves	18	0.37	2200	40	2 g/min	80	1.1[a]	Frohlich et al. (2019)
Essential oil	*Eucalyptus globulus* L.	50	0.30	350	80	12 g/min[c]	120	3.6[a]	Singh et al. (2016)
Essential oil	*Cymbopogon citronella* Leaves	200	0.18	250	35	300	120	4.4[a]	Wu et al. (2019)
Essential oil	*Pistacia lentiscus* L.	23	0.22	220	35	11.7	30	0.2[a]	Aydi et al. (2020)

[a]Yield (wt%) = Mass of extracted oil (g) / Mass of raw material (g) ×100, [b]Recovery (wt%) = Mass of extracted oil (g) / Max oil extracted of feed (g) ×100, [c]Flow rate recorded based on the pump. NR: not reported.

Table 2.7. Extraction of essential oils from plants by supercritical carbon dioxide with co-solvent.

| Matrix | Particle size (mm) | Processing Condition | | | | | Yield (%) | Reference |
		Temperature (°C)	Pressure (bar)	CO_2 flow rate (mL/min)	Co-solvent	Time (min)		
Turkish mint leaves	0.84-2	40	85	3.8	Ethanol (3.0 mole%)	120	56.6[b]	Özer et al. (1996)
Japanese Peppermint leaves	NR	20-80	88.2-196	2.0-7.8	Ethanol (2.0 mole%)	40	NR	Goto et al. (1993)
Lavandin flowers	0.60-0.85	48.5	108.7	5	Ethanol (10 mL)	120	4.7[a]	Kamali et al. (2015)
Chamaecyparis obtusa	NR	50	120	40	Methanol	90	2.9[a]	Jin et al. (2010)
Citrus grandis peel	1-2	50	120	0.5 g/min	Ethanol (80%)	120	2.4[a]	Mai et al. (2022)

[a]Yield (wt%) = Mass of extracted oil (g) / Mass of raw material (g) ×100, [b] Recovery (wt%) = Mass of extracted oil (g) / Max oil extracted of feed (g) ×100, NR: not reported.

2.5.3 Scale-up of SC-CO$_2$ extraction

After four decades of development, supercritical fluid extraction has demonstrated its technical and economic feasibility, the number of commercial plants worldwide utilizing are over 200 (Prado et al., 2011). Several studies have been conducted to investigate the scale-up of extraction of plant materials. The identification of a suitable scale-up criterion is crucial. By adopting a straightforward and practical scale-up criterion, the transition from laboratory-scale experimentation to large-scale production can be streamlined, optimizing the overall efficiency of SC-CO$_2$ extraction development (Salea et al., 2017). The widely recognized four criteria used for scale-up of an extraction process involve maintaining constant ratios such as (i) the ratio between the masses of used CO$_2$ and plant material; (ii) the ratio between CO$_2$ flow rate and plant material weight; (iii) both of the above ratios combined, (iv) or the combination of two ratios and the Reynolds number (De Melo et al., 2014).

There are various studies that have utilized the first criterion for scaling up the extraction process. Albuquerque and Meireles (2012) employed SC-CO$_2$ to extract fat from annatto seeds and successfully scaled up the extraction by around 4 times with volume of extraction vessels of 6.57 mL and 290 mL. The maximum yield achieved was 2.2% at a ratio of 35 between the masses of used CO$_2$ and plant material at 400 bar and 60 °C with a CO$_2$ flow rate of 0.2 g/s for 60 min. Similarly, Eisenmenger et al. (2006) utilized SC-CO$_2$ for wheat germ oil extraction, with an increase in the volume of the extraction vessel from 0.01 L to 4 L, they maintained a constant mass ratio of CO$_2$ and feed at 80. The highest yield obtained was 20% at 550 bar and 80 °C. Additionally, Prado et al. (2012) conducted a scale-up investigation (17 times) for SC-CO$_2$ extraction of grape seed oil, with the volume increasing from 0.29 L to 5.15 L, while maintaining a constant ratio of mass of CO$_2$ and feed at 6.6. The yield achieved was 13.42% at 350 bar and 40 °C.

Han et al. (2009) achieved successful upscaling of SC-CO$_2$ extraction of safflower seed, going from a 0.5 L to a 260 L extractor, using the second scale-up criterion.

Furthermore, Berna et al. (2000) employed the third criterion, maintaining constant ratios of 72 between the masses of used CO$_2$ and plant material, and 10 between CO$_2$ flow rate and plant material weight, for the scale-up extraction of essential oil from orange peel. The yield obtained was 0.13% at 200 bar and 40 °C with a CO$_2$ flow rate of 333 g/min for 420 min.

2.5.4. Subcritical water extraction

Subcritical water, or pressurized hot water, is the water heated to more than 100 °C, but below the critical point (374 °C) and remains liquid due to its high pressure. Subcritical water has excellent properties of high ionic products and low dielectric constant (ε). For the ionic products, the self-ionization increases when the temperature increases, as well as, the molar concentrations of hydrogen and hydroxide ions. For instance, the ionization constant (pKw) of water is 14 at 25 °C, but drops to 11 when the temperature rises to 250 °C. As the temperature rises from 25 °C to 250 °C, the ionic products increase by a factor of a thousand, thus enhancing acid- or base-catalytic hydrolysis (Chiou et al., 2019; Patrick et al., 2001; Saldaña and Valdivieso-Ramirez, 2015). The ε is the value associated with the polarizability. According to Alghoul et al. (2017), the influence of temperature on the polarity of subcritical water is greater than that of pressure. At 25 °C, the dielectric constant of water ($\varepsilon = 80$) is higher than that of methanol ($\varepsilon = 33$) and ethanol ($\varepsilon = 24$). However, when the temperature of water increases from 25°C to 250°C, its dielectric constant decreases from 80 to 27 and its polarity is close to that of methanol and ethanol (Patrick et al., 2001). Due to these properties of subcritical water including high ionic products and low dielectric constant, subcritical water is considered an excellent solvent for extraction of valuable compounds from plants, algae, and food.

In Table 2.8, subcritical water was used to recover essential oils from plants. The extraction time and temperature are the two key process parameters that have influence on the extraction yield and composition of the mint essential oil. Chiou et al. (2019) reported that the extraction yield of essential oils from Japanese mint increased from 23.6 to 29.5 mg/g-dry leaves when the extraction time increased from 5 to 30 min at a temperature of 140 °C, but the yield decreased to around 25.5 mg/g-dry leaves with further extended extraction time (60 min). Additionally, they obtained a yield of 30.3 mg/g-dry leaves at 180 °C with the extraction time of 5 min, so they concluded that the higher temperature and shorter extraction time were the optimal conditions. In the research done by Çam et al. (2018), essential oils were extracted from peppermint by subcritical water treatment. They found an increase in temperature significantly increased the extraction yield up to 130 °C, but no improvement above 130 °C at a constant pressure of 103 bar. After that, they performed extractions with four different times from 1 to 30 min and found that the extraction yield increased with the increased extraction time. Compared with conventional methods, subcritical water extraction requires less processing time (generally 5-30 min) and delivers a higher oil yield and quality (Samadi et al., 2020).

Table 2.8. Extraction of essential oil by subcritical water.

Matrix	Sample loaded (g)	Particle size (mm)	Processing Condition				Yield (%)	Reference
			Temperature (°C)	Pressure (bar)	Flow rate (mL/min)	Time (min)		
Japanese mint	5	-	180	-	-	5	3	Chiou et al. (2019)
Indian peppermint	10	-	130	103	-	30	-	Cam et al. (2019)
Sunflower seeds	10	-	130	30	-	30	1 g oil/ 20 mL water	Ravber et al. (2015)
Thymbra spicata	1.5	-	150	60	2	30	3.7	Ozel et al. (2003)
Aquilaria makaccensis	-	-	225	-	-	17	0.2 g oil/mL water	Samadi et al. (2020)
Piper betle	1.0	0.25-1	50-250	20	1-4	10	1.5-34.6	Musa et al. (2014)
Laurel	3.0	-	150	50	2	15	-	Fernández-Pérez et al. (2000)
Rosa damascena	1.5	-	150	60	2	30	0.2	Özel et al. (2006)
Coriander seeds	10	0.47	100	88	-	10	1	Zeković et al. (2016)
Coriander seeds	-	0.47	200	30	-	20	2.2	Pavlić et al. (2015)

2.6. Applications of extracted essential oils

2.6.1. Hydrogel

Hydrogel is an aggregate of water molecules and cross-linked polymer network as shown in Fig. 2.7. The cross-linked polymer networks enable hydrogels to be soft and elastic. The high-water content (> 95% by weight) of hydrogels makes hydrogels dissolve and transport ions and small molecules such as gelatin (Cheng et al., 2017) and chitosan (Qu et al., 2001).

Hydrogels can be natural or synthetic. Natural hydrogels are found in muscle and cartilage in animal tissues, and xylems and pholems in plants (Liu et al., 2021). There are a number of chemical methods used to synthesize hydrogels, such as polymerization, parallel cross-linking of multifunctional monomers, and using a cross-linking agent to promote polymers reaction (Ahmed, 2015).
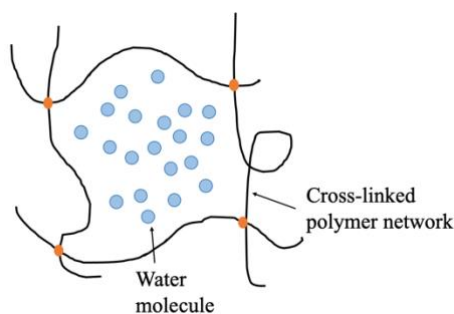
Fig. 2.7. Structure of hydrogel using polymers.

Due to the diversity of natural and synthetic hydrogels with different polymer topologies and chemical compositions, hydrogels can be applied in many fields. These applications include agriculture, where they ameliorate water availability and increase water-holding properties (Neethu et al., 2018); drug delivery systems (Li and Mooney, 2016); food science, where antibacterial compounds are incorporated into hydrogels (Li et al., 2021); tissue engineering, using

hydrogels as scaffolds for creating human-like collagen and carboxymethylated chitosan (Cao et al., 2020); and biosensors (Yang et al., 2021).

Li et al. (2014) developed (-)-menthol-based hydrogel with thixotropic property. In their experiment, menthol worked as a hydrogelator with L-lysine to form a stable and thixotropic hydrogel at a pH range of 1-12. This hydrogelator was used to further gelate antibacterial agents including Zn^{2+} aqueous solution and lincomycin hydrochloride. They found that the hydrogel loaded with Zn^{2+} showed better antimicrobial activity (with bigger bacteriostatic circles) to *Escherichia coli* than to that of the Zn^{2+} aqueous solution alone. Also, the hydrogel loaded with lincomycin hydrochloride had a better inhibition effect on the proliferation of *Staphylococcus epidermidis*. Jamshidi et al. (2020) developed a magnetic polyhydrogel based on acrylic acid-menthol deep eutectic solvent (as a function monomer), ammonium persulfate (as inhibitor), and acrylic acid-Fe_3O_4 nanoparticles (as cross-linker). This eutectic solvent based polymeric hydrogel was used to extract pesticides from contaminated water. The results showed that the use of this hydrogel significantly increased the extraction efficiency when compared with unpolymerized acrylic acid-menthol deep eutectic solvent, and recoveries were in the range of 61%-120%.

Addtionally, Jiang et al. (2022) prepared a cellulose-based hydrogel as a wound dressing. They used hydroxyethyl cellulose as a framework and epichlorohydrin as a cross-linking agent to form the hydrogel that was loaded with ZnO and cationic-β-cyclodextrin encapsulated menthol. ZnO nanoparticles and menthol provided analgesic and bactericidal effects, which are non-toxic to normal human cells.

Huerta et al. (2020) produced clove essential oil emulsion-filled cellulose nanofiber hydrogel by ultrasound with an entrapment efficiency of 33-34% with 0.5 wt% clove essential oil. They found that the increase of clove essential oil content caused the decrease of water retention value and

swelling capacity. The produced hydrogels with low viscosity and without cytotoxicity, as a result, could be a promising scaffold material for tissue engineering.

2.6.2. Encapsulation of essential oil with lipids

Essential oils have been studied for more than 60 years, and most have antioxidant, anti-inflammatory, antibacterial, wound-healing and anti-anxiety properties (Bakkali et al., 2008). However, the hydrophobicity, instability, high volatility, and toxicity risks of essential oils limit their utilization. One successful strategy to overcome these limitations is by using encapsulation as the delivery system, increasing the bioavailability and chemical stability of essential oils while reducing their volatility and toxicity. The most common delivery system is encapsulated essential oil in lipids such as blends of mono-, di- or tri-glycerides, fatty acids, and waxes (Cimino et al., 2021).

Earlier, Zhu et al. (2010) encapsulated menthol (the main component of peppermint essential oil) in beeswax by SC-CO_2 with an efficiency of 60%. They produced menthol/beeswax particles in the range of 2-50 μm using the modified particle from gas-saturated solution (PGSS) process. The results showed that the smaller particle size and narrower particle size distribution of the menthol/beeswax particles can be achieved by increasing the pressure (150 bar), decreasing the flow rate of the gas-saturated solution (0.11 mL/min) and decreasing the mass fraction of menthol (10%). They proved that menthol/beeswax particles protect menthol from its volatilization loss using the N_2-blowing method.

Later, Aredo et al. (2021) formed avocado oil or Brazil nut oil-loaded beeswax microparticles using PGSS particles from gas-saturated solutions. The particles were formed at the temperature of 60 °C and pressures of 150-300 bar with a sponge-like morphology and sizes of 162-180 μm and 96-128 μm for avocado oil and Brazil nut oil-loaded particles, respectively. The internal

37

physical structure observed by a confocal fluorescence microscope indicated that the oils were uniformly incorporated into the crystalline lattice of beeswax.

2.7 Impregnation of bioactives

2.7.1 Traditional impregnation processes

There are some traditional impregnation methods, which generally involve soaking or immersing a solid material in a solution containing the desired bioactive. For example, Pan and Tangratanavalee (2003) conducted impregnation of water in soybeans by soaking them at different temperatures (10, 20, 30, and 40 °C) for up to 8 h, resulting in a final moisture content of up to 120%. In this method, soybeans were submerged in water, and they absorbed water. However, soaking may not be suitable for impregnating certain materials with complex structures or compositions.

Vacuum impregnation is a useful technique for quickly introducing external liquids into the porous structures of animal and plant tissues (Zhao and Xie, 2004). For instance, Betoret et al. (2003) used vacuum impregnation to impregnate probiotics (*Saccharomyces cerevisiae* and *Lactobacillus casei*) into apples, achieving a content of 10^6 cfu/g.

In the case of pressure impregnation, the solid material is placed in a pressure chamber, and the substance to be impregnated is forced into the material under high pressure (~100-6000 bar). This method is often used for impregnating wood or porous materials (Lou et al., 2018). Vatankhah and Ramaswamy (2019) conducted the impregnation of ascorbic acid and chitosan into apple cubes, resulting in a yield of 250 mg/kg at 2000 bar.

Although these traditional impregnation methods have been used for various applications, they have limitations in terms of control, uniformity, and efficiency, leading to the development of more advanced and precise impregnation techniques in modern research.

2.7.2 SC-CO$_2$ assisted impregnation process

The SC-CO$_2$-assisted impregnation process is an effective approach for impregnating bioactives. Among various options, CO$_2$ is the preferred fluid because it is relatively chemically inert, not flammable, has no taste or odour, is inexpensive, and has a low critical pressure (73.8 bar) and temperature (31°C). In the supercritical state, bioactives have good solubility in CO$_2$, which allows it to dissolve numerous bioactive substances, and temporarily expand polymers. (Comin et al., 2012). In this process, three steps are distinguished, including dissolution, sorption and depressurization as presented in Fig. 2.8.
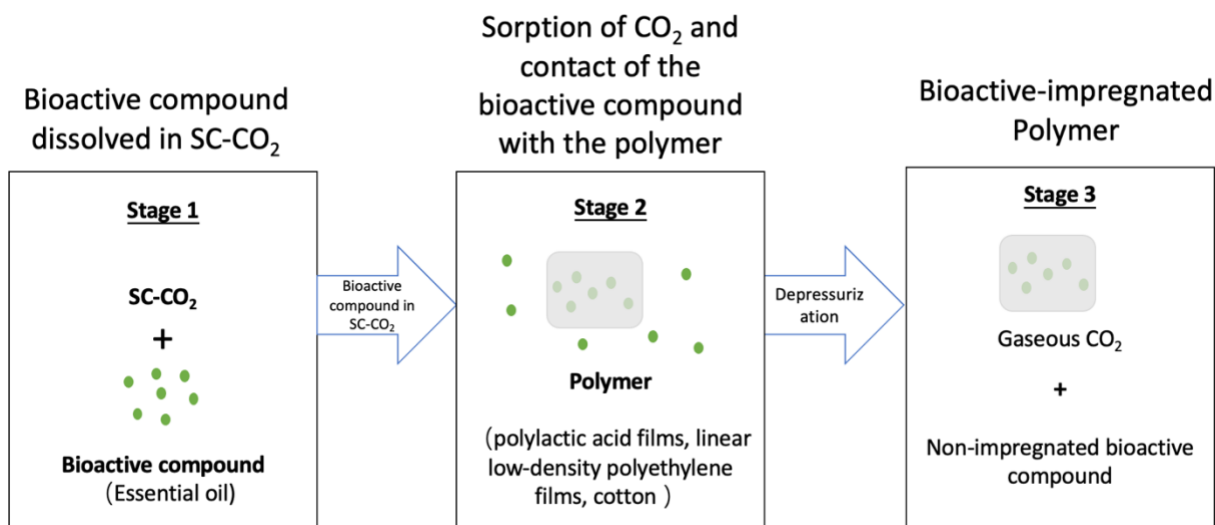
Fig. 2.8. Schematic representation of SC-CO$_2$-assisted impregnation process (Champeau et al., 2015 and Comin et al., 2012).

In the first stage, the ability of CO$_2$ to dissolve bioactives depends on their polarity and molecular weight, with nonpolar and low molecular weight solutes being more soluble than polar and high molecular weight solutes such as proteins, synthetic polymers (e.g. polyethylene), and polysaccharides. The solubility is influenced by temperature and pressure as discussed previously in the solubility section (p 12-18) (Saldana et al., 1999).

During the sorption stage, the CO_2 + bioactive solution comes into contact with the polymer, and the solution diffuses into the polymer matrix, leading to the impregnation of the bioactive into the polymer. The effectiveness of the diffusion is influenced by the operating conditions, which can impact the ability of CO_2 to swell the polymer.

In the third stage, depressurization allows CO_2 to transition from its supercritical state to a gaseous state, facilitating easy CO_2 removal from the system. As the pressure is reduced, the solubility of the bioactive in CO_2 decreases, causing it to precipitate to the bottom of the reactor or be carried out with CO_2. Then, the impregnated polymer is ready where there is no solvent remaining. By controlling the depressurization rate, the risk of foaming is minimized to maintain the structural integrity of the impregnated material (Champeau et al., 2015).

Table 2.9 summarized studies reporting the SC-CO_2-impregnation process of bioactives where the typical temperature range investigated was 35-55 °C, with pressures of 90-150 bar. However, certain studies have employed higher pressures ranging from 200 to 400 bar. The reported bioactive compound loading generally remained below 30%. The impregnated polymers were mainly biodegradable plastics such as polylactic acid films, linear low-density polyethylene films, polyethylene terephthalate, as well as polypropylene films, and pieces of cotton. The effectiveness of the impregnation process is commonly assessed using the partitioning coefficient, denoted as K (Champeau et al., 2015). This coefficient determines the relative affinity of the bioactive compound towards the polymeric phase and the CO_2 phase under specific pressure and temperature. The calculation of K value is performed using Equation 2.2:

$$K = \frac{C_{polymer}}{C_{CO_2}} \tag{2.2}$$

where, $C_{polymer}$ represents the concentration of the bioactive compound in the polymer phase (measured in grams of bioactive compound per gram of polymer), and C_{CO_2} represents the

concentration of the bioactive compound in the CO_2 phase (measured in grams of bioactive compound per gram of CO_2).

One of the main benefits of the supercritical CO_2 impregnation process is its ability to adjust bioactive compound loading by modifying operational conditions like pressure, temperature, depressurization rate and contact time. This ability is achieved through alterations in the solubility of the bioactive compound, CO_2 sorption in the matrix, and polymer swelling caused by pressure and temperature changes (Champeau et al., 2015; Comin et al., 2011).

The forthcoming sections discuss how these operational conditions (pressure, temperature, time, and depressurization rate) influence the loading of bioactive compounds and impregnation on the polymer.

Table 2.9. Impregnation of the bioactive compound on different polymers by SC-CO$_2$.

Material	Impregnated bioactive	P/B (g/g)	Process conditions				Impregnation yield (%)	Application	Reference
			P (bar)	T (°C)	DPR (bar/min)	Time (min)			
Food-related applications									
Polylactic acid films	R-carvone	2:1	98	60	6	150	30	Food packaging and preservation	Miranda-Villa et al. (2022)
Polypropylene, corona-modified polypropylene	Thymol	3:1 to 3:8.5	150	35	3.3	240	11	Antimicrobial textile	Markovic et al. (2015)
Linear low density polyethylene films	Eugenol	0.63 ± 0.05	150	45	5	240	6	Food Packaging	Goñi et al. (2016)
Polylactic acid with 5 wt% poly ε-caprolactone	Thymol and carvacrol	1:1	100	40	14	300	28	Food packaging	Lukic et al. (2020)
Polylactic acid/poly ε-caprolactone	Thymol	1:1	100	40	14	300	35.8	Food packaging	Milovanovic et al. (2018)
Pregelatinized corn starch	Flax oil	5:5	300	80	NR	480	6.6	Nutraceutical delivery	Comin et al. (2012)
Polylactic acid films	Thymol	8 pieces /1g	90	40	10	180	20.5	Food packaging	Torres et al. (2017)
Linear low density polyethylene films	Clove essential oil	NR	120 and 200	25, 35, 45	NR	0-240	4	Food packaging	Medeiros et al. (2017)
Polyethylene terephthalate/ polypropylene films	Olive leaf extract and caffeic acid	4:1	100-400	35, 55	1	1320	NR	Food Preservation	Bastante et al. (2017)

Table 2.9. Continued.

Material	Impregnated bioactive	P/B (g/g)	Process conditions				Impregnation yield (%)	Application	Reference
			P (bar)	T (°C)	DPR (bar/min)	Time (min)			
Food-related applications									
Silica and alginate aerogels	Phytol	NR	2000	40	2	1440	30.1	NR	Mustapa et al. (2016)
Cellulose acetate films	Thymol	1:5	100	35	NR	120, 300, 1680, 1920	63.8	Food packaging	Milovanovic et al. (2016)
Starch microspheres	Oregano essential oil	2.5, 1.3, 1, 0.7, 0.3	80-150	40-50	0.83-1.1	180, 360, 1440	NR	Health-promoting ingredient	Almeida et al. (2013)
Modified starch powder	Lavandin oil	1:1	100, 110, 120	40-50	0.7-1.5	120	15	NR	Varona et al. (2011)
Alginate aerogel spheres	Vitamin D3	NR	80	5, 15, 25, 35	NR	60 to 1440	12	NR	Pantić et al. (2016)
Other applications									
Cotton fabric	Ag	10 mg Ag	210	40	-	600-900	-	Antifungal textiles	Gittard et al. (2010)
Cotton gauze	Thymol	0.65 ± 0.05	155	35	3.3	1440	19.6	Wound dressing	Milovanovic et al. (2013)
Cotton gauze	Thyme extract	1:20.6	150	35	6.5	600	9	Wound dressing	Ivanović et al. (2014)

DPR: depressurization rate, NR: not reported, P: pressure, P/B: polymer/bioactive, T: temperature.

2.7.2. Effect of the processing parameters on the bioactive compound loading for impregnation

2.7.2.1. Effect of pressure

The effect of pressure on the impregnation process depends on the properties of the bioactive compound and the impregnated polymer. However, in the majority of cases, raising the pressure under isothermal conditions results in a higher impregnation yield due to the increase in the solubility of the bioactive compound, the CO_2 sorption, and the swelling of the polymer (Cortesi et al., 2000).

Comin et al. (2012) reported that the incorporation of flax oil in β-glucan aerogels increased when the pressure was raised from 80 to 150 bar under isothermal conditions (40 °C) as a result of the significant rise in the solubility of flax oil from 1.50 to 6.91 g/L.

According to Milovanovic et al. (2013), the incorporation of thymol in cellulose acetate films, increased when the pressure was raised from 100 to 150 bar. However, further increasing the pressure to 200 bar did not significantly affect the impregnation yield, as the cellulose acetate film reached its maximum loading capacity at 150 bar after 24 h. This phenomenon was similarly observed and reported by Torres et al. (2017). When the pressure was increased from 90 to 120 bar under a constant depressurization rate (10 bar/min) and temperature (40 °C), there was no significant increase in the impregnation yield. Therefore, once the polymer has reached its saturation point, raising the pressure does not lead to any further increase in the bioactive compound loading on the polymer.

In addition, the phenomenon of decreased bioactive loading with increasing pressure has also been observed by Varona et al. (2011), who reported this negative effect for the incorporation of lavandin into a starch-based material with a pressure increase from 100 to 120 bar. As the pressure increased, CO_2 exhibited greater solubility in the starch-based material and the material

experienced the increased swelling effect, leading to a weakening of the interactions between the material and the bioactive compound. At the same time, higher pressure results in increased density and solvent power of SC-CO_2, leading to stronger interactions between SC-CO_2 and lavandin, ultimately resulting in lower impregnation yields. Earlier, Almeida et al. (2013) also found a reduction in the incorporation of oregano essential oil into a starch-based material as the pressure exceeded 100 bar. This behaviour was justified by two factors: i) as the pressure increases from 100 bar to 150 bar, the density of CO_2 rises and the mass fraction of CO_2 increases. Consequently, the components of the essential oil become more diluted in the CO_2, leading to lower impregnation yields, and ii) other contributing factor is the extent of polymer swelling and the balance of interactions between CO_2, starch, and essential oil (Almeida et al., 2013). Therefore, operating impregnation at low pressure (< 100 bar) is expected to enhance the distribution of the bioactive compound in favour of the polymer phase.

2.7.2.2. Effect of temperature

Temperature is a significant variable that can influence the impregnation of bioactive compounds into a polymer structure during the SC-CO_2 assisted impregnation process. The loading of bioactive compounds has been observed to exhibit different behaviours, such as increasing, decreasing, remaining constant, or initially decreasing and then increasing, as temperature varies under isobaric conditions.

The positive effect of temperature on impregnation yield has been reported by several authors. According to Varona et al. (2011), increasing the temperature from 40 to 50 °C while maintaining pressure values between 100 and 120 bar resulted in a higher incorporation of lavandin essential oil in the modified starch powder by *n*-octenil succinate group. A similar effect was also reported by Almeida et al. (2013), when raising the temperature from 40 to 50 °C at 100 bar led to greater

incorporation of oregano essential oil into a starch-based material, resulting in higher antioxidant activity. As temperature increases under isobaric conditions, several effects occurred in the SC-CO_2-assisted impregnation process. First, the solubility of the bioactive compound in the CO_2 phase decreases, reducing the affinity between the bioactive compound and CO_2. This decrease in affinity is beneficial for the incorporation of the bioactive compound in the polymer structure; otherwise, the bioactive compound would be removed along with the CO_2 (Duarte et al., 2009). Additionally, with an increase in temperature, the density of CO_2 decreases, resulting in a decrease in the CO_2 mass fraction. As a result, the bioactive compound becomes more concentrated in the CO_2 phase. Moreover, the increase in temperature can induce changes in the structural properties of the polymer, impacting its transport characteristics. When the temperature is over the glass transition temperature, the polymer's chain mobility improves, facilitating better diffusion of SC-CO_2 and the bioactive compound. The increased mobility also enabled greater sorption of CO_2 in the polymer and enhanced polymer swelling (Rojas et al., 2022). However, Comin et al. (2012) observed the highest impregnation of lipids occurred at the lowest temperature (40 °C) and pressure (150 bar) conditions. Interestingly, when the temperature was increased to 80 °C, the impregnation of lipids decreased due to temperature's influence on vapour pressure under isobaric conditions.

Another effect of temperature was reported by Yu et al. (2011). When the operating pressure was 120 bar, the relationship between roxithromycin loading and impregnation temperature became intricate. It exhibited an increasing trend from 40 to 50 °C, but a decreasing trend from 50 to 70 °C. The reason was that the crossover pressure of the roxithromycin corresponded to 120 bar. They also found that when pressures surpassed the crossover pressure increasing the temperature under

isobaric conditions had a positive effect on impregnation yield, conversely, if pressures were below the crossover point, raising the temperature led to a decrease in impregnation yield.

2.7.2.3. Effect of depressurization rate

The depressurization step is the final stage in the SC-CO$_2$-assisted impregnation process, which involves the reduction of pressure in the system. The rate of depressurization plays a significant role in enhancing the physical-chemical interactions between the polymer and bioactive compound. Typically, depressurization rates range from 1 to 10 bar/min as shown in Table 2.9, which can enhance the strength of physical-chemical interactions between the polymer and the bioactive compound, ultimately affecting the impregnation yield (Rojas et al., 2019).

Torres et al. (2017) found that employing low depressurization rates of 1 and 10 bar/min resulted in high impregnation yields of 18% and 20%, respectively. However, when a higher depressurization rate of 100 bar/min was used, the impregnation yield significantly decreased to approximately 14%. Similarly, Goñi et al. (2016) observed that a slow depressurization rate of 5 bar/min led to a higher impregnation yield of 5.7% of eugenol on linear low-density polyethylene, while a depressurization rate of 50 bar/min resulted in a significantly lower impregnation yield of only 1.3%. Under these conditions, the use of a slow depressurization rate had a positive effect on the impregnation process due to the strong polymer/bioactive compound interactions, then, it was recommended to establish a slow depressurization rate that can facilitate the absorption or deposition of the bioactive compound into the polymer (Rojas et al., 2019).

Conversely, if the bioactive compound exhibits low affinity for the polymer, it can be readily released with CO$_2$ from the polymer matrix. In such cases, a high depressurization rate promotes the entrapment within the polymer. According to Bastante et al. (2017), the depressurization rate of 100 bar/min was the best condition for the impregnation of caffeic acid on polyethylene

terephthalate/ polypropylene films. Similarly, de Souza et al. (2014) observed the decrease on the impregnation yield (0.13-0.10%) of cinnamaldehyde in cassava starch biocomposite films with the depressurization rate increasing from 1 to 10 bar/min at 150 bar and 35 °C.

2.7.2.4. Effect of impregnation time

The SC-CO$_2$-assisted impregnation process of bioactive compounds in polymers is governed by both thermodynamics and kinetics. The kinetics of mass transfer in SC-CO$_2$-assisted impregnation mainly depends on the diffusion of the bioactive compound into the polymer matrix. The diffusion is much faster in SC-CO$_2$ impregnation compared to traditional soaking techniques due to the "molecular lubricant" effect of SC-CO$_2$, which arises from the fluid-like behaviour of SC-CO$_2$ even at low viscosities (Champeau et al., 2015; Kazarian et al., 1997). SC-CO$_2$ has dual effects in the impregnation process. First, it causes the physical alterations occurring in the amorphous and crystalline structures of the polymer matrix like the swelling and plasticization effect and enhances its free volume, in which the temperature and pressure play significant roles in this process. Secondly, SC-CO$_2$ acts as a solvent for the bioactive compound, promoting its solvation and facilitating its diffusion into the polymer matrix (Ngo et al., 2003). According to Comin et al. (2012), the incorporation of flax oil into pregelatinized corn starch increased over time under static conditions. They used a CO$_2$-phase saturated with flax oil at 150 bar and 40 °C, and the equilibrium condition was reached within 4 h of residence time.

2.7.3. Application of the SC-CO$_2$ assisted impregnation process

The SC-CO$_2$ impregnation process can be applied in both food and biomedical fields. For food-related applications, the SC-CO$_2$ impregnation process has been employed to create sustained release materials. The first objective is to produce active food packaging materials, while the second is to impregnate food-grade substances with nutraceuticals. Recently, Alvarado et al. (2018)

developed poly lactic acid (PLA) films with poly(vinyl alcohol) (PV) nanofibers/cellulose nanocrystals (CNC) and impregnated them with thymol using SC-CO_2. The resulting nanocomposite material showed improved mechanical and thermal properties, and the release rate of thymol was significantly slower compared to nanofiber-free PLA. Also, Ubeyitogullari and Ciftci (2017) used SC-CO_2 to impregnate phytosterols into nanoporous starch aerogels. The optimized conditions (90 °C and 450 bar) resulted in a high impregnation capacity of 99 mg phytosterol/g nanoporous starch aerogels and the formation of phytosterol nanoparticles (59 to 87 nm) with reduced crystallinity. The method improved the bioaccessibility and water solubility of the phytosterols, making it a promising approach for generating food-grade phytosterol nanoparticles.

For the biomedical field application, Dias et al. (2013) loaded N-carboxybutyl chitosan, collagen/cellulose, and hyaluronic acid-based polymeric matrices/dressings with an extract from jucá (*Libidibia ferrea*) to develop wound dressings with anti-inflammatory activity. The impregnation yield of the extract depended on the dressing material, with N-carboxybutyl chitosan showing the highest loading (approx. 50%). The extract-loaded dressings demonstrated cytocompatibility, reduced expression of pro-inflammatory cytokines, and exhibited suitable water vapour and oxygen permeability for managing different types of wounds at various healing stages. Kazarian and Martirosyan (2002) used SC-CO_2 to impregnate ibuprofen into poly(vinylpyrrolidone) (PVP) films with the employment of in situ ATR-IR spectroscopy to examine the process. They observed molecular dispersion of ibuprofen within the PVP matrix, with interactions occurring between ibuprofen and PVP's C-O groups. Furthermore, the presence of ibuprofen influenced both the interactions with CO_2 and the sorption of water in PVP. Overall, the impregnation of bioactives on polymers is still in its infancy and more studies are required.

2.8. Sensory evaluation of essential oils

Essential oils are well-known for their characteristic aroma, which play a crucial role in their use in various applications such as perfumery, aromatherapy, and flavouring. Sensory evaluation can be used as a quality control tool to determine the overall sensory quality of essential oils. Trained sensory panelists can detect any off-notes, deviations, or sensory defects that may impact the essential oil's quality, purity, and authenticity. This information is valuable for ensuring that only high-quality essential oils reach the market. Table 2.10 presents various studies exploring the application of essential oils as flavoring agents in different food products, along with their respective concentrations and sensory evaluation results.

Recently, Zhao et al. (2023) investigated the aroma profile of *Litsea cubeba* essential oil by five different attributes, which were lemon, fresh, woody, floral, and camphor. Each attribute was evaluated with a 10-point interval scale at room temperature with an environment at 65% relative humidity. The results showed that all kinds of *Litsea cubeba* essential oil had strong lemon flavor. In addition, Chen et al. (2022) investigated the odor perceptions of nine essential oils, including ester-alcohol type and terpene type under three concentrations. They investigated five attributes, which were pleasantness, familiarity, subjective intensity, emotional arousal and emotional perception with a scale from -10 to 10 levels. The research revealed that the chemical composition of odours played a crucial role in influencing how they were perceived, and terpene-type oil evoked stronger arousal and emotional responses compared to ester-alcohol type. Participants from the southern Yangtze river region were more familiar with the odors tested. The individual's fragrance usage habits had a notable impact on the perceived intensity and emotional response to certain odors. However, gender did not show significant differences in most of the odor perceptions.

Table 2.10. Selected studies on sensory properties of essential oil incorporated products.

Essential oil	Product	Concentration of essential oil in the product	Sensory evaluation attribute	Results	Ref.
Spearmint	White cheese	0.5, 0.75, 1.0, 1.5, 2.0, 2.5 mL/kg	Apperance and color, body and texture, odor, taste, overall acceptability	EO of 0.5 mL/kg had the highest total acceptability scores.	Foda et al. (2010)
Oregano and rosemary	Cream cheese	0.2 g EO/100 g fresh cream cheese	Colour, rancid, fermented flour, cream cheese typical flavour, sweetness, saltiness, bitterness, sourness	EO loaded cheese prevented the lipid oxidation and fermentation.	Olmedo et al. (2013)
Lemon	Salted sardines	Lemon EO micro-emulsion at 0.3 and 1.0% (v/v)	Texture (compactness, juicy and gummy), odour (salt sardines) and flavours (ham taste, rancid and putrid)	EO increased the overall acceptability.	Alfonzo et al. (2017)
Cinnamon	Milk chocolate bar	0.1, 0.3, 0.5%	Color, aroma, taste, appearance, overall	Cinnamon EO (0.1%) had the highest level of acceptance	Ilmi et al. (2017)
Pomegranate	Sunflower oil	200, 400, 800 ppm	Flavor, taste, appearance, over acceptability	Sunflower oil flavoured by pomegranate EO (800 ppm) showed better acceptability.	Wang et al. (2019)
Oregano	Chitosan films	0, 45, 90 ppm	Overall good, appearance, aroma, flavour, texture, aftertaste	EO (45 ppm) was acceptable.	Chi et al. (2006)

EO: essential oil, Ref: References.

By understanding the sensory characteristics of different essential oils, product developers can select the most appropriate oils to achieve desired sensory attributes in products such as perfumes, cosmetics, and food flavourings. Also, sensory evaluation helps in understanding consumer preferences and acceptability of essential oils. By conducting sensory tests with a diverse group of

consumers, manufacturers can gain insights into aroma preferences and sensory experiences of potential customers. This information can guide marketing strategies, product positioning, and formulation adjustments to meet consumer expectations (Kemp et al., 2009).

2.9. Conclusions

The literature review has examined the chemical composition of peppermint essential oil, specifically focusing on menthol and menthone. These compounds are well-recognized for their distinct biological activities (antioxidant, antibacterial, antifungal, and anti-inflammatory). Furthermore, this review has discussed various extraction techniques, including conventional and SC-CO_2 extraction methods. The merits of SC-CO_2 extraction, such as its selectivity and minimal environmental impact, provide valuable insights into the research undertaken in Chapter 3, which focused on the extraction of essential oil from *Mentha × piperita*. Additionally, this review has described methods for measuring solubility, laying the groundwork for the investigation into menthol impregnation onto cotton gauze in Chapter 4. In summary, this literature review has provided a comprehensive context for the research presented in Chapters 3 and 4, emphasizing their significance within the broader domain of essential oil research and the application of SC-CO_2 in this field.

Chapter 3: Supercritical CO_2 + co-solvent extraction of essential oil from *Mentha × piperita*

3.1. Introduction

Mentha × piperita, commonly known as peppermint, is a perennial herb that belongs to the Lamiaceae family. Its essential oil is a colourless or pale-yellow oil with a strong, penetrating odour of peppermint, a pungent taste and the sensation of coldness when air flows into the mouth (Nair, 2001). Due to its medicinal and aromatic properties, it is a valuable ingredient in the food, pharmaceutical, and cosmetic industries.

More than 30 compounds are identified in peppermint essential oil, but menthol (35-60%) and menthone (15-30%) are the two main components (Nair, 2001). Menthol is a cyclic monoterpene with four pairs of optical isomers: (−)- and (+)-menthol, (−)- and (+)-isomenthol, (−)- and (+)-neomenthol, and (−)- and (+)-isoneomenthol, in which (−)- menthol is the most common isomer existing in nature (Eccles, 1994). Menthol is one of the most important flavouring additives (4 mg/kg body weight), as it possesses analgesic, antifungal, antibacterial, antipruritic, anti-inflammatory, antiviral and fumigant activities (Kamatou et al., 2013; Government of Canada, 2023). Menthone is recognized for its antibacterial, antioxidant, anti-inflammatory, and antiviral properties (Chen et al., 2022).

The conventional methods of extracting essential oils from peppermint are organic solvent extraction, hydrodistillation, steam distillation and Soxhlet extraction. However, they take a long time (~10 h) and involve the use of organic solvents such as ethanol, benzene, and hexane which are associated with environmental pollution and health hazards. Also, these conventional methods are sometimes not suitable for valuable thermolabile compound extraction, as they could lead to a

reduction or loss of product (De Castro et al., 1999). For example, Ibrahim et al. (2021) investigated the extraction of the essential oil of *Mentha × piperita* by steam distillation. The optimum yield (1.36%) was obtained at 80°C, for 9 h, where menthol only accounted for 3.54%. On the other hand, carbon dioxide has a low critical temperature (31°C) and pressure (72.8 bar), and is non-toxic, non-flammable, available in high purity with low cost, and easily removed from the extract. Therefore, supercritical carbon dioxide (SC-CO$_2$) extraction is an eco-friendly and efficient method that has gained significant attention for the extraction of essential oils from various natural sources (Díaz-Reinoso et al., 2006) such as clove leaves (Frohlich et al., 2019), *Eucalyptus globulus L.* (Singh et al., 2016)*, Pistacia lentiscus* L. (Aydi et al., 2020), and *Cymbopogon citronella* leaves (Wu et al., 2019). However, to enhance the solubility of the essential oil and improve its extraction efficiency, co-solvents such as ethanol, methanol, and acetone are often added to the SC-CO$_2$ to modify the selectivity and polarity of the SC-CO$_2$.

Earlier, the use of SC-CO$_2$ extraction of essential oil from *Mentha × piperita* has been reported (Barton et al., 1992; Goto et al., 1993; Reverchon et al., 1994; Roy et al., 1996). Barton et al. (1992) extracted essential oil from peppermint at 24-43 °C and 60-180 bar with an extraction time of 4-9 h with yields of 0.9% - 2.5%. The best yield (2.5%) was achieved at 110 bar and 33°C. Goto et al. (1993) extracted at a higher temperature of 40 - 80 °C and 88 - 196 bar and found that the quantity of extracted menthol (the main component of peppermint essential oil) was smaller than the solubility of menthol. Also, they used ethanol as a co-solvent to assist the SC-CO$_2$ extraction, where 2 wt% ethanol increased the extraction of menthol threefold. Reverchon et al. (1994) performed GC-MS to analyze the composition of peppermint essential oil obtained through SC-CO$_2$ extraction as a qualitative aroma test. They found that the essential oil exhibited a better-resembled fragrance, with higher percentages of the main aroma compounds, at the extraction

conditions of 50 °C and 90 bar. The extracted essential oil contained the highest contents of menthol (25.4%) and menthone (45.0%). Roy et al. (1996) extracted essential oil and cuticular waxes, such as n-hentriacontane, n-tritriacontane, and n-nonacosane, from peppermint at 40 °C and 100-300 bar. The highest yield of essential oil obtained was 3.4%, while the yield of cuticular waxes ranged from 0.7% to 1.4%, with an increase in pressure from 100 to 300 bar.

Several previous studies have reported the scale-up of SC-CO_2 extraction, with the criteria of maintaining geometric, physical, and chemical relationships unchanged intentionally. In this study, the ratio between the mass of CO_2 used and the peppermint loading was intentionally kept constant. There are some studies that used the same criteria to scale up. For instance, Prado et al. (2011) successfully scaled up the extraction of clove and sugarcane residue from 290 mL to 5.15 L of the extraction vessel while maintaining a constant solvent mass-to-feed mass ratio of 15. The pilot scale yields were slightly higher compared to the laboratory scale, with a 20% increase for clove and a 15% increase for sugarcane residue. Similarly, Albuquerque and Meireles (2012) maintained a constant ratio of 35 for the SC-CO_2 extraction of oils from annatto seeds, resulting in a yield of 2.2%.

Therefore, there are a few aspects that were not extensively explored including the use of co-solvents (ethanol, acetone, isopropyl acetate), the influence of co-solvents and CO_2 flow rate on yield and menthol and menthone contents, and the scale-up of the essential oil extraction. These gaps in knowledge provide opportunities for further investigation and evaluation of the SC-CO_2 extraction process for peppermint essential oil.

This study aims to investigate the impact of different process parameters (pressure, temperature, time, CO_2 flow rate, co-solvent) on the extraction yield and the quality of essential oil extracted from *Mentha × piperita* using SC-CO_2 with or without co-solvents (ethanol, acetone, isopropyl

acetate). Additionally, the scale-up essential oil extraction was investigated to assess the feasibility of upscaling the extraction process. Furthermore, the antioxidant property of essential oils was evaluated. The results of this study can provide insights into the optimal conditions for the extraction of essential oil from peppermint using green SC-CO$_2$ technology and its potential to scale-up envisioning industrial applications.

3.2. Materials and Methods

3.2.1. Plant material

The dried peppermint used in this study was supplied by *Aratinga Inc* (Calgary, AB, Canada). The leaves and stalks of the peppermint were separated, and the leaves were then finely ground into a powder using a centrifugal grinding mill (ZM 200, Retsch, Inc., Newtown, PA, USA) equipped with a screen aperture size of 0.5 mm. The ground sample was placed in a plastic container and stored at 4 °C in the refrigerator.

3.2.2. Reagents

All reagents used in this experiment were purchased from commercial suppliers: carbon dioxide (Bone Dry UN1013, Linde, Edmonton, AB, Canada), ethanol (100%), acetone (Sigma-Aldrich, 270725, HPLC grade, ≥ 99.9%), isopropyl acetate (Sigma-Aldrich, 537462, ≥ 99.6%), menthol (Sigma-Aldrich, 15785, analytical specification), menthone (Sigma-Aldrich, 218235, 90%), dichloromethane (Sigma-Aldrich, 650463, ≥ 99.9%), methanol (Fisher Scientific, 164474, ACS specification), 2,2-diphenyl-1-picrylhydrazyl (Sigma-Aldrich, D9132), sodium acetate (Fisher Scientific, 127-09-3, ≥ 99.0%), iron (III) chloride (Sigma-Aldrich, 157740, 97%), 2,4,6-tri(2-pyridyl)-s-triazine (Sigma-Aldrich, T1253, ≥ 98%), hydrochloric acid (Fisher Scientific, A481-212), and acetic acid (ACP chemicals, 64-19-7).

3.2.3. Supercritical CO₂ + co-solvent extraction of essential oil

Fig. 3.1 shows a schematic of the laboratory apparatus used for the extraction of essential oil from peppermint leaves. This system was previously used by Mekala et al. (2022), and mainly consists of a CO_2 cylinder, an ISCO pump, an HPLC pump, a 25 mL high-pressure vessel, a preheater, a temperature controller, an essential oil collection vial, a gas flow meter, and valves.
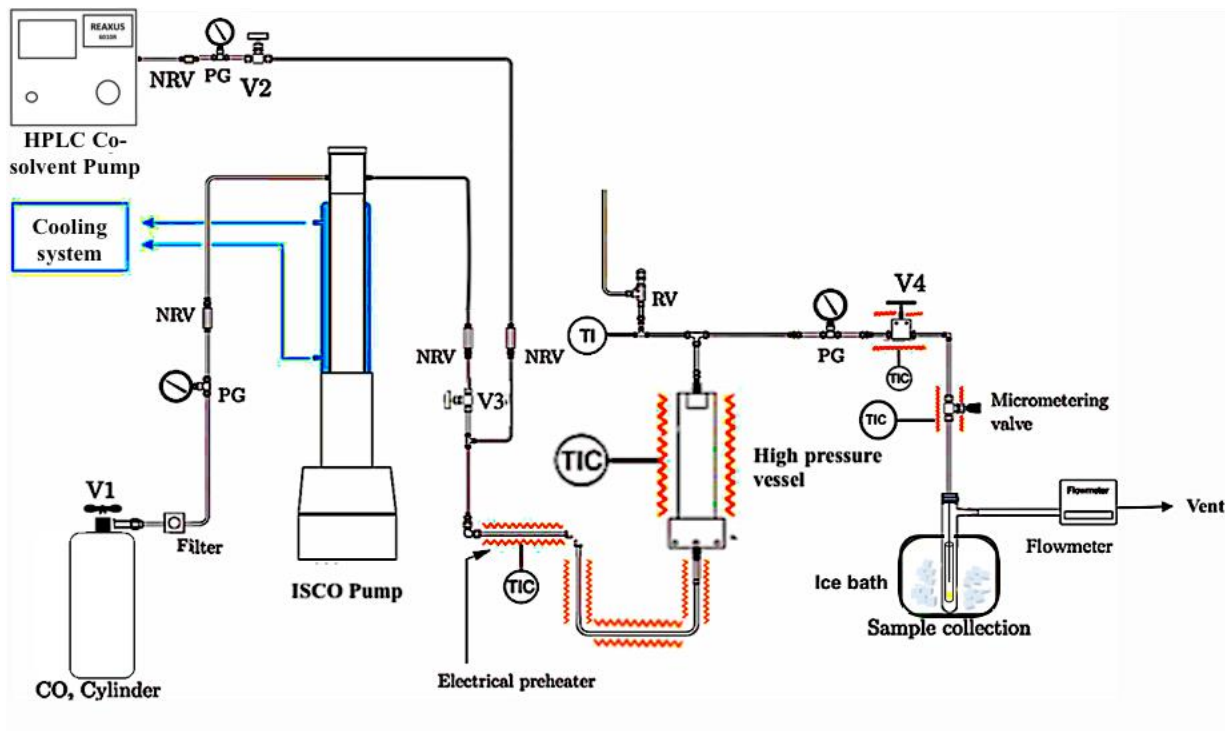
Fig. 3.1. Supercritical CO_2 laboratory extraction system 1 operating at a CO_2 flow rate of 0.5 mL/min. PG: pressure gauge, V1-4: valves, TI: temperature indicator, TIC: temperature indicator controller, NRV: one-way valve, and RV: relief valve.

A similar extraction procedure reported by Saldaña et al. (1999) was followed to perform the experiment for extracting essential oil from peppermint leaves powder. First, 4.5g of peppermint powder was weighed and placed into a basket with filters on the bottom and top. Then, the basket was loaded inside the high-pressure vessel. After that, the vessel was connected to the system with high-pressure tubing. The high-pressure vessel was also connected to a temperature controller to ensure that the desired temperature was achieved and maintained constant. The pressure in the

system was monitored by a pressure gauge. A needle valve and a flow meter were used to warrant the precise flow rate of CO_2.

By opening the valve V1, high-purity CO_2 passed through a filter and a cooling system (S&A CW-5200, Guangzhou, China) and then was fed to the high-pressure system using the syringe ISCO pump (Model 260D, Lincoln, NE, USA). The pressure was set constant in the ISCO pump. By opening valve V3, carbon dioxide was pumped into the 25 mL stainless-steel high-pressure vessel. Once the desired pressure and temperature were reached, the on/off valve V4 and needle valve, were opened. The essential oil was collected in a glass vial immersed in an ice bath and carbon dioxide was vented after flowing through the flow meter (Alicat M250SLPM, Tucson, USA). The extraction experiment was carried out for 2.5 h.

For the use of a co-solvent, liquid ethanol, acetone or isopropyl acetate inside a glass HPLC bottle was placed on the balance to know exactly how much co-solvent was used in each experiment. Then, the co-solvent was delivered into the high-pressure system by an HPLC pump that introduced the liquid co-solvent at a constant flow rate. Once the desired pressure was reached, valve V2 was opened and the carbon dioxide and the co-solvent at the same pressure were mixed before entering the high-pressure vessel to extract the essential oil from peppermint powder. Once pressure and temperature were constant, the on/off valve V4 and needle valve at the exit line were opened. The essential oil and solvent were collected for up to 180 min in a glass vial, which was placed in an ice bath. All extractions were performed at least in duplicate. After the extraction time, for the depressurization process, the pump was stopped, and the gas cylinder was closed. The collection vial was removed and replaced with a pre-weighed new vial. Valve V4 was slowly opened, along with the micrometering valve, until all the CO_2 in the system was released and the pressure gauge returned to zero.

To warrant that no essential oil and solvent remained in the tubing, the line was cleaned with the co-solvent used to recover all extracted essential oil. After that carbon dioxide was used to dry the system for 10 min before starting to load the high-pressure vessel for the next experiment.

As co-solvent together with the essential oil was collected in the glass vial, the solvent was removed using a gentle flow of nitrogen gas to avoid the loss of any essential oil under the fume hood.

The yield of extraction was calculated by the mass of extracted essential oil and the mass of total peppermint powder loaded in the high-pressure vessel using Equation 3.1.

$$Yield\ (\%) = \left(\frac{Extracted\ essential\ oil\ (g)}{Total\ feed\ (g)}\right) \times 100 \tag{3.1}$$

Table 3.1 shows the processing parameters, such as extraction time, pressure, temperature, use of co-solvent, and CO_2 flow rate evaluated in this study for the extraction of essential oil.

Table 3.1. Process parameter range for the SC-CO_2 extraction of peppermint essential oil.

No.	Parameter	Unit	Range
1	Pressure	bar	100-400
2	Temperature	°C	45-55
3	Extraction Time	min	15-180
4	Co-solvent (ethanol, acetone, or isopropyl acetate)	mol%	3
5	Flow rate	mL/min	0.5-3

The extraction kinetic of essential oil in SC-CO_2 was investigated by collecting and weighing extracted essential oil at first 15 min and after that every 30 min up to 180 min. The pressure and temperature conditions affect the solubility of the essential oil in SC-CO_2. The pressure and temperature must be carefully optimized to ensure that the target compound is adequately extracted while minimizing the degradation of heat-sensitive compounds. A series of experiments were

performed to optimize these two parameters. The use of co-solvent (ethanol, acetone, isopropyl

acetate) at a constant concentration of 3 mol% was also evaluated.

For the evaluation of the high CO_2 flow rates, another SC-CO_2 system set-up was used as shown

in Fig. 3.2.
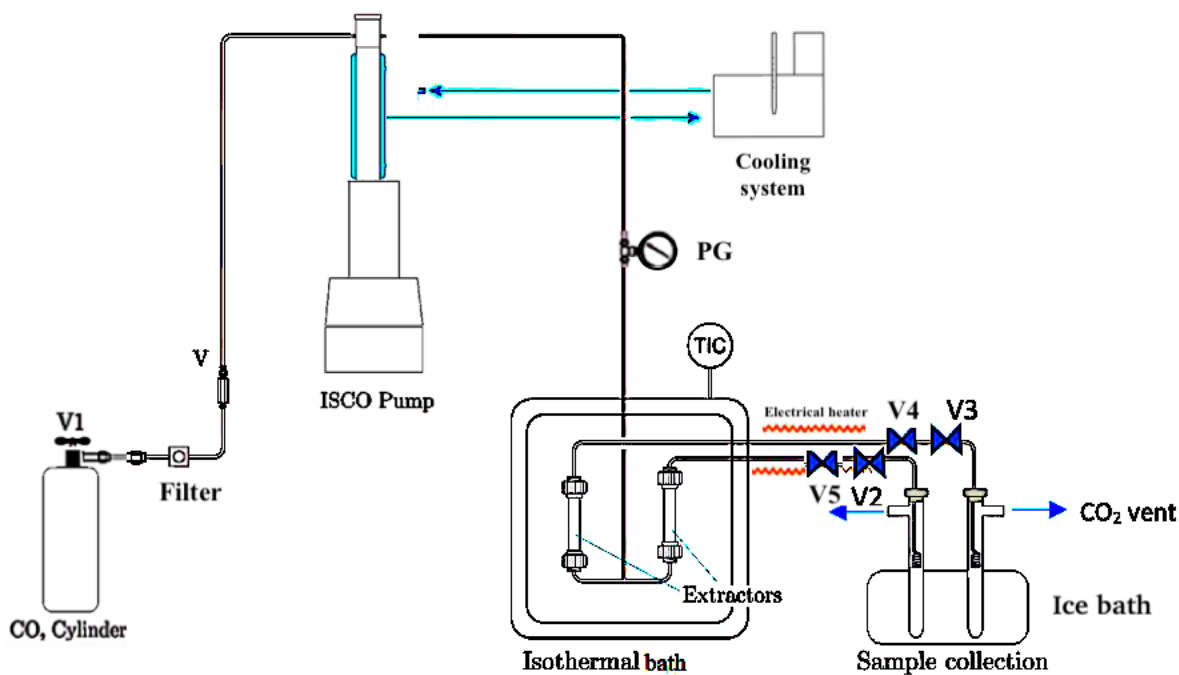
Fig. 3.2. SC-CO_2 laboratory extraction system 2 operating at a high CO_2 flow rate (3 mL/min). V: check valve, V1: cylinder valve, V2 and V3: micro metering valves, V4 and V5: on/off valve, and TIC: temperature indicator controller.

This SC-CO_2 laboratory extraction system (ISCO SFX 220, Lincoln, NE, USA) operates at a

higher CO_2 flow rate (3-10 mL/min). First, 3g of peppermint powder were accurately weighed and

placed inside an extraction cell equipped with filters at the top and bottom. The loaded cell was

then placed into the extraction chamber. The temperature inside the chamber was lowered to below

0 °C using a cooler, and the one-way valve between the CO_2 tank and extraction chamber was

opened. The operating temperature of the extractor, the desired extraction pressure and time were

then set. Once the desired temperature and pressure conditions were achieved, the extraction process started. The essential oil was collected in a glass vial immersed in an ice bath and carbon dioxide was vented.

The extraction experiment was carried out for 120 min. All extractions were performed at least in duplicate. During the depressurization process, the pump was stopped, and the gas cylinder was closed. The collection vial was exchanged with a pre-weighed new vial. Valves V2 to V5 were gradually opened, allowing the release of all the CO_2 from the system until the pressure gauge indicated zero. The extracts were measured gravimetrically using a balance with an accuracy of ± 0.0001 g. The extracts were stored at 4 °C for further analysis.

3.2.4. Scale-up of SC-CO_2 extraction of essential oil

Scale-up experiments were performed using a Newport Scientific, Inc. apparatus (Jessup, Md, USA) equipped with a 300 mL extraction vessel and a 50 mL basket, as depicted in Fig. 3.3.

For each experiment, 9, 15, or 30 g of peppermint powder was loaded into the 50 mL basket, which was then placed inside the 300 mL extraction cell. The procedure used was similar to the reported method by Saldaña et al. (2006). The carbon dioxide used in the experiments had a purity of 99.95% (Bone Dry UN1013, Linde, Edmonton, AB, Canada) that was pressurized using a diaphragm compressor. The pressure was regulated with a back-pressure regulator, maintaining a ± 10 bar tolerance. The extraction vessel was heated using a heating jacket, and the temperature was controlled with a thermostat, ensuring a ± 1 °C accuracy.

The CO_2 flow rate, measured at ambient conditions, was approximately 1.5 L/min and controlled by a heated micro-metering valve. A glass collection vial was connected to the micrometering valve and placed in a refrigerated bath at -20 °C. After each experiment, all tubings in the system

were thoroughly cleaned with ethanol. Sample weights were determined gravimetrically, and the collected samples were stored at 4 °C for further analysis with GC.

The scale-up criterion involved maintaining a constant ratio of solvent mass to feed mass. The same ratio for peppermint essential oil extracted at laboratory scale was used as a reference where the optimal operational conditions were 110 bar and 50 °C. The solvent flow rate was calculated using this scale-up criterion so that the mass of CO_2/mass of feed was ~ 78 which was maintained. The experimental design with all runs is presented in Table 3.4.
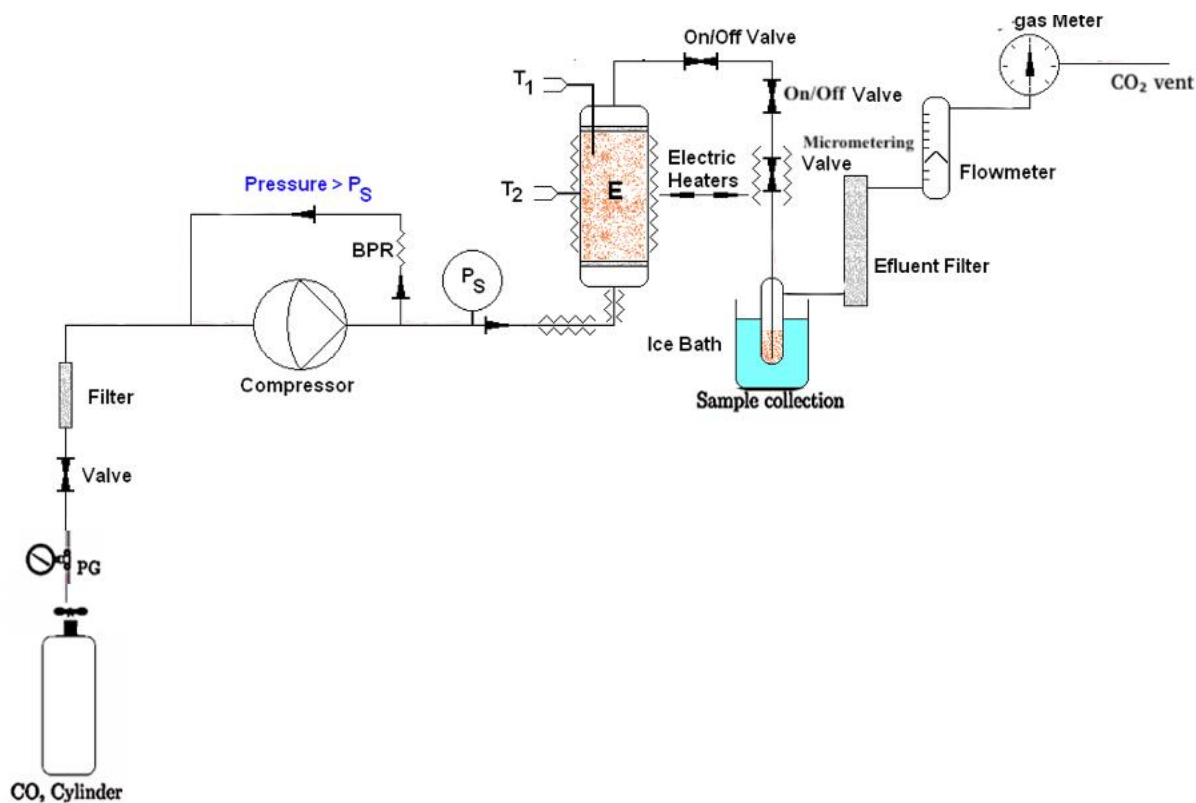
Fig. 3.3. SC-CO_2 scale-up extraction system. BPR: back pressure regulator, PG: tank pressure, PS: system pressure, T1: extractor temperature, T2: heating sensor, E: extractor and basket inside, PE: extractor pressure.

3.2.5. Characterization of extracts by gas chromatography

A gas chromatograph (Varian 430GC, Walnut Creek, CA, USA) was connected to a flame ionization detector. The inlet temperature was 250°C and the detector was 300°C. The column was a Restek Stabilwax-DA (length: 15m, diameter: 0.25mm) using helium as the carrier gas at 10 mL/min and a split ratio of 50. The oven program was at 50°C held for 2 min, then increased to 200°C at 30°C/min then held at 200°C for 0.5min. The sample was dissolved in 1 mL of dichloromethane and 1 µL was injected into the GC. The menthol and menthone contents were calculated by the standard curve (See Figs. A1 and A2 in the appendix).

3.2.6. DPPH radical scavenging capacity assay

The assessment of peppermint essential oil's (obtained at 110 bar, 50 °C) scavenging capacity against the 2,2-diphenyl-1-picrylhydrazyl (DPPH) radical followed the procedure outlined in Hejna et al. (2021) and Zhou et al. (2011). Briefly, different concentrations (50, 100, 200, 500 mg/mL) of the peppermint essential oil dissolved in methanol were added to 3.9 mL of DPPH solution (25 mg/L in methanol). A control solution with DPPH and methanol was also prepared. The mixture was then shaken and left to incubate at room temperature in a dark environment for 30 minutes, after which the absorbance at 517 nm was measured using a UV-Vis spectrophotometer (Rose Scientific, Edmonton, AB, Canada). The inhibitory percentage of DPPH was determined using Equation 3.2.

$$\text{DPPH inhibition \%} = \frac{A_1 - A_2}{A_1} \times 100 \qquad (3.2)$$

Where, A1 = the absorbance of the control reaction; A2 = the absorbance in the presence of the sample.

3.2.7. Ferric reducing antioxidant power (FRAP) method

The antioxidant property of peppermint essential oil, obtained at 110 bar and 50 °C, was evaluated using the FRAP method at different concentrations of 50, 100, 200, and 500 mg/mL where methanol was used to dilute the essential oil. The procedure described by Moller et al. (2020) was followed. The FRAP solution was prepared by mixing $FeCl_3 \cdot 6H_2O$ in distilled water (resulting in a final concentration of Fe(III) of 20 mM), 2,4,6-tri(2-pyridyl)-s-triazine (TPTZ) in 40 mM HCl (resulting in a final concentration of TPTZ of 10 mM), and 0.3 M CH_3COOH/CH_3COONa buffer solution at pH = 3.6. The FRAP reagent was freshly prepared by mixing acetic acid buffer, TPTZ solution, and FRAP test solution in a volume ratio of 10:1:1.

In the FRAP assay, 3.0 mL of the FRAP reagent was mixed with 300 μL of deionized water and 100 μL of the peppermint essential oil solution (50, 100, 200, 500 mg/mL). The mixture was vigorously shaken for 30 seconds and then incubated in the dark at 37 °C for 30 min. After incubation, the absorbance was measured at 593 nm using methanol as the blank solution. The obtained absorbance values were compared to the ascorbic acid calibration curve (ranging from 0 to 100 μM), and the FRAP values were expressed in μM ascorbic acid equivalent (AAE) antioxidant capacity (See Fig. A3 in the appendix).

3.2.8. Chemical structure of essential oil by Fourier transform infrared spectroscopy

The FTIR spectra of peppermint essential oil was obtained using a Nicolet iS50 spectrometer (ThermoFischer Scientific, Waltham, MA, USA) in the ATR mode. The spectra were recorded with a resolution of 2 cm^{-1} and covered the wavelength range of 500-4000 cm^{-1}, similar to the method employed by Zhao and Saldaña (2019). This analysis allowed for a detailed examination of the functional groups present in the peppermint essential oil.

3.2.9. Statistical analysis

The data are presented as mean ± standard deviation, derived from a minimum of two independent experiments and analyses. Statistical analysis was performed with the Minitab version 18.0 (Minitab Inc., State College, PA, USA), utilizing one-way analysis of variance (ANOVA) and Tukey's test for multiple comparisons of means at a significance level of $p < 0.05$ and a confidence interval of 95%.

3.3. Results and Discussion

3.3.1. Effect of extraction time on the essential oil extraction

Fig. 3.4 shows the effect of extraction time on the yield of essential oil extracted from *Mentha × piperita* using two SC-CO_2 extraction equipment with different CO_2 flow rates at 50°C and 110 bar. The results indicated that the yield of essential oil extracted from *Mentha × piperita* increased with increasing extraction time up to 180 min for equipment 1 and 120 min for equipment 2. In the case of equipment 2, there was an initial extraction of approximately 0.5% of essential oil within the first 60 min, primarily due to the solubility effect. From 60 to 120 min, the yield increased further to 0.76%, indicating that the extraction process was dominated by solubility and mass transfer, and above 120 min, the process was dominated by mass transfer.
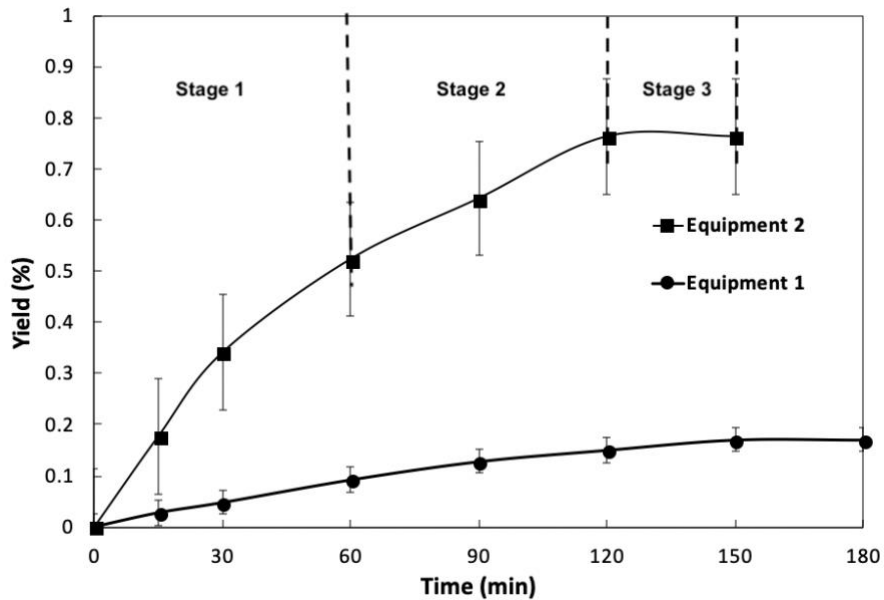
Fig. 3.4. Effect of time on the extraction yield at 110 bar and 50°C using Equipment 1 (0.5 mL CO_2/min) and Equipment 2 (3 mL CO_2/min).

The SC-CO_2 extraction curves with respect to time can be divided into three main stages. In the initial stage, the free essential oil present on the surface of the peppermint was dissolved in SC-CO_2 and transported by convection at a constant extraction rate, primarily influenced by solubility. Typically, approximately 50% of the total essential oil can be extracted during this phase. The second stage was marked by a decline in the extraction rate, as the available surface essential oil decreased, and the diffusion of CO_2 began to dissolve the remaining essential oil. The final stage corresponded to a diffusion-controlled regime, where the mass transfer mechanism was predominantly governed by the diffusion of CO_2 within the matrix of the peppermint powder (Fig. 3.4).

Beyond these times, the yield did not increase significantly, suggesting that the extraction had reached its maximum yield. The observed increase in yield with increasing extraction time was

likely due to the fact that longer exposure to SC-CO_2 can improve the solubility of the essential oil components and facilitate their transfer into the SC-CO_2.

A similar trend was reported by Shahsavarpour et al. (2017) for the extraction of spearmint essential oil from *Mentha spicata*, where the yield had a positive relation (0.17 – 0.65%) with the extraction time (20 – 120 min). Also, Wu et al. (2019) observed that the extraction yield of essential oil from *Cymbopogon citronella* leaves increased from 2.2% to 4% as the extraction time was extended from 30 to 150 min. A significant amount of essential oil was extracted from *Cymbopogon citronella* leaves during the initial 60 min of the extraction process, which corresponded to the first stage dominated by solubility. Furthermore, Zarrinpashne and Kandi (2018) reported a 13% increase in the extraction recovery of essential oil from Persian black cumin as the extraction time was extended from 2 to 12 h. Thus, the optimal extraction time varied, depending on the specific characteristics of the plant material such as particle size, cell wall structure and moisture content, and the extraction vessel used (dimensions). For example, the differences in the optimal extraction time observed between equipment 1 and 2 could be attributed to differences in the CO_2 flow rate. A low flow rate increased the contact between the CO_2 and the essential oil in the matrix, facilitating its dissolution but requiring a longer time, while a high flow rate enhanced the mass transfer efficiency (Mezzomo et al., 2009). As a result, equipment 1 showed a single stage of extraction predominantly dominated by solubility. The low flow rate of equipment 1 limited its ability to efficiently extract more essential oil from the peppermint matrix. Beyond a certain extraction time, prolonged exposure to SC-CO_2 can extract undesirable compounds like cuticular wax such as n-Hentriacontane, n-Tritriacontane and n-Dotriacontane from peppermint (Reverchon et al., 1994), which can compromise its quality and antioxidant

property. Therefore, it is crucial to optimize the extraction time to achieve the maximum yield while maintaining the quality and antioxidant activity of the extracted essential oil.

The following studies investigated the effect of different operating parameters, such as pressure, temperature, co-solvent and flow rate on the yield of essential oil at a constant extraction time of 180 min and 120 min for equipment 1 and 2, respectively.

3.3.2. Effect of pressure and temperature on the essential oil extraction

The extraction process using SC-CO_2 was affected by two crucial physical parameters, pressure and temperature, which combined modified the density of the supercritical fluid (See Table A2 in the appendix). Fig. 3.5 shows the effect of pressure and temperature on essential oil extraction yield from peppermint. Increasing the pressure above 120 bar generally resulted in an increase in essential oil extraction yield. At 50 °C, increasing the pressure from 100 to 400 bar resulted in a significant increase in the yield from 0.060% to 0.340% due to the increased solubility of the essential oil in SC-CO_2 at high pressures. As the pressure increased, the density and solvating power of the SC-CO_2 also increased, resulting in better penetration of the CO_2 into the peppermint matrix, hence better extraction of the essential oil (Carlson et al., 2001). A similar trend was observed in the studies conducted by Shahsavarpour et al. (2017) and Wu et al. (2019) for the extraction of essential oils from different plants. In the study by Shahsavarpour et al. (2017), the extraction of essential oils from *Mentha spicata* showed an increase in yield, from 0.207% to 0.283%, when the pressure increased from 85 to 120 bar. The extractions were performed at 38 °C with a CO_2 flow rate of 0.177 g/min for 120 min. Likewise, Wu et al. (2019) reported an increase in the extraction yield of essential oil from lemongrass leaves from 2.7% to 4.0% when the extraction pressure raised from 100 to 250 bar at 40 °C with a CO_2 flow rate of 333 mL/min.
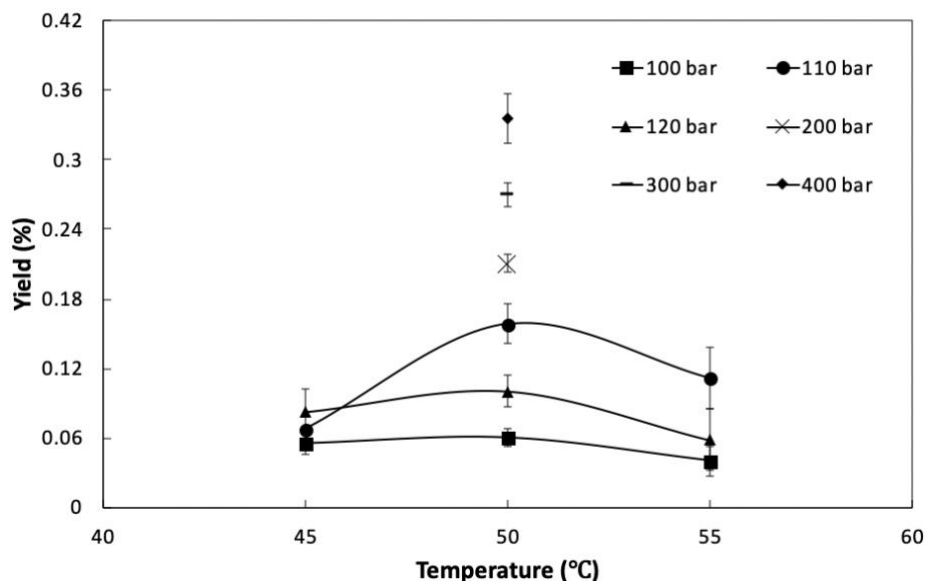
Fig. 3.5. Effect of pressure and temperature on essential oil extraction yield from *Mentha × piperita* using Equipment 1 (0.5 mL CO_2/min at pump).

Regarding temperature, Fig 3.5 illustrates a complex relationship between temperature and extraction yield. The extraction yield of peppermint essential oil showed a significant increase as the temperature rose from 45 to 50 °C. However, a decrease in extraction yield was observed as the temperature was further increased from 50 to 55 °C, at each pressure level (100 bar, 110 bar, and 120 bar). Near the critical point, even a slight change in temperature can cause significant changes in the density of the solvent (Saldaña et al., 1999). When the temperature increased at a constant pressure, the density of the SC-CO_2 decreased, affecting the ability of CO_2 to remove the essential oil from the peppermint matrix. Also, according to Porter and Lammerink (1994), the density of essential oils decreased as temperature increased at atmospheric pressure. For example, when the temperature increased from 20 to 60 °C at atmospheric pressure, the density of parsley essential oil decreased from 1.0660 to 1.0324 g/cm^3, and the density of wild thyme essential oil decreased from 0.9247 to 0.8939 g/cm^3, respectively. Then, the solubility of essential oil in SC-

CO_2 also decreased with increasing temperature. Earlier, Frohlich et al. (2019) observed a decline in the apparent solubility of eugenol from clove leaves in SC-CO_2, decreasing from 0.0056 to 0.0043 g/g CO_2 as the temperature raised from 40 to 60 °C at 220 bar. Consequently, the extraction yields also decreased from 1.08 to 1.03%. However, when the extraction temperature increased, it caused an increase in the kinetic energy of the essential oil molecules, leading to a rise in the sublimation pressure of essential oil and a greater likelihood of removal (Shahsavarpour et al., 2017). Furthermore, the increase in extraction temperature caused a reduction in the viscosity of the supercritical fluid, leading to a subsequent increase in the diffusion coefficient of the fluid. Additionally, the elevated temperature enhanced the Brownian motion of the essential oil molecules within the peppermint sample, thereby accelerating the mass transfer process (Wu et al., 2019). Hence, the impact of temperature on the extraction yield was determined by the combined influence of these competing factors.

Table 3.2 presents the impact of pressure and temperature on the composition of the extracted peppermint essential oil, with a particular focus on its main components, menthol and menthone, using Equipment 1 and 2.

Table 3.2. Yield of essential oil extracted from *Mentha × piperita,* and menthol and menthone contents in the extract.

P (bar)	T (°C)	CO_2 density (kg/m^3)	μ $(10^{-6}$ Pa S)	Yield (%)	Menthol content (%)	Menthone content (%)
Equipment 1 (0.5 mL CO_2/min at pump)						
100	45	506.55	38.09	0.055±0.010[efE]	24.838±2.254[bcdCDEF]	0.030±0.009[bcE]
100	50	384.40	28.34	0.060±0.008[efE]	28.849±1.857[bcCD]	0.039±0.003[bcE]
100	55	337.20	26.04	0.040±0.012[fE]	23.357±1.515[cdCDEF]	0.049±0.009[bcE]
110	45	553.25	42.91	0.067±0.002[efE]	32.796±0.235[abBC]	0.008±0.003[cE]
110	50	447.48	33.98	0.158±0.017[cdE]	38.853±2.629[aAB]	0.061±0.013[bcE]
110	55	400.13	31.09	0.110±0.027[deE]	26.355±3.772[bcCDE]	0.028±0.006[bcE]
120	45	599.95	47.72	0.083±0.019[efE]	7.953±3.673[fHI]	0.033±0.017[bcE]
120	50	510.56	39.62	0.100±0.013[defE]	25.588±1.059[bcCDEF]	0.043±0.009[bcE]
120	55	463.06	36.15	0.058±0.026[efE]	4.016±0.048[fI]	0.010±0.003[cE]
200	50	784.40	68.93	0.210±0.008[bcE]	16.698±2.919[deFGH]	0.286±0.037[aDE]
300	50	870.60	85.50	0.270±0.010[bE]	9.709±1.610[efGHI]	0.199±0.062[aDE]
400	50	923.4	98.36	0.340±0.021[aDE]	4.480±0.194[fI]	0.104±0.013[bE]
Equipment 2 (3 mL CO_2/min at pump)						
110	50	447.48	33.98	0.707±0.080[bCD]	47.539±1.156[aA]	2.287±0.076[aA]
200	50	784.40	68.93	0.964±0.217[bBC]	38.809±4.637[aAB]	1.553±0.403[abB]
300	50	870.60	85.50	1.165±0.291[bB]	18.536±2.031[bEFG]	0.546±0.015[cCD]
400	50	923.4	98.36	1.970±0.107[aA]	22.667±2.201[bDEF]	0.783±0.081[bcC]

[a-e] Different letters in the same column and same flow rate indicate significant differences ($p < 0.05$), [A-I] Different letters in the same column and different flow rates indicate significant differences ($p < 0.05$), P: pressure, T: temperature, μ: CO_2 dynamic viscosity.

Fig. 3.6 shows that the concentrations of menthol and menthone vary with changes in pressure and temperature with the CO_2 flow rate of 0.5 mL/min. The decrease in menthol content observed at 55 °C compared to 45 °C and 50 °C at the same pressures of 100 bar, 110 bar and 120 bar could be attributed to the solubility of menthol in SC-CO_2 (Fig 3.6A). The solubility of menthol in SC-CO_2 decreased when the temperature increased at constant pressure (Galushko et al., 2006). For example, the solubility of menthol decreased from 18.1×10^{-3} to 3.7×10^{-3} with the temperature increasing from 50 to 60 °C at 113 bar.

The menthone contents were influenced by pressures of 200-400 bar, resulting in a significant increase in menthone contents at a lower CO_2 flow rate. The menthone content was lower than values reported in the literature (11.07-26.26%) (Barton et al., 1992). The possible reason for this low value in this thesis is the different growth environments or drying methods used, which may result in a lower amount of menthone.

Nevertheless, both menthol and menthone content were significantly influenced by the CO_2 flow rate. As the flow rate increased from 0.5 to 3 mL/min, there was an increase in both menthol and menthone contents due to the enhanced mass transfer efficiency at high flow rates (Table 3.2). The highest menthol content (47.539%) and menthone (2.287%) content were obtained at 110 bar and 50 °C with a CO_2 flow rate of 3 mL/min.
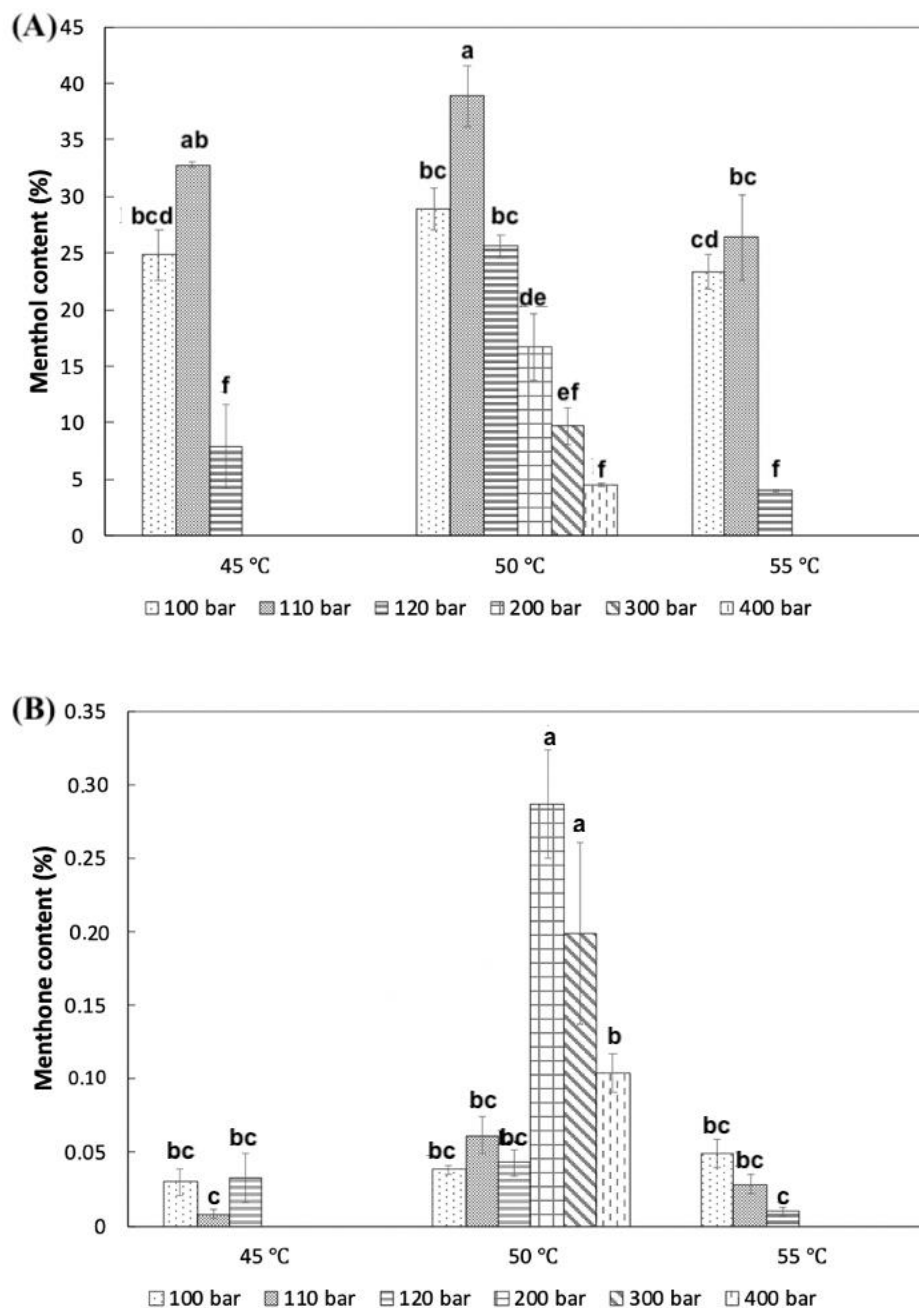
Fig. 3.6. Effect of temperature and pressure on: (A) menthol and (B) menthone contents in SC-CO_2 extracted essential oil from *Mentha × piperita* using Equipment 1 (0.5 mL CO_2/min at pump). [a-f]Bars that do not share a letter are significantly different.

The obtained results in Table 3.2 revealed a remarkable selectivity for menthol under the specific conditions of SC-CO_2 extraction. Particularly, at 50 °C and 110 bar, with a CO_2 flow rate of 0.5 mL/min, the extracted essential oil had a high menthol content of 38.853% and a low menthone

content of 0.061%. This high selectivity for menthol at this condition holds significant promise for fractionation purposes.

3.3.3. Effect of co-solvent on the essential oil extraction

Table 3.3 shows data for the use of co-solvents such as ethanol, acetone, or isopropyl acetate with SC-CO_2 for essential oil extraction from *Mentha × piperita*. In general, ethanol and acetone are recognized as safe solvents by the FDA and are commonly used in the food and pharmaceutical industries. Isopropyl acetate is regarded as a Class 3 solvent by FDA, which means it is less toxic and has a lower risk to human health (FDA, 2017). Also, isopropyl acetate is commonly used as a solvent in the food and cosmetic industry and is considered safe for use in food and personal care products.

Table 3.3. Comparison of extraction yield, menthol and menthone contents between neat CO_2 extraction and CO_2+co-solvent extraction at 110 bar and 50 °C using Equipment 1 (0.5 mL CO_2/min at pump).

Co-solvent	Yield (%)	Menthol content (%)	Menthone content (%)
Neat CO_2	0.158±0.017[b]	38.853±2.629[a]	0.061±0.013[b]
Ethanol	0.241±0.077[b]	26.570±3.243[ab]	0.502±0.045[a]
Acetone	0.758±0.157[a]	18.619±2.270[b]	0.379±0.008[a]
Isopropyl acetate	0.337±0.083[b]	26.329±4.677[ab]	0.370±0.053[a]

[a-b] Different letters in the same column indicate significant differences ($p<0.05$).

The addition of co-solvent significantly affects the yield and composition of the essential oil extracted from *Mentha × piperita* using SC-CO_2 extraction (See Table A3 in the appendix). All three co-solvents resulted in a significant increase in the menthone content, ranging from 0.061%

to 0.502%. However, the addition of co-solvents led to a decrease in the menthol content, with values ranging from 38.853% to 18.619% in the extracts.

Among the co-solvents evaluated (Fig. 3.7), acetone resulted in the highest yield (0.758%), more than three times higher than that of neat CO_2 extraction (0.158%) at 50 °C and 110 bar. Isopropyl acetate also showed an increase in yield compared to neat CO_2 extraction, with a yield of 0.337 ±0.083%. However, the increase was not as high as that obtained with acetone. Although ethanol did not significantly increase the yield of the extract (0.241%), it was the most suitable co-solvent in terms of preserving the essential oil composition with high menthol content (26.570%) and menthone content (0.502%).
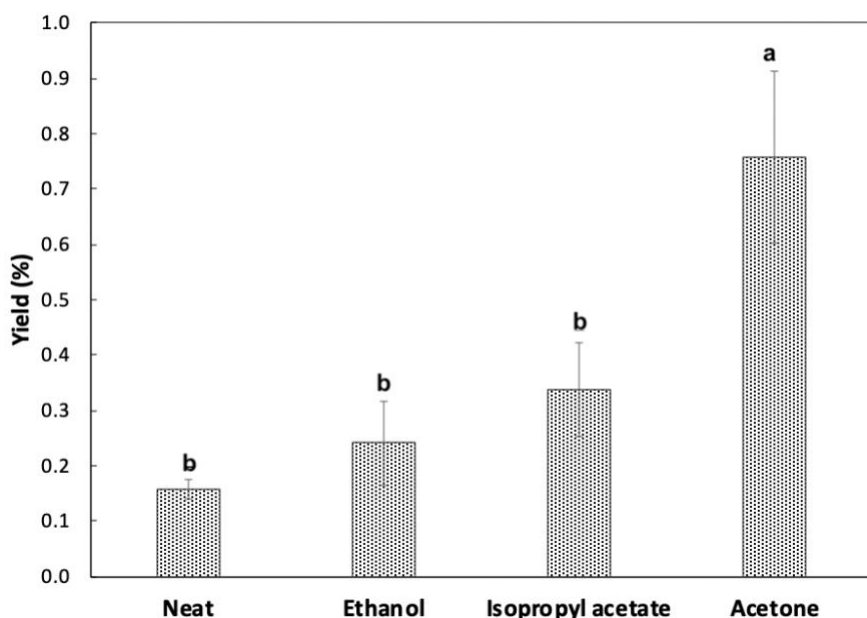
Fig. 3.7. Effect of co-solvent on extraction yield using Equipment 1 at 110 bar and 50 °C with a flow rate of 0.5 mL CO_2/min at pump. [a-b] Bars that do not share a letter are significantly different.

Earlier, Bensebia et al. (2009) used 3% of ethanol to assist SC-CO_2 extraction of essential oil from rosemary and the yield increased from 1.7% to 2.3% at 40 °C and 100 bar, as the ethanol penetrated the cellular walls and improved the mass transfer. Also, Quitain et al. (2006) showed that 10 mol%

ethanol as an entrainer increased the recovery of oil components of okara by three times. Nemoto et al. (1997) reported the effect of co-solvent on yield by changing the polarity, surface interactions, matrix accessibility, and desorption kinetics of the bioactives. In summary, adding co-solvents to SC-CO_2 increases its polarity and solvent strength, resulting in greater solubility of the compounds. Also, co-solvents have the potential to mask active sites on the surface of the sample matrix, thereby preventing the re-adsorption or partitioning of the compounds onto the matrix active sites. Co-solvents may alter the sample matrix to enable SC-CO_2 to access distant sites in the matrix, facilitating the transportation of the compounds to the bulk fluid. Finally, co-solvents can interact with the compound-matrix complex and lower the activation energy barrier for desorption. However, the increased yield did not correspond to an increase in menthol content, which remained lower than that obtained with neat CO_2 extraction as shown in Table 3.3. On the other hand, the content of menthone increased with the use of co-solvents. Therefore, the use of co-solvents can have both positive and negative effects on the quality of the extract.

For instance, it can increase the yield and improve the extraction of certain compounds like menthone. However, it can also extract undesired compounds such as chlorophyll (greenish coloration of the extract and an earthy or grassy taste), waxes (waxy texture or coating in the extract), which can lead to potential alterations in the aroma, flavour, and purity of the essential oil. This resulted in the menthol content being lower than in neat SC-CO_2 extraction when the total yield increased. Therefore, the selection of a co-solvent for SC-CO_2 extraction of peppermint oil should be based on the desired yield and target compounds of interest. Acetone can provide the highest yield but may not be ideal for obtaining high menthol content.

3.3.4. Effect of CO₂ flow rate on the essential oil extraction

Fig. 3.8 shows the effect of CO_2 flow rate and pressure at 50 °C on the SC-CO_2 extraction yield from *Mentha × piperita*. The results showed that increasing the CO_2 flow rate from 0.5 mL/min to 3 mL/min led to higher extraction yields at constant temperature and pressure conditions.

At 110 bar and 50 °C, when the CO_2 flow rate increased from 0.5 mL/min to 3 mL/min, the yield increased from 0.158 to 0.707%. The essential oil obtained at 110 bar and 50 °C had the highest menthol (47.539%) and menthone (2.287%) contents (Table 3.2).
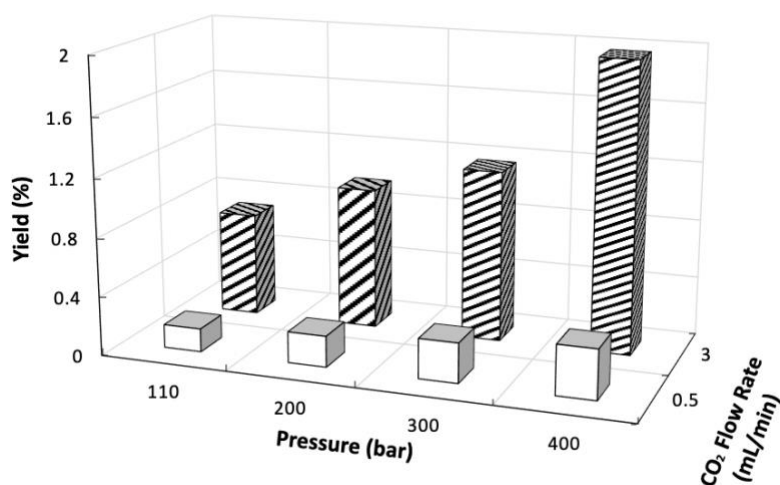
Fig. 3.8. Effect of CO_2 flow rate at pump and pressure on the extraction yield at 50 °C.

The results suggested that increasing the CO_2 flow rate had a positive impact on the extraction yield of essential oil from *Mentha × piperita*. Increasing the flow rate of CO_2 during extraction led to the enhancement of mass transfer of essential oil from peppermint matrix to SC-CO_2, resulting in a higher quantity of essential oil being extracted from the system to enhance extraction efficiency. Earlier, Shahsavarpour et al. (2017) observed a similar relationship between CO_2 flow rate (0.059 – 0.177 g/min) and yield (0.281 – 0.429%) of extraction of essential oil from spearmint at a temperature of 45 °C and pressure of 100 bar. This indicated that an increase in CO_2 flow rate

resulted in enhanced mass transfer coefficient, which in turn reduced mass transfer resistance through increased convection. However, Bensebia et al. (2009) observed that two different CO_2 flow rates (1 and 5 g/min) had a negligible influence on the extraction yield of essential oil from rosemary and concluded that the process might be controlled by internal mass transfer. Therefore, different competing factors determine whether the flow rate can lead to an increase or decrease in extraction efficiency.

3.3.5. Scale-up of essential oil extraction from *Mentha × piperita*

The scale-up of the SC-CO_2 extraction of essential oil from *Mentha × piperita* was successfully achieved with a 3-fold, 5-fold, and 10-fold increase in peppermint powder loading compared to the laboratory scale. To ensure consistent scaling up, the ratio of CO_2 mass to feed mass was maintained constant at approximately 78. From the data presented in Fig. 3.9, it can be observed that the ratio of total CO_2 mass to feed mass was 77.8 for a 3-h extraction using a 10 mL extraction vessel, resulting in a yield of 0.707% at 110 bar and 50 °C. When using a larger 300 mL extraction vessel and feed loadings of 9g, 15g, and 30g, and maintaining the CO_2/feed ratio at 78, the extraction yields after a 5-h extraction were 0.937%, 0.787%, and 0.768%, respectively. Therefore, the scale-up experiments yielded slightly higher extraction yields (0.937%, 0.787%, and 0.768%) compared to the laboratory-scale extraction (0.707%) using a 3g feed loading (Table 3.4.). The scale-up experiments yielded slightly higher extraction yields using 5h and the CO_2 flow rate of 7 mL/min compared to the laboratory scale using 3h and the CO_2 flow rate of 3 mL/min.
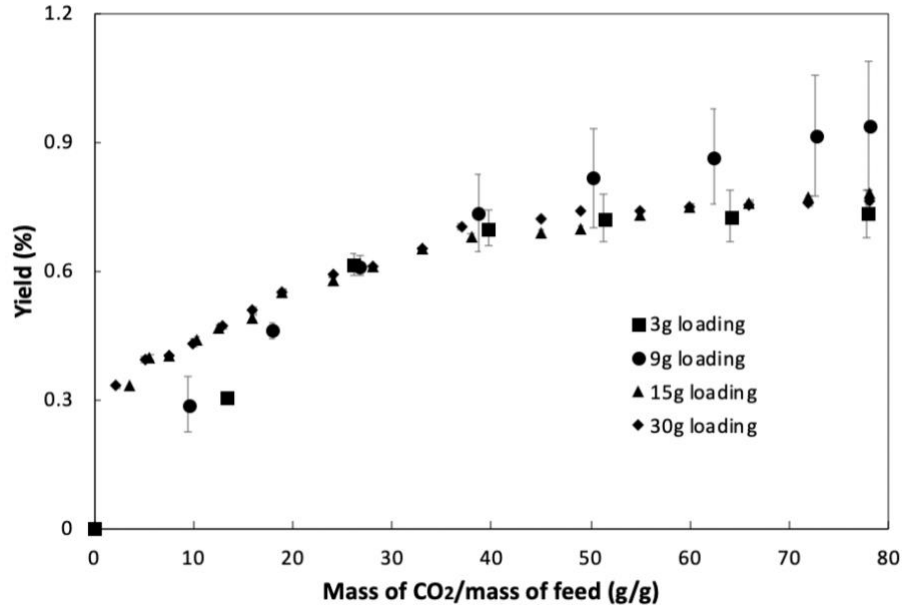
Fig. 3.9. Extraction yield variation with constant CO_2/feed (g/g) ratio at 110 bar and 50 °C.

Additionally, there was a slightly higher content of menthol (47.539-49.808%), but a significantly lower content of menthone (2.287-1.899%) in the scale-up extracts. These results indicated the potential for improved efficiency and productivity in the scale-up process.

Earlier, Prado et al. (2011) observed a similar pattern in their study on the SC-CO_2 extraction of clove. They conducted a 15-fold scale-up extraction, which was significantly larger (5.15 L) compared to the laboratory-scale extraction (290 mL). The results revealed an increase in the extraction yield, with a 20% higher yield for clove in the scale-up extraction. The researchers attributed this improved yield to the higher flow rate of SC-CO_2 utilized in the scale-up extraction, which led to mechanical dragging to entrain the essential oil that was not fully dissolved in SC-CO_2. Later, Salea et al. (2017) similarly reported a higher yield of 3.83% during a 15-fold scale-up extraction of ginger oil from *Zingiber officinale* var. Amarum using SC-CO_2, compared to a yield of 3.10% obtained in the laboratory-scale extraction. These findings suggest that the geometries of the extractor, as well as factors such as channelling and biomass aggregation, can have an impact on the performance of the extraction process.

79

In contrast, studies conducted by Kotnik et al. (2007) and Taher et al. (2014) reported different results, showing a decrease in extraction yield during pilot-scale experiments. For example, a 67-fold scale-up extraction of chamomile flower head with 1 kg loading resulted in a decrease in yield from 3.81% to 2.5% at 500 bar and 120 °C with a CO_2 flow rate of 13 kg/h (Kotnik et al., 2007). Similarly, Taher et al. (2014) maintained a constant ratio of reactor height and diameter at 3.3 and conducted an eight-fold scale-up extraction of microalgae lipids with 25 g loading. However, the scale-up extraction led to a drop-in yield from 7.06% to 6.2% at 500 bar and 53 °C, using a CO_2 flow rate of 1.9 g/min. The variation in extraction yield observed during pilot-scale experiments can be attributed to several factors. The scale-up process itself introduces changes in reactor geometry, flow rate, contact time, and mass transfer dynamics, which can impact extraction efficiency (Prado et al., 2012).

Table 3.4. Comparison of extraction yield, menthol and menthone contents between laboratory and scale-up conditions with the same CO_2/feed (g/g) ratio at 110 bar and 50 °C.

Extraction vessel volume (mL)	Peppermint loading (g)	CO_2 flow rate at pump (mL/min)	Yield (%)	Menthol content (%)	Menthone content (%)
10	3	3.0	0.707±0.080[a]	47.539±1.156[a]	2.287±0.076[a]
	9		0.937±0.149[a]	49.808±0.289[a]	1.899±0.107[b]
300	15	7	0.787±0.005[a]	48.186±0.759[a]	2.001±0.035[ab]
	30		0.768±0.007[a]	47.362±0.465[a]	2.128±0.064[ab]

[a-b] Different letters in the same column indicate significant differences (p<0.05).

3.3.6. Antioxidant Activity of *Mentha × piperita* essential oil

The DPPH scavenging activity and ferric reducing antioxidant power (FRAP) of peppermint essential oil were evaluated at various concentrations (50 mg/mL, 100 mg/mL, 200 mg/mL, and 500 mg/mL) using the method described earlier. Fig. 3.10 shows a dose-dependent increase in the scavenging activity, indicating that higher concentrations of peppermint essential oil corresponded

to higher inhibitory percentages of DPPH radical. At the lowest concentration of 50 mg/mL, the scavenging activity was 34.7%, demonstrating the ability of peppermint essential oil to neutralize free radicals. At the highest concentration of 500 mg/mL, the peppermint essential oil exhibited a scavenging activity of 77.9%.
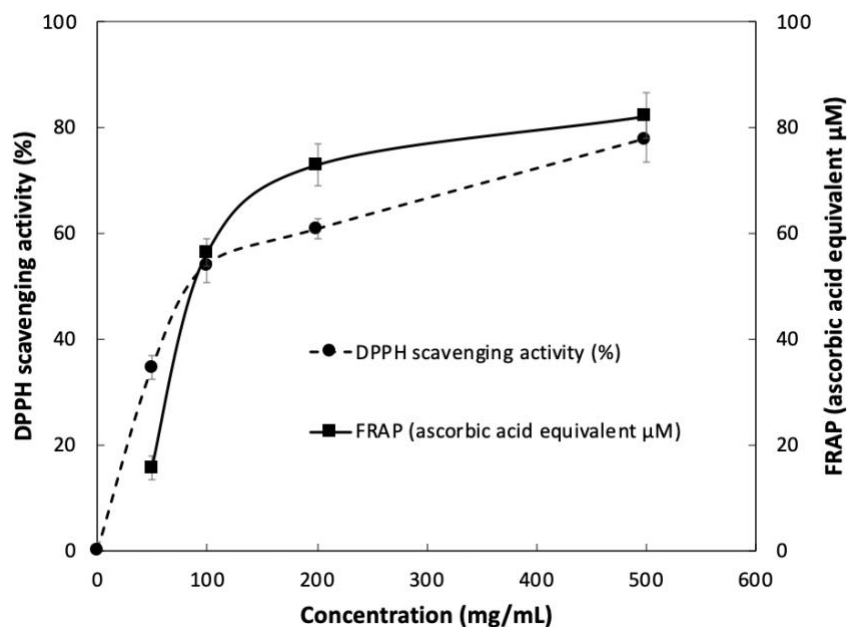
Fig. 3.10. Antioxidant activity of peppermint essential oil obtained at 110 bar and 50 °C: DPPH and FRAP assays at different methanol concentrations (50 mg/mL, 100 mg/mL, 200 mg/mL, and 500 mg/mL).

These findings align with results from previous studies that have highlighted the antioxidant properties of peppermint essential oil (Hejna et al., 2021, Wu et al., 2019). The strongest response (~70%) was observed at the highest concentration of peppermint essential oil (600 mg/mL). Fig. 3.10 also shows the FRAP results of peppermint essential oil evaluated at various concentrations (50 mg/mL, 100 mg/mL, 200 mg/mL, and 500 mg/mL). As the concentration of the peppermint essential oil in methanol increased from 50 mg/mL to 500 mg/mL, the FRAP values increased from 15.621 to 82.253 µM ascorbic acid equivalent (See Table A1 in the appendix). It has a similar trend with DPPH results, in which peppermint essential oil possesses dose-dependent

antioxidant activity, where higher concentrations exhibited greater antioxidant capacity. A similar trend was also reported by Hejna et al. (2021), as they found that 600 mg/mL of peppermint essential oil exhibited an antioxidant activity of around 65 μM ascorbic acid equivalent, which is consistent with this study.

The antioxidant properties found in peppermint essential oils are linked to its major monoterpenoids, such as menthol, menthone, carvone, and 1,8-cineole. Additionally, minor constituents containing active methylene groups, like terpinolene, α- and γ-terpinene, have also shown antioxidant activity (Wu et al., 2019).

3.3.7. Structural analysis of peppermint essential oil by Fourier transform infrared spectroscopy

The structural analysis of peppermint essential oil was performed using FT-IR to investigate the presence of chemical bonds and functional groups in the essential oil obtained at 110 bar and 50 °C. Figure 3.11 shows distinct peaks within the wavelength range of 500 to 4000 cm^{-1} in the spectrum. The extracted essential oil exhibited significant bands, including a strong peak at 3540 cm^{-1} attributed to -OH group vibrations. Additionally, bands at 2924 and 2854 cm^{-1} indicated the presence of $-CH_3$ and $-CH_2$ groups, respectively. The appearance of a peak at 1742 cm^{-1} indicated C=O vibrations (Yilmaztekin et al., 2019). The peak at 1464 cm^{-1} was associated with C-H bonding in the alkane methylene group, while the peak at 1378 cm^{-1} suggested phenol-alcohol group presence (Sorour et al., 2021). These spectral features were consistent with previously reported FT-IR analyses of peppermint essential oil (Sorour et al., 2021; Yilmaztekin et al., 2019).
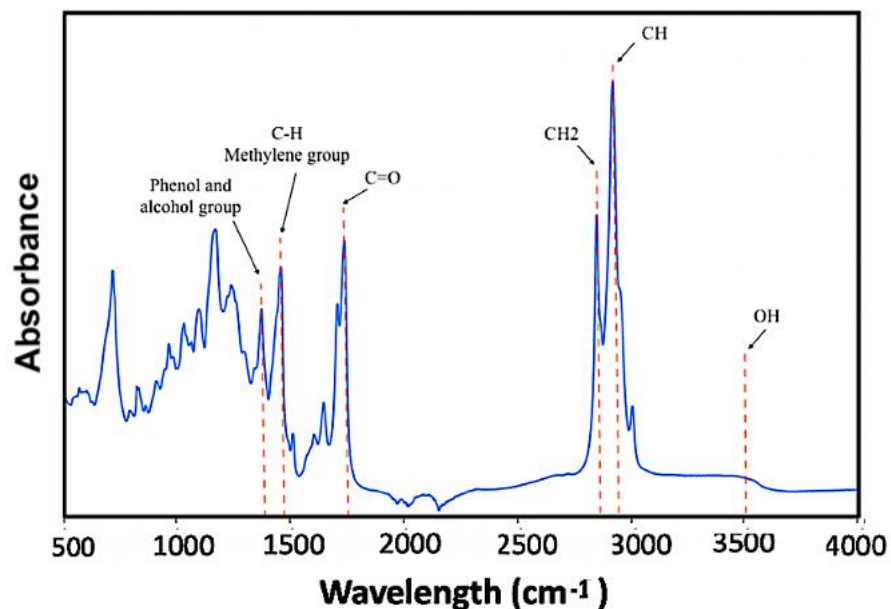
Fig. 3.11. FT-IR spectra of essential oil extracted from *Mentha × piperita* at 110 bar and 50°C.

3.4. Conclusion

This study demonstrated the effectiveness of using SC-CO_2 and SC-CO_2 + co-solvents to extract peppermint essential oil from peppermint leaves. Through a series of carefully designed experiments, the optimal extraction parameters were determined to be 110 bar, 50°C, 120 min, and a CO_2 flow rate of 3 mL/min. The extracts contained high levels of menthol (47.539%), which is the most abundant compound in peppermint essential oil.

The addition of co-solvents had a significant impact on both the yield and composition of the extracted oil. The three co-solvents evaluated showed a significant increase in the menthone content, while causing a decrease in the menthol content. Among the co-solvents, acetone resulted in the highest yield (0.758%), followed by isopropyl acetate (0.337%), while ethanol did not significantly increase the yield (0.241%) but preserved the essential oil composition with high menthol (26.570%) and menthone (0.502%) contents. The use of co-solvents altered the polarity, surface interactions, matrix accessibility, and desorption kinetics of the compounds, thereby

affecting the extraction process. It is important to consider the trade-off between yield and desired compound composition when selecting a co-solvent for the SC-CO_2 extraction.

The scale-up of SC-CO_2 extraction of essential oil from *Mentha × piperita* demonstrated successful scaling with 3-fold, 5-fold, and 10-fold increases in peppermint powder loading compared to the laboratory scale (3g). The consistent maintenance of the CO_2 mass to feed mass ratio at approximately 78 ensured reliable scaling up. The scale-up experiments yielded slightly higher extraction yields compared to the laboratory scale, with values of 0.937%, 0.787%, and 0.768% obtained using a larger extraction vessel and higher feed loadings. These results indicate the potential for improved efficiency and productivity in the scale-up process. Furthermore, the essential oil collected from the scale-up experiment exhibited a slightly higher content of menthol (47.539 to 49.808%) and a significantly lower content of menthone (2.287 to 1.899%). Peppermint essential oil at different concentrations showed remarkable DPPH scavenging activity and ferric reducing power. The antioxidant activity of peppermint essential oil exhibited a concentration-dependent pattern, with higher concentrations (500 mg/mL) leading to increased inhibition of DPPH radicals (77.9%) and ferric reducing power (82.253 µM ascorbic acid equivalent). The structural analysis of the extracted peppermint essential oil by FT-IR revealed distinct peaks corresponding to various chemical bonds and functional groups, consistent with previous FT-IR analyses of peppermint essential oil. These findings provide valuable insights into the extraction of peppermint essential oil that can have practical applications in the food and pharmaceutical industries. Further research and refinement of the extraction parameters are warranted to maximize the extraction efficiency and quality of essential oil from *Mentha × piperita* using SC-CO_2 extraction.

In addition to the conclusions drawn from this study, there are also some limitations and future perspectives to consider. One of the limitations of this study is to focus only on the extraction of menthol and menthone, the two most abundant compounds in peppermint essential oil. Future research could explore the extraction of other compounds found in peppermint essential oil such as 1,8-cineole and menthyl acetate, as well as the potential health benefits associated with these compounds.

Chapter 4: Solubility of menthol in supercritical carbon dioxide and its impregnation on cotton gauze

4.1. Introduction

Menthol [5-methyl-2-(1-methylethyl) cyclohexanol; 2-isopropyl-5-methylcyclohexanol or *p*-methan-3-ol] is a cyclic monoterpene alcohol found as the main constituent in essential oils of *Mentha canadensis* (cornmint) and *Mentha × piperita* (peppermint) (Kamatou et al., 2013). Menthol ranks as the third most important flavoring substance, following vanilla and citrus. In 2022, a global production of approximately 34,000 metric tons was reported (Dylong et al., 2022). Initially menthol was used as an additive in the 1920s. Then, menthol has been used in various applications of several products, including toothpaste, preshave lotions, and numerous cosmetic products (Etzold et al., 2009). In addition to its role as a flavour enhancer, menthol has valuable applications in pharmacy and medicine. Its cooling (Yosipovitch et al., 1996), analgesic (Galeotti et al., 2002), antifungal (Edris and Farrag, 2003), antibacterial (Kotan et al., 2007), antipruritic (Koga et al., 2009), anti-inflammatory (Baylac and Racine, 2003), antitussive (Kumar et al., 2012), and antiviral (Schuhmacher et al., 2003) effects make menthol a versatile ingredient in the pharmaceutical and medical fields.

Earlier, Yosipovitch et al. (1996) conducted a study that demonstrated the cooling sensation of menthol (10 wt%) on the skin. Their research revealed that in approximately 65% of human subjects, this cooling sensation could persist for up to 70 min. However, a high concentration of 40% menthol could decrease the cold and mechanical pain threshold (Binder et al., 2011). When applied topically, menthol functions as a counter-irritant by delivering a cooling sensation. It achieves this by initially stimulating nociceptors (pain receptors) and subsequently desensitizing them (Pergolizzi et al., 2018). The mechanism behind menthol's action involves the inhibition of

Na^+ channels on concentration, voltage, and frequency. By promoting both fast and slow inactivation states, menthol effectively reduces the activity of Na^+ channels in a use-dependent manner. In the research of Gaudioso et al. (2012), it was observed that low concentrations of menthol provided analgesic effects in mice, relieving pain caused by a toxin that targets Na^+ channels. The anti-inflammatory property of menthol was reported by Juergens et al. (1998). By an *in vitro* investigation, it was observed that menthol effectively suppressed the production of three inflammation mediators by monocytes. At a concentration of 10^{-7} mg/mL, menthol exhibited effects on inflammation mediators, which reduced IL-1-b (pro-inflammatory cytokines involved in immune defence against infection) by $64 \pm 7\%$. Therefore, it was suggested that menthol could be utilized as a promising compound in the treatment of wound healing for burns, muscle aches, and some sports injuries by reducing pain, inflammation, and contributing to the overall comfort of the affected area.

On the other hand, for an effective wound dressing system, it is crucial to possess specific properties that align with its intended application. These properties include flexibility, controlled adherence to the surrounding tissue, gas permeability, durability or biodegradability, as well as the ability to absorb fluids released from the wound while simultaneously regulating water loss (Dias et al., 2011). Woven absorbent cotton gauze has been utilized since 1891 to cover wounds and facilitate the process of wound healing (Dhivya et al., 2015). The natural composition and properties of cotton gauze meet all the requirements for an effective wound dressing, as it provides a gentle and comfortable interface with the wound, absorbs exudate, and helps maintain an appropriate moisture balance for optimal wound healing conditions (Katayama et al., 2012).

The conventional method used for impregnating bioactives in cotton gauze is immersion. In the immersion method, the cotton gauze is fully immersed in the desired solution, allowing for

thorough impregnation of the material. For example, Souza et al. (2019) dipped cotton gauze into a chitosan solution with different concentrations of 0.063 to 0.5 wt% and dried it in the oven for 12h to achieve impregnation with the highest weight increase of 5.1%. Similarly, Rashmi et al. (2020) prepared the iodine-loaded cotton gauze by immersing it into the iodine solution for 4h to achieve the impregnation yield of 21.3 wt%. The drawback of the immersion method is the potential for uneven distribution of the impregnating substance. Depending on the viscosity and properties of the solution used, the impregnation may not penetrate the gauze uniformly, leading to variations in the final product's properties or performance.

Supercritical carbon dioxide (SC-CO₂) is known for its dual capabilities as a solvent for extracting valuable compounds and its exceptional diffusion properties in organic materials when operating above the critical conditions of 73.8 bar and 31.1 °C. This excellent diffusion ability can be employed for impregnating polymers with natural bioactives. The SC-CO₂ is selected due to its high solvent capacity, cost-effectiveness, non-toxic nature, and non-flammability. The process of SC-CO₂ impregnation can be considered as a reversed extraction process, where the performance is determined by mass transfer and thermodynamic equilibrium (Alvarado et al., 2018). Some studies have utilized SC-CO₂ to impregnate various materials. Some examples include phytol-impregnated silica aerogels (30.1%) (Mustapa et al., 2016), carvone-impregnated polylactic acid films (30%) (Miranda-Villa et al., 2022), eugenol-impregnated polyethylene films (6%) (Goñi et al., 2016), and thymol-impregnated cotton gauze (9% and 19.6%, respectively) (Ivanović et al., 2014; Milovanovic et al., 2013). All these investigations highlighted the potential of SC-CO₂ as an effective impregnation method, yielding impregnation efficiencies ranging from 6% to 30%.

To achieve efficient impregnation of menthol on cotton gauze, solubility data of menthol in SC-CO₂ are essential. Earlier, Sovová and Jež (1994) measured the solubility of menthol in CO₂ within

the pressure range of 67 to 115.6 bar and temperature range of 35 to 55 °C, utilizing a dynamic method. The highest solubility (1.3×10^{-2}) was obtained at 90.7 bar and 40 °C. Subsequently, Galushko et al. (2006) conducted a similar investigation, examining the solubility of menthol in CO_2 within the pressure range of 66 to 144 bar and temperature range of 30 to 60 °C, while the highest solubility (4×10^{-2}) was obtained at 143.7 bar and 60 °C. The results of Galushko et al. (2006) and Sovová and Jež (1994) were similar with each other. However, to date, there is no available data on the solubility of menthol in SC-CO_2 at pressures exceeding 150 bar. In this study, the solubility of menthol in SC-CO_2 was investigated at 100-300 bar, and 45-55 °C using a dynamic method. Based on the obtained solubility data, this study identified the optimum operating conditions for impregnating cotton gauze with menthol using SC-CO_2. In addition, the efficiency of impregnation relies on various variables, such as the properties of the polymer such as porosity, the chemical interactions between the impregnated compound and the SC-CO_2, and operational processing factors like impregnation time and depressurization rate (Goñi et al., 2016). In this study, the impregnation time and depressurization rate were assessed to determine their impact on the impregnation process. Additionally, the colour, structure, and thermal properties of both the original cotton gauze and the menthol-impregnated cotton gauze were investigated.

4.2. Materials and Methods

4.2.1. Materials

All materials used were purchased from commercial suppliers: carbon dioxide (Bone Dry UN1013, Linde, Edmonton, AB, Canada), menthol (Sigma-Aldrich, 15785, analytical specification), and 5 cm × 5 cm sterilized gauze pads (SAFE-TEX manufacturing company, Houston, TX, United States).

4.2.2. Solubility determination

Fig. 4.1 shows the schematic of the dynamic SC-CO_2 system used for solubility measurements. The system mainly consists of a CO_2 cylinder, an ISCO pump, a 25 mL high-pressure vessel, a preheater, a temperature controller, a solute collection vial, a gas flow meter, and valves (Mekala et al., 2022).

To perform a solubility experiment using the dynamic SC-CO_2 system, a similar solubility procedure previously reported by Saldaña et al. (1999) was followed. Briefly, menthol powder (~ 0.2 g) was placed inside a stainless-steel frit basket with 5 μm openings equipped with a filter on the top and loaded inside the high-pressure vessel (25 mL). Then, the vessel was connected to the system with the high-pressure tubing. The high-pressure vessel was also connected to a temperature controller (DINICO DZ47-63) to ensure that the desired temperature was achieved. Then, pressure in the system was monitored by a pressure gauge. A precise micrometering valve (Swagelok, Solon, OH, United States) and a flow meter (M250SLPM, Alicat Scientific, Tucson, AZ, United States) were installed to warrant the low flow rates needed for the solubility measurements.
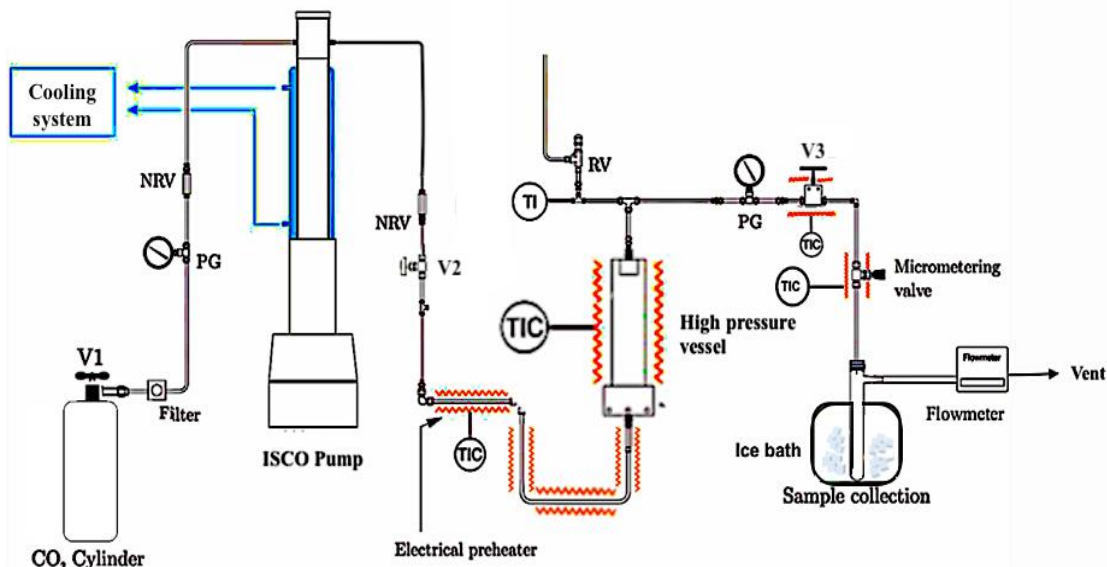
Fig. 4.1. Schematic representation of the SC-CO₂ dynamic system. PG: pressure gauge, V1-3: valves, TI: temperature indicator, TIC: temperature indicator controller, NRV: one-way valve, RV: relief valve.

By opening the valve V1, high purity carbon dioxide (Bone Dry UN1013) liquefied through a chiller (S&A CW-5200) was fed to the high-pressure system using the syringe ISCO pump (Model 260D). The system pressure was set in the ISCO pump. After, carbon dioxide was pumped into the 25 mL stainless steel high-pressure vessel by opening valve V2. Once the desired pressure and temperature were reached, the on/off valve V3 and the micrometering valve were opened. The micrometering valve was used to control the flow rate. The menthol precipitated in a glass vial immersed in an ice bath, and the carbon dioxide was vented after flowing through the flow meter.

The solubility experiment was carried out for 3 h at 100-300 bar and 45-55 °C as shown in Table 4.1, collecting samples every hour. To clean the system, the tubing was cleaned by pumping with acetone or ethanol to recover all menthol that remained in the tubing. After that, carbon dioxide

was used to dry the system for 1 h before starting to load the high-pressure vessel for the next experiment. All measurements were performed at least in duplicate.

Table 4.1. Experimental design to measure menthol solubility in SC-CO_2 using the dynamic method.

Run	Temperature (°C)	Pressure (bar)	CO_2 density (kg/m³)
1		100	506.55
2		110	553.25
3	45	120	599.95
4		200	812.15
5		300	890.30
6		100	384.40
7		110	447.48
8	50	120	510.56
9		200	784.40
10		300	870.60
11		100	337.20
12		110	400.13
13	55	120	463.06
14		200	754.10
15		300	850.30

The mass of menthol was calculated by the difference between the mass collected in the glass vial and the mass of the empty glass vial.

The solubility value was determined by considering the mass of the collected menthol, along with the mass and molecular weight of carbon dioxide and menthol. To calculate solubility, the masses of menthol and carbon dioxide were converted into moles using their respective molecular weights. Subsequently, the mole of menthol was divided by the total moles of CO_2 and menthol to obtain the solubility value using Equation 4.1.

$$\text{Solubility} = \frac{\frac{\text{mass of menthol (g)}}{\text{molecular weight of menthol (g/mole)}}}{\frac{\text{mass of } CO_2 \text{ (g)}}{\text{molecular weight of } CO_2 \text{ (g/mole)}} + \frac{\text{mass of menthol (g)}}{\text{molecular weight of menthol (g/mole)}}} \quad (4.1)$$

Carbon dioxide mass was calculated by the flow rate at the outlet multiplied by the time and density at ambient conditions using Equation 4.2.

$$\text{Mass of } CO_2 = \text{flow rate (L/min)} \times \text{density of } CO_2 \text{ (g/L)} \times \text{time (min)} \tag{4.2}$$

4.2.3. Supercritical CO₂ impregnation

The impregnation of cotton gauze with menthol was carried out using the apparatus described in Chapter 3 (Fig. 3.1). The high-pressure stainless-steel vessel had a volume of 25 mL and was equipped with a heater to reach the desired temperature of 45 °C. First, menthol was placed in a stainless-steel frit basket positioned at the bottom of the vessel, and a stainless-steel mesh was placed above the basket. Then, the cotton gauze (5 cm × 5 cm), folded twice to form four layers, was positioned above the mesh. The gauze/menthol ratio was maintained at 2.5 ± 0.05 g/g. This ratio was chosen to prevent excessive menthol loading, as achieving complete impregnation of menthol resulted in a yield of only 40%. The stainless-steel mesh with a pore diameter of 0.09 mm was used to prevent menthol from splashing onto the gauze.
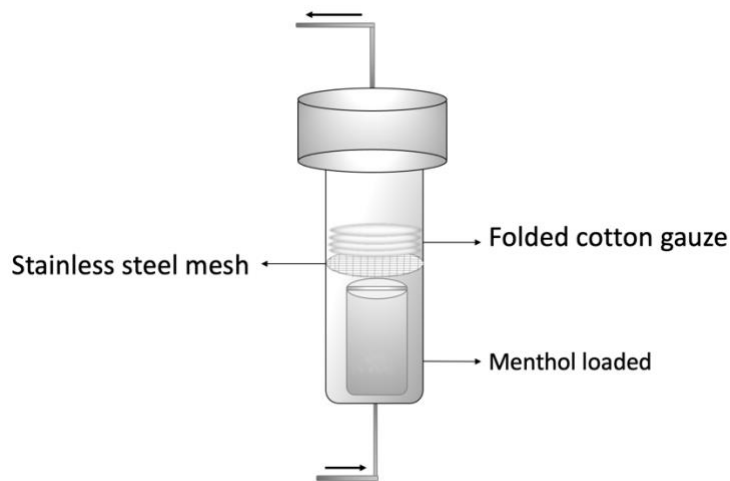
Fig. 4.2. Schematic for the SC-CO₂ menthol impregnation high pressure vessel: an inner high-pressure basket with placement of menthol, cotton gauze, and stainless-steel mesh. Cotton gauze:menthol mass ratio 2.5g/g.

SC-CO$_2$ impregnation operating conditions, such as pressure and temperature, were based on the obtained solubility data (45 °C and 120 bar). Menthol loaded in a basket and cotton gauze were placed inside the vessel, and the vessel was connected to the system with high-pressure tubing. The high-pressure vessel was also connected to a temperature controller to ensure that the desired temperature was achieved and maintained constant. The pressure in the system was monitored by a pressure gauge, and CO$_2$ was introduced into the system using the ISCO pump until the desired pressure was reached. Valve V2 was then closed, and the pump was turned off. The SC-CO$_2$ impregnation system was maintained at a constant temperature and pressure for specific time intervals (30 or 300 min), as indicated in Table 4.2.

Table 4.2. Experimental design for the impregnation of menthol on cotton gauze using SC-CO$_2$ at 120 bar and 45 °C.

No.	Time (min)	Depressurization rate (bar/min)
1	30	6
2		60
3	300	6
4		60

At the end of the process, either a slow decompression rate (6 bar/min) or a fast depressurization rate (60 bar/min) was applied. The amount of impregnated menthol was determined gravimetrically by weighing the impregnated gauze on an analytical scale with an accuracy of ±0.0001 g. The menthol loading was calculated by the weight of menthol impregnated divided by the mass of raw cotton gauze using Equation 4.3. All experiments were conducted at least in duplicate to ensure reliability of the results.

$$Impregnation\ yield\ (\%) = \frac{m_f - m_i}{m_i} \times 100 \tag{4.3}$$

where, m_i and m_f are the masses of cotton gauze before and after the SC-CO$_2$ impregnation process, respectively.

4.2.4. Characterization of the menthol-impregnated cotton gauze by SC-CO$_2$

The impregnated cotton gauze was characterized using various methods, including color analysis, Fourier-transform infrared spectroscopy (FTIR), scanning electron microscopy (SEM), and thermogravimetric analysis (TGA). In the color analysis, the impregnated cotton gauze was examined for any visible changes in color or appearance. FTIR was used to identify any functional groups present in the impregnated gauze, while SEM provided insights into the surface morphology and microstructure. TGA was utilized to analyze the thermal stability and decomposition behavior of the impregnated cotton gauze.

4.2.4.1. Color

The color characteristics of the control cotton gauze and the SC-CO$_2$ menthol-impregnated cotton gauze were assessed using a Hunter lab colorimeter (CR-400/410, Konica Minolta, Ramsey, NJ, USA) following the ASTM D2244 method described by Billmeyer and Hammond (1990). Each sample was placed on a glass plate with a diameter of 60 mm. The colour values, including L (lightness), a (red to green), and b (blue to yellow), were recorded for both the control and menthol-impregnated cotton gauze.

To quantify the difference in colour between the control and menthol-impregnated cotton gauze, the colour difference (ΔE) was calculated using Equation (4.4):

$$\Delta E \ = \ \sqrt{(L^* - \ L)^2 + \ (a^* - \ a)^2 \ + \ (b^* - \ b)^2} \qquad\qquad (4.4)$$

where, L^*, a^*, and b^* represent the color parameters of the control cotton gauze, while L, a, and b represent the color parameters of the SC-CO$_2$ menthol-impregnated cotton gauze. L represents

darkness to lightness (0-100), *a* represents greenness to redness (-128 to +127), and *b* represents blueness to yellowness (-128 to +127).

4.2.4.2. Chemical structure by Fourier transform infrared spectroscopy

The FTIR spectra of both the control cotton gauze and the cotton gauze impregnated with menthol were obtained using a Nicolet iS50 spectrometer (ThermoFischer Scientific, Waltham, MA, USA) in the ATR mode. The spectra were recorded with a resolution of 2 cm^{-1} and covered the wavelength range of 500-4000 cm^{-1}, similar to the method employed by Zhao and Saldaña (2019). This analysis allowed for a detailed examination of the functional groups present in the impregnated cotton gauze compared to the control sample.

4.2.4.3 Morphology by scanning electron microscopy

The morphology of the original and menthol-impregnated cotton gauze by SC-CO_2 was analyzed with a scanning electron microscope (SEM) (Zeiss Sigma SEM, Carl Zeiss AG, Oberkochen, Germany) using methodology reported by Huerta and Saldaña (2018). Cotton gauze samples were placed on aluminum specimen stubs using double-sided adhesive carbon tape and coated with platinum. The photomicrographs were captured at an accelerating voltage of 20 kV.

4.2.4.4. Thermal stability by thermogravimetric analysis (TGA)

TGA was conducted using a TGA instrument (Q600 SDT, TA Instruments, USA) at a heating rate of 10 °C/min to assess the thermal stability of the gauze samples at different temperatures. A small amount of cotton gauze sample (~10 mg) was placed in a standard alumina crucible and positioned in the sample slot of the thermogravimetric analyzer. The analysis was carried out within a temperature range of 30-600 °C. Additionally, kinetic plots were generated using the thermogram data to determine the order of decomposition.

4.2.5. Statistical analysis

The data are presented as mean ± standard deviation, derived from a minimum of two independent experiments and analyses. Statistical analysis was performed using Minitab version 18.0 (Minitab Inc., State College, PA, USA), utilizing one-way analysis of variance (ANOVA) and Tukey's test for multiple comparisons of means at a significance level of $p < 0.05$ and a confidence interval of 95%.

4.3. Results and Discussion

4.3.1. Solubility of menthol in SC-CO$_2$

Fig 4.3 shows solubility data of menthol in SC-CO$_2$ at different temperature (45-55 °C) and pressure (100- 300 bar) conditions with SC-CO$_2$ densities ranging from 337.20 to 890.30 kg/m^3. The solubility of menthol significantly increased with increasing pressure from 100 to 200 bar for all isothermals. The solubility of menthol also significantly increased by decreasing temperature from 55 to 45 °C for all isobars from 100 to 200 bar as depicted in Fig. 4.3.

At a constant temperature of 45 °C, as the pressure increased from 100 to 200 bar, the solubility of menthol ranged from $9.20 \pm 0.19 \times 10^{-3}$ to $1.25 \pm 0.05 \times 10^{-2}$ mole fraction. However, at a constant pressure of 200 bar, as the temperature increased from 45 °C to 55 °C, the solubility of menthol significantly decreased from $1.25 \pm 0.05 \times 10^{-2}$ to $1.09 \pm 0.11 \times 10^{-2}$ mole fraction (See Table B2 in the appendix). These results indicated that higher pressure and lower temperature favoured the solubility of menthol in SC-CO$_2$. Saldaña et al. (1999) pointed out the retrograde behavior (a decrease in solubility with the increase in temperature) at pressures lower than 190 bar. This behaviour can be attributed to the increased density of CO$_2$ at a higher pressure of 200 and a lower temperature of 45 °C, providing more opportunities for interaction and dissolution of menthol

molecules. Additionally, lower temperatures reduced the kinetic energy of the system, allowing for stronger intermolecular interactions between menthol and CO_2.

Another factor that may contribute to the solubility was the change in CO_2 viscosity with pressure (See Table B2 in the appendix). The increased viscosity of SC-CO_2 at higher pressures may hinder the movement. According to the Fig. 4.3, the highest solubility was observed at 120 bar and 45 °C compared to other conditions. As a result, a temperature of 45 °C and a pressure of 120 bar, were selected for the impregnation process.
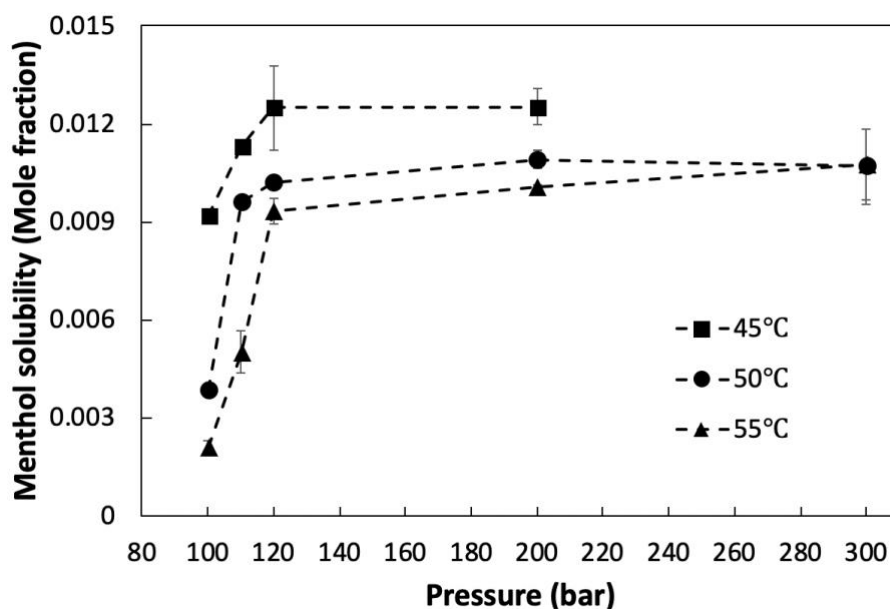
Fig. 4.3. Solubility of menthol in SC-CO_2 as a function of pressure and temperature.

In Table 4.3, the solubility of menthol in SC-CO_2 measured in this study was compared to the literature values reported in two studies that used dynamic methods (Galushko et al., 2006; Sovova and Jez, 1994).

At a temperature of 50 °C, the measured solubilities of menthol in SC-CO_2 in this study at pressures of 100 bar and 110 bar were $3.85 \pm 0.11 \times 10^{-3}$ and $9.62 \pm 0.03 \times 10^{-3}$ mole fraction, respectively. These values were consistent with the solubilities reported by Sovova and Jez (1994) and Galushko

et al. (2006) at similar conditions, demonstrating the accuracy and reliability of the solubility experimental results.

Table 4.3. Comparisons of menthol solubility in SC-CO_2 with published literature data.

Run	Temperature (°C)	Pressure (bar)	Solubility (mole fraction)	Sovova and Jez (1994)	Galushko et al. (2006)
1	45	100	$0.92\pm0.19\times10^{-2}$	1.09×10^{-2} (45°C, 99.1 bar)	
6	50	100	$3.85\pm0.11\times10^{-3}$	3.96×10^{-3} (50°C, 101.5 bar)	3.79×10^{-3} (50°C, 97.3 bar)
7	50	110	$9.62\pm0.03\times10^{-3}$	9.11×10^{-3} (50°C, 106.9 bar)	1.81×10^{-2} (50°C, 113.7 bar)
8	50	120	$1.02\pm0.02\times10^{-2}$		2.34×10^{-2} (50°C, 121.3 bar)
11	55	100	$2.10\pm0.21\times10^{-3}$	2.27×10^{-3} (55°C, 103.3 bar)	
12	55	110	$5.02\pm0.64\times10^{-3}$	5.10×10^{-3} (55°C, 109.8 bar)	
13	55	120	$9.33\pm0.41\times10^{-3}$	9.13×10^{-3} (55°C, 115.6 bar)	

The solubility of essential oil components in SC-CO_2 can vary widely depending on the molecular properties, such as polarity, molecular weight, and functional groups. Earlier, Milovanovic et al. (2013) reported the solubility of thymol in SC-CO_2 (9×10^{-4} – 1.47×10^{-2} mole fraction) at temperatures of 35, 40 and 50 °C and pressures ranging from 78 to 250 bar (SC-CO_2 density range 335.89–849.60kg/m^3) using a static method. This solubility range for thymol was almost similar to the solubility range of menthol in SC-CO_2, which may attribute to the similar molecular weight (menthol: 156.27 g/mol; thymol: 150.22 g/mol). Among other essential oils, Di Giacomo et al. (1989) investigated the solubility of limonene and citral in SC-CO_2 using a dynamic method under specific conditions of 95-100 bar and 35-50 °C. The results revealed that the solubility of limonene

varied within the range of 2.2×10^{-4} to 4.38×10^{-2} mole fraction, whereas the solubility of citral ranged from 3×10^{-5} to 2.23×10^{-2} mole fraction. Overall, limonene exhibited a higher solubility in SC-CO_2 compared to menthol, thymol, and citral, indicating its greater affinity for dissolving in SC-CO_2. Limonene has a relatively non-polar structure due to its hydrocarbon backbone, which is less hindered by polar functional groups. In contrast, menthol (hydroxy group), thymol (hydroxy group), and citral (aldehyde group) contain polar functional groups that can impede their interaction with the non-polar SC-CO_2. Additionally, the molecular weight (136.24 g/mol) of limonene may also play a role, as smaller molecules can more easily dissolve in SC-CO_2.

4.3.2. Preliminary studies on impregnation

In this preliminary study, the objective was to create peppermint essential oil-impregnated cotton gauze by loading peppermint powder and cotton gauze in the high-pressure vessel. Initially, peppermint powder was placed in a stainless-steel basket, while the cotton gauze was positioned above it, separated by a stainless-steel metal. However, the impregnation yield was very low due to the limited capacity of the stainless-steel basket, which accommodated only 3 g of powder, thus resulting in approximately 0.03 g of peppermint essential oil. Consequently, the impregnation yield was low. As a solution, pure menthol was employed to achieve the desired impregnation.

4.3.3. SC-CO_2 impregnation of menthol in cotton gauze

The impregnation process of menthol onto cotton gauze using SC-CO_2 involved the following steps: First, the SC-CO_2 acts as a solvent, allowing the dissolution of menthol. Next, the high menthol solubility in SC-CO_2 and exceptional diffusion properties of SC-CO_2 enable it to penetrate the cotton gauze matrix and allow interactions of menthol and cotton gauze. The dissolved menthol fills the void spaces within the cotton gauze, leading to its impregnation. The impregnation process continues for a specific duration to ensure sufficient contact between the menthol and the cotton

gauze. Lastly, the depressurization stage facilitates the transition of SC-CO_2 into gas and its removal from the cotton gauze. During this stage, the depressurization rate plays a crucial role in determining the impregnation yield. Rapid depressurization can result in the rapid expansion of trapped CO_2 and the formation of foam within the polymer, which can lead to undesirable structural polymer changes (Champeau et al., 2015). Therefore, impregnation time and depressurization rate need to be carefully controlled to optimize the impregnation process and achieve the desired level of impregnation.

Table 4.4. Impregnation yields of menthol into cotton gauze at different processing conditions.

No.	Time (min)	Depressurization rate (bar/min)	Impregnation yield (%)
1	30	6	11.15±1.49[c]
2		60	6.00±0.19[d]
3	300	6	30.65±1.03[a]
4		60	22.22±0.87[b]

[a-d] Different letters in the same column indicate significant differences ($p < 0.05$).

Table 4.4 presents the impregnation yields, calculated using Equation 4.3, for all the experimental conditions evaluated. Overall, significant menthol impregnation was achieved, resulting in impregnation yields ranging from 6% to 30.65%, depending on the specific process variables. The highest impregnation yield of 30.65% was obtained when employing a time duration of 300 min and a depressurization rate of 6 bar/min.

The different concentrations of menthol-loaded cotton gauze in this study can be applied in different areas. For example, 10% of menthol has been found effective in relieving thermal pain and itch sensation (Yosipovitch et al., 1996), while topical application of low concentrations of menthol (1-8% does-response) has been shown to increase blood flow in the cutaneous microvasculature (Craighead and Alexander, 2016). Additionally, a 5% menthol concentration has been reported to provide a strong cooling effect (Pergolizzi Jr et al., 2018). On the other hand, high

concentrations of menthol (>30%) can induce cold hyperalgesia in humans, making it a valuable tool for studying polyneuropathy (Pergolizzi Jr et al., 2018). The utilization of high concentrations of topical menthol (>30%) for causing cold hyperalgesia in human subjects has recently been demonstrated in research, providing a reliable model for assessing neuropathic pain features (Pergolizzi Jr et al., 2018).

Furthermore, the range of loading values obtained in this study was consistent with those reported in the literature for the impregnation of other compounds into cotton gauze. For example, previous studies reported loading values of thymol ranging from 1% to 19.6% (155 bar and 35 °C) on cotton gauze (Milovanovic et al., 2013), as well as loading values of thyme extract ranging from 1.1% to 8.9% (150 bar and 35 °C) on cotton gauze (Ivanović et al., 2014). However, Pajnik et al. (2017) reported a much lower impregnation yield (0.5% and 1%) for SC-CO_2-assisted impregnation of pyrethrum extract on cotton fabric as a tick repellent. The difference in loading can be attributed to the solubility variations of the compound or interest and application envisioned. Pajnik et al. (2017) selected impregnation conditions with the lowest solubility of pyrethrum extract to achieve the desired impregnation yield. This approach may have been influenced by regulatory guidelines set by the United States Environmental Protection Agency (1250 mg/m^2) and the German Federal Institute for Risk Assessments (1300 mg/m^2), which imposed limits on the concentration of permethrin in textiles.

In general, the impregnation time had a positive effect on the impregnation yield. The results presented in Table 4.4 demonstrated that increasing the time from 30 to 300 min led to a significant increase in the impregnation yield, ranging from 11.15% to 30.65% and from 6.00% to 22.22% at depressurization rates of 6 and 60 bar/min, respectively. This trend aligned with the findings of Pajnik et al. (2017), who observed an increase in impregnation yield of pyrethrum extract on cotton

fabric from 0.5% to 1% as the time increased from 1 to 2 h. Similarly, Rojas et al. (2018) conducted experiments using a 100 mL high-pressure cell with 1 g of thymol placed in a vial. They tested different impregnation times (30, 60, 120, 180, and 300 min) along with three CO_2 pressures (90, 120, and 150 bar) and two different depressurization rates (100 bar/min and 10 bar/min) at 40 °C. The study revealed that extending the impregnation time from 30 to 180 min at 90 bar and 40 °C resulted in an increased impregnation yield of thymol on LDPE-based nanocomposites (Low-density polyethene with organo-modified montmorillonite), showing a rise from 0.92% to 1.33%. Milovanovic et al. (2013) reported an impregnation yield of 19.6% for pure thymol on cotton gauze (17 threads/cm^2) using SC-CO_2 with a 24-h impregnation time, while they achieved a yield of 11% with a 2-h impregnation time. However, as stated by Rojas et al. (2020), the impregnation time was influenced by the diffusion process of the solute into the polymer matrix. This diffusion was determined by the diffusion coefficient, which is influenced by the affinity between the active compound and the polymer. The diffusion coefficient generally increases with pressure and temperature, indicating that the active compound can be absorbed or deposited more efficiently into the polymer matrix (Yu et al., 2011). The diffusion coefficient was determined by the concentration of the compound in the polymer, the thickness of the polymer, the concentration of the compound in SC-CO_2 and impregnation time (Rojas et al., 2018).

In terms of the effect of depressurization rate on impregnation yield, the results in Table 4.4 indicate that a low depressurization rate (6 bar/min) resulted in higher yields (11.15% or 30.65%) compared to a high depressurization rate (60 bar/min) at 120 bar and 45 °C.

This suggests that a slow depressurization rate can facilitate the absorption or deposition of menthol into the cotton gauze, so it is likely that menthol exhibited a greater affinity for cotton gauze than for CO_2. Earlier, Almeida et al. (2013) reported that the highest antioxidant activity

(678 µmol TEAC/g) of oregano essential oil (antioxidant, antimicrobial and anti-inflammatory properties) impregnated native sorghum and rice starch was achieved when using a low depressurization rate (0.83 bar/min). Similarly, Rojas et al. (2018) observed a higher impregnation of thymol (0.42%) on LDPE when employing a low depressurization rate (10 bar/min) compared to 0.26% impregnation at a depressurization rate of 100 bar/min. Also, Masmoudi et al. (2011) reported that the impregnation yield of cefuroxime sodium (antibiotics) on intraocular lenses (0.2%) was too low to be quantified gravimetrically at a rapid depressurization rate (few minutes). Conversely, when the solute exhibited a low affinity for the polymer, it can be readily removed from the matrix along with the CO_2. In such cases, a high depressurization rate promotes the trapping of the solute within the polymer (Champeau et al., 2015). For example, Dias et al. (2013) reported higher amounts (0.5%) of jucá extract with anti-inflammatory properties impregnated onto wound dressing polymers when employing a higher depressurization rate of 100 bar/min compared to 30 bar/min.

4.3.4. SC-CO_2 menthol-impregnated cotton gauze characterization

4.3.4.1. Colour

Table 4.5 shows the colour difference (ΔE) between the original cotton gauze and the menthol-impregnated cotton gauze under different SC-CO_2 impregnation conditions. Different impregnation conditions resulted in varying impregnation yields that corresponded to colour differences.

For example, impregnation times of 30 min and 300 min combined with depressurization rates of 6 bar/min and 60 bar/min, yielded different impregnation yields ranging from 6.00% to 30.65%. These different impregnation yields, in turn, led to varying ΔE ranging from 0.25 to 0.68. According to Hunter (1975), an ΔE value of around 0.3 indicates an excellent colour match, an ΔE

value of around 1 indicates a fair match, an ΔE value of around 2 indicates a poor match and an ΔE value of 3 or greater indicates an unsatisfactory match in the textile industry.

The measured ΔE values indicated that the colour difference between the SC-CO_2 menthol-impregnated cotton gauze and the original cotton gauze was < 1, indicating a good colour match. This low value is important in applications where maintaining the fabric's original colour is desired. These results suggested that the impregnation of menthol onto cotton gauze by SC-CO_2 had a minimal impact on the overall colour of the fabric. Also, it was observed that the higher impregnation yields of 30.65% and 22.22% resulted in slightly higher ΔE values of 0.68 and 0.65 compared to lower impregnation yields of 6.00% and 11.5% with the ΔE values of 0.30 and 0.25, respectively. This suggests that the incorporation of more menthol into the cotton gauze contributed to the non-significant change in colour.

For example, impregnation times of 30 min and 300 min combined with depressurization rates of 6 bar/min and 60 bar/min, yielded different impregnation yields ranging from 6.00% to 30.65%. These different impregnation yields, in turn, led to varying ΔE ranging from 0.25 to 0.68. According to Hunter (1975), an ΔE value of around 1 indicates a fair match, an ΔE value of around 2 indicates a poor match and an ΔE value of 3 or greater indicates an unsatisfactory match in the textile industry.

The measured ΔE values indicated that the colour difference between the SC-CO_2 menthol-impregnated cotton gauze and the original cotton gauze was < 1, indicating a good colour match. This low value is important in other applications where maintaining the original colour is desired. These results suggested that the impregnation of menthol onto cotton gauze by SC-CO_2 had a minimal impact on the overall colour of the fabric. Also, it was observed that the higher impregnation yields of 30.65% and 22.22% resulted in slightly higher ΔE values of 0.68 and 0.65

compared to lower impregnation yields of 6.00% and 11.5% with the ΔE values of 0.30 and 0.25, respectively. This suggests that the incorporation of more menthol into the cotton gauze contributed to the non-significant change in colour.

Table 4.5. Colour measurement of menthol-impregnated cotton gauze with SC-CO$_2$ and colour difference from original cotton gauze.

Experimental condition	Colour			ΔE
	L	a	b	
30 min and	83.11	-0.58	3.07	0.30 ± 0.16^a
6 bar/min	83.54	-0.32	2.74	
30 min and	83.45	-0.4	3.09	0.25 ± 0.02^a
60 bar/min	83.53	-0.5	3.04	
300 min and	83.46	-0.42	3.55	0.68 ± 0.02^a
6 bar/min	84.04	-0.43	3.03	
300 min and 60	83.47	-0.47	3.7	0.65 ± 0.28^a
bar/min	83.32	-0.41	3.3	

[a]The same letter in the ΔE column indicates no significant color difference (p>0.05). *L* (0-100): darkness to lightness; *a* (-128-127): greenness to redness; *b* (-128-127): blueness to yellowness.

4.3.4.2. Structural analysis by Fourier transform infrared spectroscopy

Fig. 4.4 shows the FT-IR spectra of pure cellulose (A1), original cotton gauze (A2), menthol (B1) and the SC-CO$_2$ menthol-impregnated cotton gauze (B2) to understand any potential changes in chemical structure. The FT-IR results revealed characteristic peaks in the spectrum of the original cotton gauze (90-95% of cellulose) (Fig. 4.4 (A2)) that corresponded to different functional groups present in cellulose (Fig. 4.4 (A1)), the main component of cotton gauze. For instance, a broad peak at 3340 cm^{-1} indicated O-H stretching, while a peak at 2912 cm^{-1} represented asymmetric stretching of C-H bonds (Chung et al., 2004). Other observed peaks included C-H plane bending, deformation stretch, and wagging vibrations at 1410, 1368, and 1341 cm^{-1}, respectively (Milovanovic et al., 2013). The peak at 1243 cm^{-1} originated from plane bending vibrations of C-H bonds, while peaks at 1085 and 1054 cm^{-1} indicated the presence of asymmetric bridge C-O-C bonds (Chung et al., 2004). The peak at 1015 cm^{-1} corresponded to C-O stretching vibrations, and

the peak at 898 cm^{-1} indicated the presence of β-glucosidic bonds (C_1-O-C_4) in the cellulose structure. Additionally, absorbed water was detected at 1715 cm^{-1}. Overall, the observed FT-IR bands in the original cotton gauze were consistent with the expected spectral features reported in the literature (Chung et al., 2004).

Fig. 4.4 (B1) shows the FT-IR spectrum of menthol, where the peak at 3253 cm^{-1} indicated O-H stretching vibrations of the hydroxyl group in the menthol molecule, while peaks at 2868 and 2929 cm^{-1} represented C-H stretching vibrations of the methyl group (Al-Bayati, 2009). In addition, the peaks at 1368 and 1445 cm^{-1} were attributed to C-H bending vibrations of the isopropyl group, and the peaks at 1025 and 1043 cm^{-1} suggested the presence of C-O stretching vibrations (Mathur et al., 2011).

In Fig. 4.4 (B2), the FT-IR analysis of the menthol-impregnated cotton gauze samples at different impregnation conditions particularly at 300 min and 6 bar/min or 60 bar/min revealed specific peaks at wavenumbers of 1025, 1043, 1368, 1445, 2868, 2929, and 3253 cm^{-1}. These peaks were associated with various vibrational modes related to the presence of menthol (Fig. 4.4 (B1)) in the samples. These specific peaks provided evidence of the successful impregnation of menthol onto the cotton gauze by SC-CO_2. However, for the samples impregnated with 30 min and 6 bar/min, and 60 bar/min, no significant shifts or distinct peaks were observed compared to the control cotton gauze. This behaviour suggests that the impregnation process may not have caused significant changes in the chemical structure of the SC-CO_2 menthol impregnated cotton gauze at these specific conditions. These results were in agreement with the low values obtained for ΔE during the 30-min impregnation process at different depressurization rates of 6 and 60 bar/min (Table 4.5).
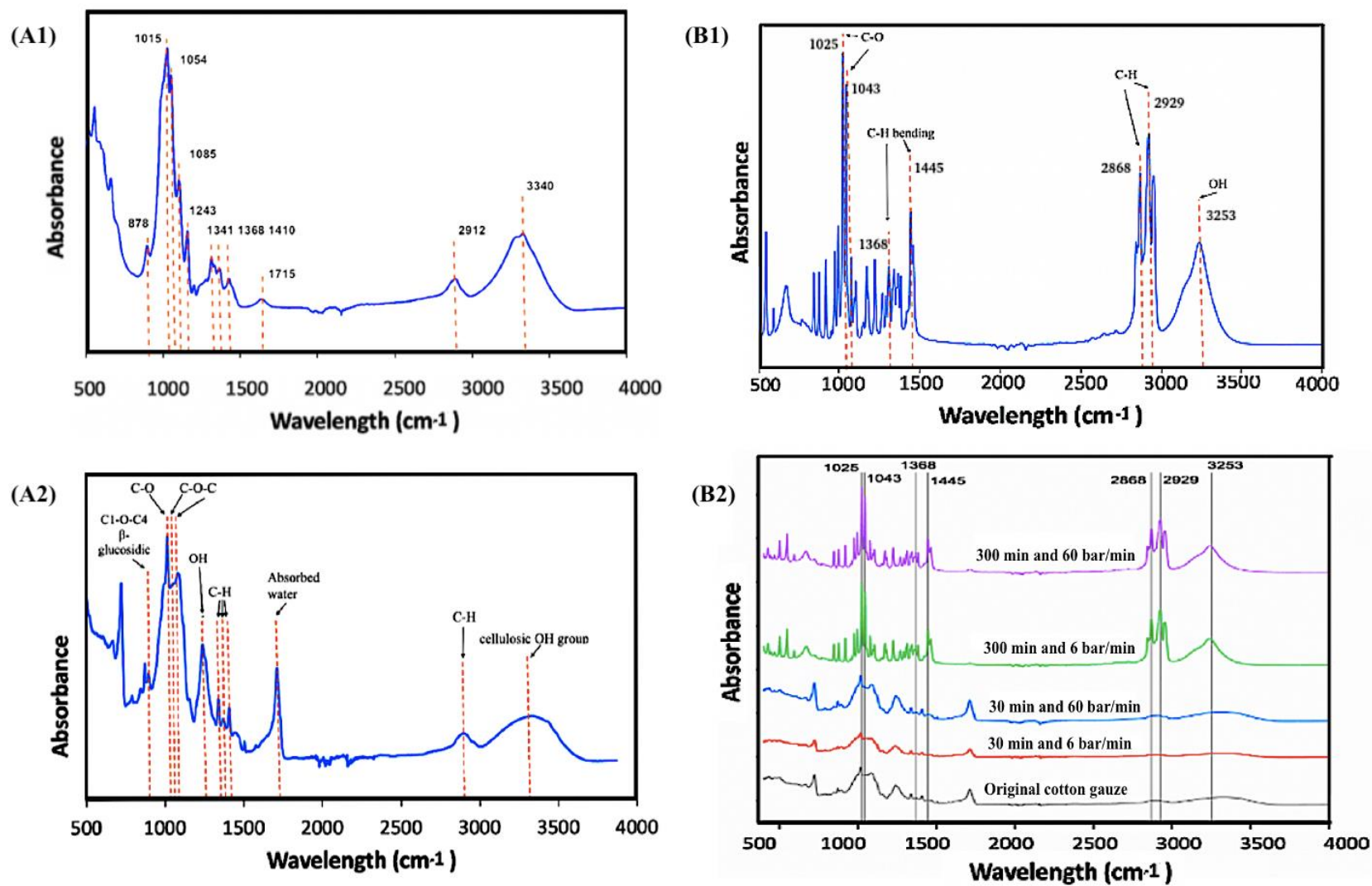
Fig. 4.4. FT-IR spectra of (A1) pure cellulose, (A2) original cotton gauze, (B1) pure menthol and (B2) SC-CO$_2$ menthol-impregnated cotton gauze at 120 bar and 45 °C.

4.3.4.3. Morphology of impregnated cotton gauze by scanning electron microscope

Fig. 4.5 displays scanning electron micrographs of original cotton gauze, SC-CO$_2$ 6% menthol-impregnated, and SC-CO$_2$ 30.65% menthol-impregnated cotton gauze samples at a magnification of 300X. While the presence of menthol crystallites on the cotton surface was not visible as discussed earlier in Table 4.5 by the low ΔE values (<1), noticeable changes in the fibre morphology were evident.
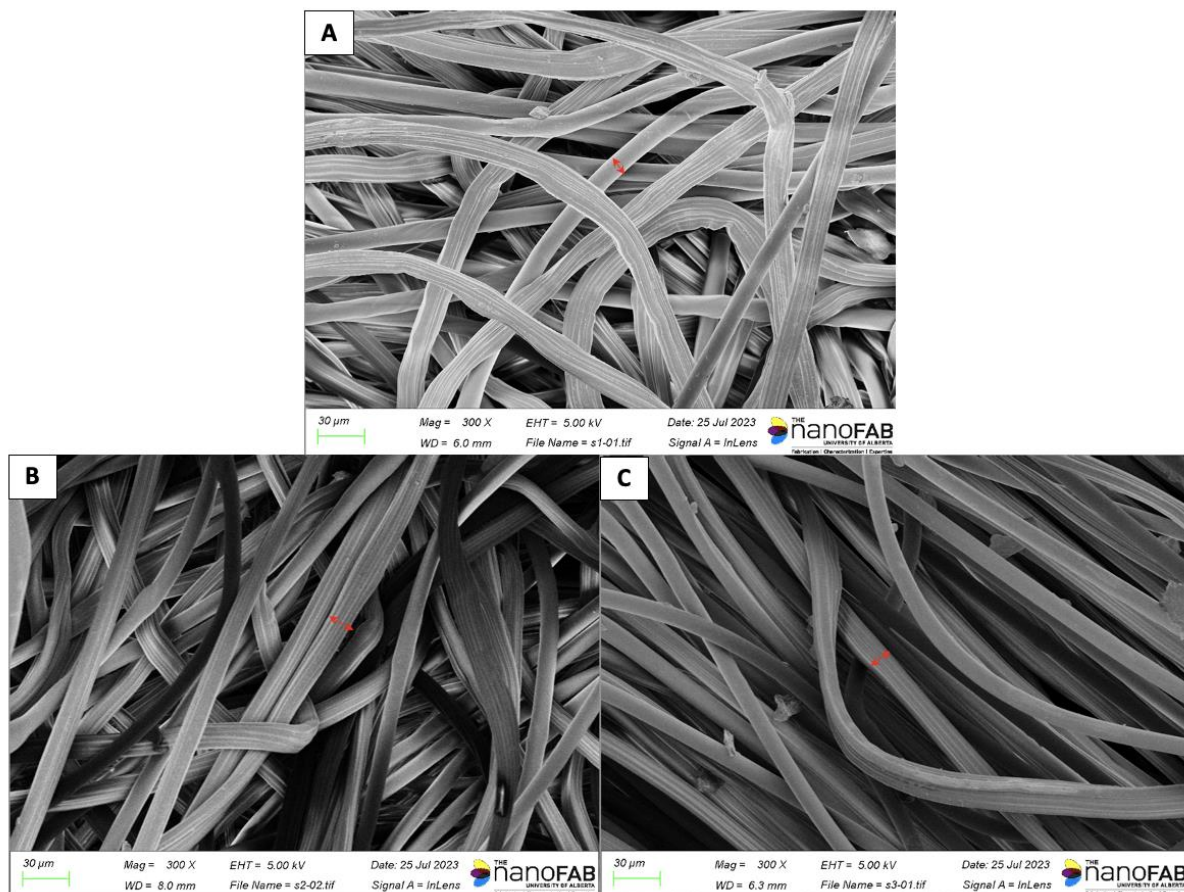
Fig. 4.5. SEM images of cotton gauze: (A) Original cotton gauze, (B) SC-CO$_2$ 6% menthol-impregnated cotton gauze, and (C) SC-CO$_2$ 30.65% menthol-impregnated cotton gauze.

Previous research by Milovanovic et al. (2013) highlighted the formation of fine wrinkles running parallel to the cotton fibre axis and an increase in specific surface areas on thymol-impregnated

cotton gauze with a depressurization rate of 3.3 bar/min. A similar phenomenon of wrinkle formation was observed in this study, following the treatment of cotton gauze with SC-CO$_2$ for menthol impregnation (Fig. 4.5B and C). This formation of wrinkles can be attributed to the degasification speed between the surface and interior of the cotton fibres during the depressurization step, leading to differential shrinkage between these two segments (Milovanovic et al., 2013). The formation of large pleat-like wrinkles (1 μm wide) on the surface of cotton due to the SC-CO$_2$ treatment was also confirmed by Katayama et al. (2012), who modified the surface of cotton by SC-CO$_2$ treatment. They observed that SC-CO$_2$ promoted the formation of large pleat-like wrinkles in the cotton at 200 bar and 40 °C with treating times of 60 min and a rapid depressurization rate of 8 bar/min.

Furthermore, Rashmi et al. (2020) observed an increase in the thickness of cotton fibres in grafted and iodine-loaded cotton gauze, resulting in a straighter appearance and improved absorbency of exudates, making it a convenient dressing option for wound healing. This study aligns with these findings, as the SC-CO$_2$ 33.65% menthol-impregnated cotton gauze exhibited more straightened fibres (Fig. 4.5 C), while the original cotton gauze showed a more bent structure (Fig. 4.5 A). Furthermore, the fibre thickness of SC-CO$_2$ menthol-impregnated cotton gauze increased to 15 μm, compared to the original cotton gauze thickness of 10 μm, as measured using the scale.

4.3.4.4. Thermal stability by thermogravimetric analysis

Thermal analysis was conducted using TGA to examine the thermal stability and decomposition behaviour of SC-CO$_2$ menthol-impregnated cotton gauze in comparison to the original cotton gauze. As depicted in Fig 4.6, the weight of the original cotton gauze displayed minimal loss (approximately 5%) in the temperature range of 30-80 °C, primarily attributed to the dehydration of cellulose fibres (Rashmi et al., 2020). However, beyond 300 °C, a single decomposition

characteristic of polysaccharides was observed in the original cotton gauze, due to the rapid breakdown of cellulose and the release of degradation products (Ciftici and Saldaña, 2015). Additionally, the residual weight of the original cotton gauze, after reaching 450 °C and up to 600 °C, remained relatively constant at approximately 10% (Hiriart-Ramírez et al., 2012).
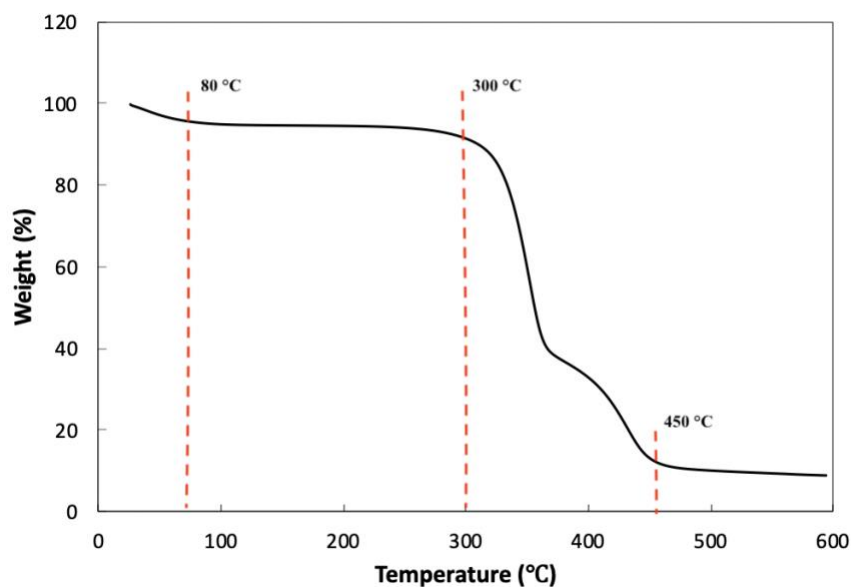
Fig. 4.6. Thermal analysis by TGA of original cotton gauze.

The iodine-loaded cotton gauze showed a different decomposition, including three stages (Rashmi et al., 2020). The initial stage involved the dehydration of cellulosic fibers, followed by the second stage (95-220 °C) where carbonization of cellulosic fibers took place. In the final stage (220-386 °C), there was a weight loss of approximately 40% due to the destruction of bonds in the poly(N-vinylpyrrolidone)-iodine complex and the intermolecular bonds of poly(N-vinylpyrrolidone).

Recently, Romero-Fierro et al. (2022) reported the difference in decomposition stages between original cotton gauze and poly (acrylic acid) and poly (methacrylic acid)-loaded cotton gauzes. The modified gauzes underwent four weight losses at different decomposition stages. The first loss

111

(30-100 °C) was due to the dehydration of grafted carboxylic groups, the second stage (200-350 °C) involved decarboxylation processes, the third stage was related to the decomposition of the cellulose polymeric matrix, and the fourth stage (above 380 °C) corresponded to the complete decomposition of the graft polymer residue with the formation of various residue products like anhydrous rings.

4.4. Conclusion

The solubility of menthol in SC-CO$_2$ was investigated under varying temperature and pressure conditions. The highest solubility of menthol in SC-CO$_2$ was 1.25×10^{-2} at 120 bar and 45 °C, while the lowest solubility of menthol in SC-CO$_2$ was 5.02×10^{-3} at 110 bar and 55 °C. Overall, the results demonstrated that high pressures up to 200 bar and lower temperatures favoured the solubility of menthol in SC-CO$_2$, which can be attributed to the increased density of CO$_2$ and stronger intermolecular interactions at lower temperatures. However, at pressures above 200 bar and a temperature of 45 °C, the solubility of menthol decreased due to the saturation effect and changes in CO$_2$ viscosity.

At the conditions of the highest solubility of menthol, the SC-CO$_2$ impregnation of menthol onto cotton gauze was successful, achieving impregnation yields ranging from 6 to 30.65% under different processing conditions (30 min and 300 min, and depressurization rates of 6 bar/min and 60 bar/min). The impregnation process involved dissolution, penetration, and interaction between menthol and the cotton gauze, and the impregnation yield was influenced by the impregnation time and depressurization rate. Based on the results, it was observed that a longer impregnation time of 300 min and a slow depressurization rate of 6 bar/min resulted in a higher impregnation yield of 30.65%.

The characterization of the modified cotton gauze revealed that the SC-CO$_2$ menthol impregnation had minimal impact on the colour of the cotton gauze, as indicated by low colour differences. Fourier transform infrared spectroscopy and scanning electron microscopy confirmed the presence of menthol in the impregnated samples, and SEM showed the formation of wrinkles on the cotton surface.

In addition, the thermal analysis revealed the decomposition behaviour of the original cotton gauze, which displayed different weight loss stages associated with the dehydration and degradation of cellulose fibres.

Overall, this study provided valuable insights into the solubility behaviour of menthol in SC-CO$_2$ at 100-300 bar and 45-55 °C and the successful impregnation process onto cotton gauze with different yields, depending on the further potential application. These findings can have implications for various applications, including wound dressings and textile treatments.

Chapter 5: Conclusions and Recommendations

5.1. Conclusions

Peppermint (*Mentha × piperita*) is a perennial herb from the Lamiaceae family, cultivated worldwide. Its essential oil is characterized by a pale yellow colour and refreshing flavour, due to its distinct profile of monoterpenes like menthol and menthone. Among the more than 30 compounds found in peppermint essential oil, menthol (35-60%) and menthone (15-30%) are the main compounds (Nair, 2001). Menthol serves as an important food additive at 4 mg/kg body weight for imparting cooling and refreshing sensations to various food and beverage products (Trident mint gum, Halls, Celestial seasonings mint magic herbal tea). Moreover, menthol finds applications as a medicinal compound in topical analgesic and anti-inflammatory products (Binder et al., 2011), and as a fragrance compound valued for its strong and recognizable minty aroma. On the other hand, menthone possesses antibacterial, antioxidant, anti-inflammatory, and antiviral properties (Chen et al., 2022).

To extract peppermint essential oil in an environmentally friendly manner while maintaining its quality and purity, SC-CO_2 extraction was employed. Furthermore, SC-CO_2 was utilized as a solvent for impregnating menthol onto cotton gauze.

In the first study of this thesis research, the extraction of peppermint essential oil was conducted using SC-CO_2 with(out) co-solvents such as ethanol, acetone, and isopropyl acetate. Various extraction processing parameters, namely pressure (ranging from 100 to 400 bar), temperature (45-55 °C), CO_2 flow rate (0.5 and 3 mL/min), extraction time (15-180 min), and co-solvent type (ethanol, acetone, and isopropyl acetate), were investigated to assess their influence on the yield and quality of the extracted essential oil. Gas chromatography analysis was employed to characterize the extracts and determine their quality. Additionally, a scale-up study was conducted

using a larger extraction vessel (300 mL) while maintaining the same CO_2/feed mass ratio of 78. Finally, the antioxidant properties of the essential oil were evaluated.

The peppermint leaves were initially processed into a fine powder with particle sizes of 0.5 mm, to facilitate SC-CO_2 extraction under various processing conditions. The SC-CO_2 extraction process comprised three distinct stages. In the initial stage, the solubility of the desired compound in SC-CO_2 played a dominant role. As the extraction progressed into the intermediate stage, both solubility and mass transfer mechanisms became crucial, allowing SC-CO_2 to penetrate deeper layers of the peppermint leaves to extract more essential oil. Finally, in the last stage, mass transfer mechanisms primarily governed the extraction process.

Considering these principles, the extraction time was evaluated for two different equipment setups (equipment 1 and equipment 2), resulting in 180 min and 120 min as the respective optimal extraction times. Subsequent investigations focused on exploring the impact of pressure, temperature, co-solvent usage, and flow rate on the yield and quality of essential oil while maintaining a constant extraction time.

Under constant temperature conditions (50 °C), an increase in pressure from 100 bar to 400 bar resulted in a significant rise in yield from 0.06% to 0.34%. However, this increase in pressure also caused a significant decrease in menthol content from 28.85% to 4.48%, while the menthone content increased from 0.04% to 0.10%. The rise in pressure led to an increase in the density and solvating power of SC-CO_2, which enhanced its ability to penetrate the peppermint leaves and extract essential oil.

Regarding temperature, at constant pressure, an increase in temperature led to a decrease in the density of SC-CO_2, affecting its ability to carry essential oil from the peppermint. Additionally, the density of essential oil decreased with rising temperature. Simultaneously, high extraction

temperatures increased the kinetic energy of essential oil molecules, resulting in a high sublimation pressure and an increased likelihood of evaporation. Consequently, the effect of temperature on extraction yield depended on the interplay of these competing factors. The most favourable conditions for extraction were 110 bar and 50 °C, which yielded 0.16% essential oil with good menthol content (38.85%) and menthone content (0.06%).

The addition of co-solvents (ethanol, acetone, or isopropyl acetate) to improve SC-CO_2 extraction led to increased yields, primarily due to changes in polarity, surface interactions, matrix accessibility, and desorption kinetics of compounds. Among the evaluated co-solvents, acetone yielded the highest extraction result (0.76%), surpassing neat CO_2 extraction by more than three times (0.16%) at 50 °C and 110 bar with a CO_2 flow rate of 0.5 mL/min. All three co-solvents resulted in a significant increase in the menthone content, ranging from 0.06% to 0.50%, and a significant decrease in menthol content, with values ranging from 38.85% to 18.62% in the extracted essential oil. These findings indicated the potential use of co-solvents for the fractionation of peppermint essential oil.

Also, increasing the CO_2 flow rate from 0.5 mL/min to 3 mL/min resulted in higher extraction yields of 0.16% to 0.71% at a constant temperature and pressure of 110 bar and 50 °C, respectively. This improvement in yield can be attributed to an enhanced mass transfer coefficient, which reduced mass transfer resistance through increased convection. However, a high flow rate also led to an increase in linear velocity, potentially reducing extraction efficiency by decreasing the contact between the supercritical fluid and the peppermint. As a result, the net effect of these competing factors determined whether the flow rate ultimately led to an increase or decrease in extraction yield.

The successful scale-up of the SC-CO_2 extraction of essential oil from *Mentha × piperita* involved increasing the peppermint powder loading by 3-fold, 5-fold, and 10-fold compared to the laboratory-scale extraction. The scale-up experiments resulted in slightly higher extraction yields (0.94%, 0.79%, and 0.77%) compared to the laboratory-scale extraction (0.71%). Additionally, the menthol content remained consistent, with a significant decrease in menthone content.

The antioxidant property of peppermint essential oil was evaluated at various concentrations (50 mg/mL, 100 mg/mL, 200 mg/mL, and 500 mg/mL) using DPPH scavenging activity. The results demonstrated a concentration-dependent increase in antioxidant activity, indicating that higher concentrations of peppermint essential oil corresponded to higher antioxidant activity.

In the second study of this thesis research, the solubility of menthol in SC-CO_2 was examined across a range of temperature (45-55 °C) and pressure conditions (100-300 bar). The objective was to impregnate menthol onto cotton gauze using SC-CO_2, with different impregnation times (30 or 300 min) and depressurization rates (6 or 60 bar/min). Then, the original cotton gauze and menthol-impregnated cotton gauze were subjected to analysis using colour assessment, FT-IR, SEM, and TGA.

The solubility of menthol showed an increase with rising pressure from 100 to 200 bar, as well as a decrease when temperature increasing from 45 to 55 °C. This behaviour was attributed to the higher density of CO_2 at these conditions, facilitating extensive interaction and dissolution of menthol molecules. Ultimately, a solubility value of 1.25×10^{-2} mole fraction at 120 bar and 45 °C was selected as the optimal condition for the impregnation process.

The highest impregnation yield (30.65%) was achieved with an impregnation time of 300 min and a depressurization rate of 6 bar/min. The slow depressurization rate promoted the absorption or

deposition of menthol into the cotton gauze effectively. However, the different percentages of menthol obtained through various processing parameters offer versatility for different applications. The menthol-impregnated cotton gauze with a concentration of 6% can offer a robust cooling effect. At an impregnation concentration of 11.15%, the menthol-impregnated gauze can alleviate thermal pain and itch sensations. Meanwhile, the cotton gauze impregnated with 30.65% menthol concentration can induce cold hyperalgesia in individuals.

In the characterization of cotton gauze, it was observed that incorporating a larger amount of menthol into the cotton gauze did not result in a significant change in colour. The FT-IR analysis provided evidence of successful menthol impregnation onto the cotton gauze, as indicated by the presence of specific peaks corresponding to the hydroxyl (3253 cm^{-1}), methyl (2868, and 2929 cm^{-1}), and isopropyl (1368, and 1445 cm^{-1}) groups of menthol.

Furthermore, SEM analysis revealed noticeable alterations in the cotton gauze morphology, with the appearance of wrinkles after impregnation with menthol. Additionally, the decomposition behavior of the menthol-impregnated cotton gauze differed from that of the original cotton gauze. Typically, the decomposition of the original cotton gauze involved processes such as cellulose dehydration, breakdown, and the release of dehydrated cellulose. In contrast, the impregnated cotton gauze exhibited a different decomposition pathway, involving the breakdown of chemical bonds of menthol, leading to the volatilization of menthol molecules.

The results of this investigation demonstrated the immense potential of SC-CO$_2$ as a highly promising technique for extracting peppermint essential oil with exceptional quality and purity, making it a practical choice for applications in the food and pharmaceutical industries. Moreover, SC-CO$_2$ proved to be an effective solvent for impregnating menthol, the main component of peppermint essential oil, into cotton gauze, thereby enabling diverse applications. The menthol-

impregnated cotton gauze holds promise for applications in wound dressing and textile treatment. In conclusion, this research has successfully accomplished its objectives, revealing the valuable contributions of SC-CO$_2$ in essential oil extraction and menthol impregnation, with potential implications for various industrial sectors. This research represents the initial endeavor to scale up the extraction of peppermint essential oil and the impregnation of menthol into cotton gauze.

5.2. Recommendations and future work

Some recommendations to advance research of Chapter 3 are:

- Investigate the impact of particle size on extraction yield by varying the size of peppermint leaves to 0.25 mm and 1 mm. This will provide valuable insights into the influence of particle size on the efficiency of SC-CO$_2$ extraction. The current study in Chapter 3 employed a particle size of 0.5 mm.

- Explore the extraction of other valuable compounds present in peppermint essential oil, such as 1,8-cineole (eucalyptol) at ~C$18/mL and menthyl acetate at ~C$5/mL, to further enrich the understanding of the essential oil's composition and potential health benefits associated with these additional components. Eucalyptol is recognized for its capacity to promote respiratory well-being, whereas menthyl acetate is acknowledged for its ability to alleviate digestive discomfort.

- Conduct a comprehensive assessment of the stability of essential oil by observing physical appearance, monitoring odour changes, analyzing chemical composition through techniques like GC-MS, measuring the refractive index, and exposing the essential oil to different conditions (e.g., temperature, light, air) to observe any changes. Also, evaluate the shelf life of the extracted essential oil under different storage conditions, including

room temperature (22 °C), refrigeration (4 °C), and freezing (-18 °C) to provide information on the longevity and quality of the extracted essential oil over time.

- Consider scaling up the extraction process beyond the 300 mL level, such as 1 L, 10 L, or even at industrial scale (20 L), to assess the feasibility and reliability of the findings on a larger scale.

- Explore the fractionation of specific components within peppermint essential oil, such as menthol and menthone, by employing varying pressure and temperature conditions.

Some recommendations to advance research of Chapter 4 are:

- Assess the oxygen permeability of the menthol-impregnated cotton gauze, particularly for wound dressing applications, using a permeometer under controlled conditions of room temperature and 100% relative humidity. Additionally, conducting water vapor sorption studies to understand the gauze's moisture management properties involved exposing dried samples to an atmosphere of 95% RH (at 23 °C) in a desiccator containing a potassium sulfate saturated solution. The samples can then be periodically weighed to measure water vapor sorption loading.

- Explore the antimicrobial activity of the menthol-impregnated cotton gauze by evaluating its effectiveness against gram-negative bacteria *E. coli*, gram-positive bacterial strains *S. aureus*, and fungus *Candida albicans*. This will provide valuable insights into its potential as a wound dressing with antimicrobial properties.

- Conduct *in vitro* studies to investigate the potential cytotoxic effects of the menthol-impregnated gauze on specific cell lines (dermal fibroblasts or keratinocytes) relevant to the intended application, using established cell viability assays such as MTT or cell

counting methods. This assessment will help determine the safety and biocompatibility of the gauze for medical applications.

- Explore the applications in other fields like menthol-impregnated food packaging (PLA film) and menthol-impregnated pillows as aromatherapy to relieve stress.

References

Abourehab, M. A., Alsubaiyel, A. M., Alshehri, S., Alzhrani, R. M., Almalki, A. H., Abduljabbar, M. H., Venkatesan, K., and Kamal, M. (2022). Laboratory determination and thermodynamic analysis of alendronate solubility in supercritical carbon dioxide. *Journal of Molecular Liquids*, 367, 120242. https://doi.org/10.1016/j.molliq.2022.120242.

Ahmed, E. M. (2015). Hydrogel: Preparation, characterization, and applications: A review. *Journal of Advanced Research*, 6(2), 105-121. https://doi.org/10.1016/j.jare.2013.07.006.

Al-Bayati, F. A. (2009). Isolation and identification of antimicrobial compound from *Mentha longifolia L.* leaves grown wild in Iraq. *Annals of Clinical Microbiology and Antimicrobials*, 8, 1-6. DOI: 10.1186/1476-0711-8-20.

Albuquerque, C. L., and Meireles, M. A. A. (2012). Defatting of annatto seeds using supercritical carbon dioxide as a pretreatment for the production of bixin: experimental, modeling and economic evaluation of the process. *The Journal of Supercritical Fluids*, 66, 86-95. https://doi.org/10.1016/j.supflu.2012.01.004.

Alghoul, Z. M., Ogden, P. B. and Dorsey, J. G. (2017). Characterization of the polarity of subcritical water. *Journal of Chromatography A*, 1486, 42-49. https://doi.org/10.1016/j.chroma.2016.12.072.

Almeida, A. P., Rodríguez-Rojo, S., Serra, A. T., Vila-Real, H., Simplicio, A. L., Delgadilho, I., da Costa, S.B., da Costa, L.B., Nogueira, I.D., and Duarte, C. M. (2013). Microencapsulation of oregano essential oil in starch-based materials using supercritical fluid technology. *Innovative Food Science & Emerging Technologies*, 20, 140-145. https://doi.org/10.1016/j.ifset.2013.07.009.

Alvarado, N., Romero, J., Torres, A., de Dicastillo, C. L., Rojas, A., Galotto, M. J., and Guarda, A. (2018). Supercritical impregnation of thymol in poly (lactic acid) filled with electrospun poly (vinyl alcohol)-cellulose nanocrystals nanofibers: Development an active food packaging material. *Journal of Food Engineering*, 217, 1-10. https://doi.org/10.1016/j.jfoodeng.2017.08.008.

Ansari, K. and Goodarznia, I. (2012). Optimization of supercritical carbon dioxide extraction of essential oil from spearmint (*Mentha spicata L.*) leaves by using Taguchi methodology. *The Journal of Supercritical Fluids*, 67, 123-130. https://doi.org/10.1016/j.supflu.2012.03.011.

Arango-Ruiz, Á., Martin, Á., Cosero, M.J., Jiménez, C. and Londoño, J. (2018). Encapsulation of curcumin using supercritical antisolvent (SAS) technology to improve its stability and solubility in water. *Food Chemistry*, 258, pp.156-163. https://doi.org/10.1016/j.foodchem.2018.02.088.

Aredo, V., Bittencourt, G. M., Pallone, E. M. D. J. A., Guimarães, F. E. C. and de Oliveira, A. L. (2021). Formation of edible oil-loaded beeswax microparticles using PGSS–Particles from Gas-Saturated Solutions. *The Journal of Supercritical Fluids*, 169, 105106. https://doi.org/10.1016/j.supflu.2020.105106.

Asl, A. H. and Khajenoori, M. (2013). Subcritical water extraction. *Mass Transfer-Advances in Sustainable Energy and Environment Oriented Numerical Modeling*, 17, 459-487. DOI: 10.5772/54993.

Aydi, A., Zibetti, A.W., Al-Khazaal, A.Z., Eladeb, A., Adberraba, M. and Barth, D. (2020). Supercritical CO_2 extraction of extracted oil from *Pistacia lentiscus* L.: mathematical modeling, economic evaluation and scale-up. *Molecules*, 25(1), 199. https://doi.org/10.3390/molecules25010199.

Azwanida, N. N. (2015). A review on the extraction methods use in medicinal plants, principle, strength and limitation. *Medicinal Aromatic Plants*, 4(196), 2167-0412. DOI: 10.4172/2167-0412.1000196.

Bakkali, F., Averbeck, S., Averbeck, D., and Idaomar, M. (2008). Biological effects of essential oils–a review. *Food and Chemical Toxicology*, 46(2), 446-475. https://doi.org/10.1016/j.fct.2007.09.106.

Barbieri, C. and Borsotto, P. (2018). Essential oils: market and legislation. *Potential of Essential Oils*, 107-127. DOI: 10.5772/intechopen.77725.

Bastaki, S. M., Adeghate, E., Amir, N., Ojha, S., and Oz, M. (2018). Menthol inhibits oxidative stress and inflammation in acetic acid-induced colitis in rat colonic mucosa. *American Journal of Translational Research*, 10(12), 4210. PMID: 30662664; PMCID: PMC6325525.

Bastante, C. C., Cardoso, L. C., Serrano, C. M., and de la Ossa, E. M. (2017). Supercritical impregnation of food packaging films to provide antioxidant properties. *The Journal of Supercritical Fluids*, 128, 200-207. https://doi.org/10.1016/j.supflu.2017.05.034.

Barton, P., Hughes Jr, R.E. and Hussein, M.M. (1992). Supercritical carbon dioxide extraction of peppermint and spearmint. *The Journal of Supercritical Fluids*, 5(3), 157-162. https://doi.org/10.1016/0896-8446(92)90002-2.

Baylac, S., and Racine, P. (2003). Inhibition of 5-lipoxygenase by essential oils and other natural fragrant extracts. *International Journal of Aromatherapy*, 13(2-3), 138-142. https://doi.org/10.1016/S0962-4562(03)00083-3.

Bensebia, O., Barth, D., Bensebia, B., and Dahmani, A. (2009). Supercritical CO_2 extraction of rosemary: Effect of extraction parameters and modelling. *The Journal of Supercritical Fluids*, 49(2), 161-166. https://doi.org/10.1016/j.supflu.2009.01.007.

Berna, A., Tárrega, A., Blasco, M., and Subirats, S. (2000). Supercritical CO_2 extraction of essential oil from orange peel; effect of the height of the bed. *The Journal of Supercritical Fluids*, 18(3), 227-237. https://doi.org/10.1016/S0896-8446(00)00082-6.

Betoret, N., Puente, L., Dıaz, M.J., Pagan, M.J., Garcıa, M.J., Gras, M.L., Martínez-Monzó, J. and Fito, P. (2003). Development of probiotic-enriched dried fruits by vacuum impregnation. *Journal of Food Engineering*, 56(2-3), 273-277. https://doi.org/10.1016/S0260-8774(02)00268-6.

Billmeyer Jr, F. W., and Hammond III, H. K. (1990). ASTM standards on color-difference measurements. *Color Research & Application*, 15(4), 206-209. https://doi.org/10.1002/col.5080150406.

Binder, A., Stengel, M., Klebe, O., Wasner, G., and Baron, R. (2011). Topical high-concentration (40%) menthol—somatosensory profile of a human surrogate pain model. *The Journal of Pain*, 12(7), 764-773. https://doi.org/10.1016/j.jpain.2010.12.013.

Bouyahya, A., Mechchate, H., Benali, T., Ghchime, R., Charfi, S., Balahbib, A., Burkov, P., Shariati, M. A., Lorenzo, J. M. and Omari, N. E. (2021). Health benefits and pharmacological properties of carvone. *Biomolecules*, 11(12), 1803. doi: 10.3390/biom11121803.

Çam, M., Yüksel, E., Alaşalvar, H., Başyiğit, B., Şen, H., Yılmaztekin, M., Ahhmed, A. and Sağdıç, O. (2019). Simultaneous extraction of phenolics and essential oil from peppermint by pressurized hot water extraction. *Journal of Food Science and Technology*, 56(1), 200-207. DOI: 10.1007/s13197-018-3475-5.

Cao, J., Wang, P., Liu, Y., Zhu, C. and Fan, D. (2020). Double crosslinked HLC-CCS hydrogel tissue engineering scaffold for skin wound healing. *International Journal of Biological Macromolecules*, 155, 625-635. DOI: 10.1016/j.ijbiomac.2020.03.236.

Carlson, L. H. C., Machado, R. A. F., Spricigo, C. B., Pereira, L. K., and Bolzan, A. (2001). Extraction of lemongrass essential oil with dense carbon dioxide. *The Journal of Supercritical Fluids*, 21(1), 33-39. https://doi.org/10.1016/S0896-8446(01)00085-7.

Champeau, M., Thomassin, J. M., Tassaing, T., and Jérôme, C. (2015). Drug loading of polymer implants by supercritical CO_2 assisted impregnation: A review. *Journal of Controlled Release*, 209, 248-259. https://doi.org/10.1016/j.jconrel.2015.05.002.

Chao, S. C., Young, D. G., and Oberg, C. J. (2000). Screening for inhibitory activity of essential oils on selected bacteria, fungi and viruses. *Journal of Essential Oil Research*, 12(5), 639-649. https://doi.org/10.1080/10412905.2000.9712177.

Cheng, H., Yue, K., Kazemzadeh-Narbat, M., Liu, Y., Khalilpour, A., Li, B., Zhang, Y.S., Annabi, N. and Khademhosseini, A. (2017). Mussel-inspired multifunctional hydrogel coating for

prevention of infections and enhanced osteogenesis. *ACS Applied Materials & Interfaces*, 9(13), 11428-11439. DOI: 10.1021/acsami.6b16779.

Chen, J., Zhang, N., Pei, S., and Yao, L. (2022). Odor perception of aromatherapy essential oils with different chemical types: Influence of gender and two cultural characteristics. *Frontiers in Psychology*, 13, 998612. https://doi.org/10.3389/fpsyg.2022.998612.

Chen, X., Wu, Q., Gong, Z., Ren, T., Du, Q., Yuan, Y., Zuo, Y., Miao, Y., He, J., Qiao, C. and Zheng, Z., 2022. A natural plant ingredient, menthone, regulates T cell subtypes and lowers pro-inflammatory cytokines of rheumatoid arthritis. *Journal of Natural Products*, 85(4), 1109-1117. https://doi.org/10.1021/acs.jnatprod.1c01231.

Chiou, T.Y., Konishi, M., Nomura, S., Shimotori, Y., Murata, M., Ohtsu, N., Kohari, Y., Nagata, Y. and Saitoh, T. (2019). Recovery of mint essential oil through pressure-releasing distillation during subcritical water treatment. *Food Science and Technology Research*, 25(6), 793-799. https://doi.org/10.3136/fstr.25.793.

Chi, S., Zivanovic, S., and Penfield, M. P. (2006). Application of chitosan films enriched with oregano essential oil on bologna–active compounds and sensory attributes. *Food Science and Technology International*, 12(2), 111-117. https://doi.org/10.1177/1082013206063845.

Chung, C., Lee, M., and Choe, E. K. (2004). Characterization of cotton fabric scouring by FT-IR ATR spectroscopy. *Carbohydrate Polymers*, 58(4), 417-420. https://doi.org/10.1016/j.carbpol.2004.08.005.

Ciftci, D., and Saldaña, M. D. (2015). Hydrolysis of sweet blue lupin hull using subcritical water technology. *Bioresource Technology*, 194, 75-82. https://doi.org/10.1016/j.biortech.2015.06.146.

Ciftci, O.N., and Temelli, F. (2014). Melting point depression of solid lipids in pressurized carbon dioxide. *Journal of Supercritical Fluids,* 92, 208–214. https://doi.org/10.1016/j.supflu.2014.05.009.

Cimino, C., Maurel, O. M., Musumeci, T., Bonaccorso, A., Drago, F., Souto, E. M. B., Pignatello, R., and Carbone, C. (2021). Essential oils: Pharmaceutical applications and encapsulation strategies into lipid-based delivery systems. *Pharmaceutics*, 13(3), 327. DOI: 10.3390/pharmaceutics13030327.

Comin, L. M., Temelli, F., and Saldaña, M. D. (2012). Impregnation of flax oil in pregelatinized corn starch using supercritical CO_2. *The Journal of Supercritical Fluids*, 61, 221-228. DOI: 10.3390/pharmaceutics13030327.

Conde-Hernández, L. A., Espinosa-Victoria, J. R., and Guerrero-Beltrán, J. Á. (2017a). Supercritical extraction of essential oils of *Piper auritum* and *Porophyllum ruderale*. *The Journal of Supercritical Fluids*, 127, 97-102. https://doi.org/10.1016/j.supflu.2017.03.026.

Conde-Hernández, L. A., Espinosa-Victoria, J. R., Trejo, A. and Guerrero-Beltrán, J. Á. (2017b). CO_2-supercritical extraction, hydrodistillation and steam distillation of essential oil of rosemary (*Rosmarinus officinalis*). *Journal of Food Engineering*, 200, 81-86. https://doi.org/10.1016/j.jfoodeng.2016.12.022.

Corso, M.P., Fagundes-Klen, M.R., Silva, E.A., Cardozo Filho, L., Santos, J.N., Freitas, L.S. and Dariva, C. (2010). Extraction of sesame seed (*Sesamun indicum* L.) oil using compressed propane and supercritical carbon dioxide. *The Journal of Supercritical Fluids*, 52(1), 56-61. DOI:10.1016/j.supflu.2009.11.012.

Cortesi, A., Alessi, P., Kikic, I., Kirchmayer, S., and Vecchione, F. (2000). Supercritical fluids chromatography for impregnation optimization. *The Journal of Supercritical Fluids*, 19(1), 61-68. https://doi.org/10.1016/S0896-8446(00)00071-1.

Craighead, D. H., and Alexander, L. M. (2016). Topical menthol increases cutaneous blood flow. *Microvascular Research*, 107, 39-45. doi: 10.1016/j.mvr.2016.04.010.

d'Alessio, P. A., Ostan, R., Bisson, J. F., Schulzke, J. D., Ursini, M. V. and Béné, M. C. (2013). Oral administration of d-limonene controls inflammation in rat colitis and displays anti-inflammatory properties as diet supplementation in humans. *Life science*s, 92(24-26), 1151-1156. https://doi.org/10.1016/j.lfs.2013.04.013.

Dambolena, J. S., López, A. G., Cánepa, M. C., Theumer, M. G., Zygadlo, J. A. and Rubinstein, H. R. (2008). Inhibitory effect of cyclic terpenes (limonene, menthol, menthone and thymol) on *Fusarium verticillioides* MRC 826 growth and fumonisin B1 biosynthesis. *Toxicon*, 51(1), 37-44. https://doi.org/10.1016/j.toxicon.2007.07.005.

Dangkulwanich, M. and Charaslertrangsi, T. (2020). Hydrodistillation and antimicrobial properties of lemongrass oil (*Cymbopogon citratus, Stapf*): An undergraduate laboratory exercise bridging chemistry and microbiology. *Journal of Food Science Education*, 19(2), 41-48. https://doi.org/10.1111/1541-4329.12178.

De Carvalho, C. C. and Da Fonseca, M. M. R. (2006). Carvone: Why and how should one bother to produce this terpene. *Food Chemistry*, 95(3), 413-422. https://doi.org/10.1016/j.foodchem.2005.01.003.

De Castro, M. L., Jiménez-Carmona, M. M., and Fernandez-Perez, V. (1999). Towards more rational techniques for the isolation of valuable essential oils from plants. *TrAC Trends in Analytical Chemistry*, 18(11), 708-716. https://doi.org/10.1016/S0165-9936(99)00177-6.

De Melo, M.M.R., Domingues, R.M.A., Sova, M., Lack, E., Seidlitz, H., Lang Jr, F., Silvestre, A.J.D. and Silva, C.M. (2014). Scale-up studies of the supercritical fluid extraction of triterpenic acids from *Eucalyptus globulus* bark. *The Journal of Supercritical Fluids*, 95, 44-50. https://doi.org/10.1016/j.supflu.2014.07.030.

Dhifi, W., Bellili, S., Jazi, S., Bahloul, N. and Mnif, W. 2016. Essential oils' chemical characterization and investigation of some biological activities: A critical review. *Medicines*, 3(4), 25.

Dhivya, S., Padma, V. V., and Santhini, E. (2015). Wound dressings–a review. *BioMedicine*, 5(4), 22. doi: 10.7603/s40681-015-0022-9.

Dias, A. M. A., Braga, M. E. M., Seabra, I. J., Ferreira, P., Gil, M. H., and De Sousa, H. C. (2011). Development of natural-based wound dressings impregnated with bioactive compounds and using supercritical carbon dioxide. *International Journal of Pharmaceutics*, 408(1-2), 9-19. https://doi.org/10.1016/j.ijpharm.2011.01.063.

Díaz-Reinoso, B., Moure, A., Domínguez, H., and Parajó, J. C. (2006). Supercritical CO_2 extraction and purification of compounds with antioxidant activity. *Journal of Agricultural and Food Chemistry*, 54(7), 2441-2469. https://doi.org/10.1021/jf052858j.

Di Giacomo, G., Brandani, V., Del Re, G., and Mucciante, V. (1989). Solubility of essential oil components in compressed supercritical carbon dioxide. *Fluid Phase Equilibria*, 52, 405-411. https://doi.org/10.1016/0378-3812(89)80346-2.

Duarte, A. R. C., Mano, J. F., and Reis, R. L. (2009). Dexamethasone-loaded scaffolds prepared by supercritical-assisted phase inversion. *Acta Biomaterialia*, 5(6), 2054-2062. https://doi.org/10.1016/j.actbio.2009.01.047.

Dylong, D., Hausoul, P. J., Palkovits, R., and Eisenacher, M. (2022). Synthesis of (−)-menthol: industrial synthesis routes and recent development. *Flavour and Fragrance Journal*, 37(4), 195-209. https://doi.org/10.1002/ffj.3699.

Eccles, R. (1994). Menthol and related cooling compounds. *Journal of Pharmacy and Pharmacology*, 46(8), 618-630. DOI: 10.1111/j.2042-7158.1994.tb03871.x.

Edris, A. E., and Farrag, E. S. (2003). Antifungal activity of peppermint and sweet basil essential oils and their major aroma constituents on some plant pathogenic fungi from the vapor phase. *Food/Nahrung*, 47(2), 117-121. DOI:10.1002/food.200390021.

Esfandiari, N., and Sajadian, S. A. (2022). Experimental and modeling investigation of Glibenclamide solubility in supercritical carbon dioxide. *Fluid Phase Equilibria*, 556, 113408. https://doi.org/10.1016/j.fluid.2022.113408.

Essential oils in Canada. OEC. (2020). Retrieved March 13, 2023, from https://oec.world/en/profile/bilateral-product/essential-oils/reporter/can?redirect=true&shareMarket=shareMarket.

Etzold, B., Jess, A., and Nobis, M. (2009). Epimerisation of menthol stereoisomers: Kinetic studies of the heterogeneously catalysed menthol production. *Catalysis Today*, 140(1-2), 30-36. https://doi.org/10.1016/j.cattod.2008.07.009.

FAOSTAT (2018). *Food and Agriculture Organization of the United Nations, Statistical database*. Accessed on April 2, 2023, at https://www.fao.org/faostat/en/#data/QCL/visualize.

Fernández-Pérez, V., Jiménez-Carmona, M.M. and de Castro, M.D.L. (2000). An approach to the static–dynamic subcritical water extraction of laurel essential oil: comparison with conventional techniques. *Analyst*, 125(3), 481-485. https://doi.org/10.1039/A907244F.

Foda, M. I., El-Sayed, M. A., Hassan, A. A., Rasmy, N. M., and El-Moghazy, M. M. (2010). Effect of spearmint essential oil on chemical composition and sensory properties of white cheese. *Journal of American Science*, 6(5), 272-279.

FoodData Central. (2019). *Peppermint, fresh. U.S. Department of Agriculture*. Accessed on Dec 12, 2022, at https://fdc.nal.usda.gov/fdc-app.html#/food-details/173474/nutrients.

Frohlich, P. C., Santos, K. A., Palu, F., Cardozo-Filho, L., da Silva, C., and da Silva, E. A. (2019). Evaluation of the effects of temperature and pressure on the extraction of eugenol from clove (*Syzygium aromaticum*) leaves using supercritical CO_2. *The Journal of Supercritical Fluids*, 143, 313-320. https://doi.org/10.1016/j.supflu.2018.09.009.

Fuchs, L.K., Holland, A.H., Ludlow, R.A., Coates, R.J., Armstrong, H., Pickett, J.A., Harwood, J.L. and Scofield, S. (2022). Genetic manipulation of biosynthetic pathways in mint. *Frontiers in Plant Science*, 13, 928178.https://doi.org/10.3389/fpls.2022.928178.

Galeotti, N., Mannelli, L. D. C., Mazzanti, G., Bartolini, A., and Ghelardini, C. (2002). Menthol: a natural analgesic compound. *Neuroscience Letters*, 322(3), 145-148. DOI: 10.1016/s0304-3940(01)02527-7.

Galushko, A. A., Sovová, H., and Stateva, R. P. (2006). Solubility of menthol in pressurized carbon dioxide: Experimental data and thermodynamic modeling. *Chemical Industry and Chemical Engineering Quarterly*, 12(3), 152-158. DOI:10.2298/CICEQ0603152G.

Gañán, N. and Brignole, E.A. (2011). Fractionation of essential oils with biocidal activity using supercritical CO_2—Experiments and modeling. *The Journal of Supercritical Fluids*, 58(1), 58-67. https://doi.org/10.1016/j.supflu.2011.04.010.

Gañán, N.A., Dambolena, J.S., Martini, R.E. and Bottini, S.B. (2015). Supercritical carbon dioxide fractionation of peppermint oil with low menthol content–Experimental study and simulation analysis for the recovery of piperitenone. *The Journal of Supercritical Fluids*, 98, 1-11. https://doi.org/10.1016/j.supflu.2014.12.018.

Gaudioso, C., Hao, J., Martin-Eauclaire, M. F., Gabriac, M., and Delmas, P. (2012). Menthol pain relief through cumulative inactivation of voltage-gated sodium channels. *Pain*, 153(2), 473-484. https://doi.org/10.1016/j.pain.2011.11.014.

Gittard, S. D., Hojo, D., Hyde, G. K., Scarel, G., Narayan, R. J., and Parsons, G. N. (2010). Antifungal textiles formed using silver deposition in supercritical carbon dioxide. *Journal of Materials Engineering and Performance*, 19, 368-373. DOI:10.1007/s11665-009-9514-7.

Giuliani, C., and Maleci Bini, L. (2008). Insight into the structure and chemistry of glandular trichomes of *Labiatae*, with emphasis on subfamily *Lamioideae*. *Plant Systematics and Evolution*, 276(3), 199-208. DOI:10.1007/s00606-008-0085-0.

Goñi, M. L., Gañán, N. A., Strumia, M. C., and Martini, R. E. (2016). Eugenol-loaded LLDPE films with antioxidant activity by supercritical carbon dioxide impregnation. *The Journal of Supercritical* Fluids, 111, 28-35. https://doi.org/10.1016/j.supflu.2016.01.012.

Goto, M., Sato, M. and Hirose, T. (1993). Extraction of peppermint oil by supercritical carbon dioxide. *Journal of Chemical Engineering of Japan*, 26(4), 401-407. https://doi.org/10.1016/0896-8446(92)90002-2.

Gupta, R. B., and Kompella, U. B. (2006). Supercritical Fluid Technology for Particle Formation. *Nanoparticle technology for drug delivery. [electronic resource]. Taylor & Francis*. https://doi.org/10.1201/9780849374555.

Gupta, R.B. and Shim, J.-J. (2007). Introduction. *Solubility in supercritical carbon dioxide. [electronic resource]*. CRC Press. Accessed on 15 June 2023, at https://search-ebscohost-com.login.ezproxy.library.ualberta.ca/login.aspx?direct=true&db=cat03710a&AN=alb.7617993&site=eds-live&scope=site. https://doi.org/10.1201/9781420005998.

Han, X., Cheng, L., Zhang, R., and Bi, J. (2009). Extraction of safflower seed oil by supercritical CO_2. *Journal of Food Engineering*, 92(4), 370-376. https://doi.org/10.1016/j.jfoodeng.2008.12.002.

Hansen, J. S., Nielsen, G. D., Sørli, J. B., Clausen, P. A., Wolkoff, P. and Larsen, S. T. (2013). Adjuvant and inflammatory effects in mice after subchronic inhalation of allergen and ozone-initiated limonene reaction products. *Journal of Toxicology and Environmental Health, Part A*, 76(19), 1085-1095. https://doi.org/10.1080/15287394.2013.838915.

Hejna, M., Kovanda, L., Rossi, L., and Liu, Y. (2021). Mint oils: In vitro ability to perform anti-inflammatory, antioxidant, and antimicrobial activities and to enhance intestinal barrier integrity. *Antioxidants*, 10(7), 1004. https://doi.org/10.3390/antiox10071004.

Hezave, A. Z., Mowla, A., and Esmaeilzadeh, F. (2011). Cetirizine solubility in supercritical CO_2 at different pressures and temperatures. *The Journal of Supercritical Fluids*, 58(2), 198-203. https://doi.org/10.1016/j.supflu.2011.05.017.

Hiriart-Ramírez, E., Contreras-García, A., Garcia-Fernandez, M. J., Concheiro, A., Alvarez-Lorenzo, C., and Bucio, E. (2012). Radiation grafting of glycidyl methacrylate onto cotton gauzes for functionalization with cyclodextrins and elution of antimicrobial agents. *Cellulose*, 19, 2165-2177. DOI:10.1007/s10570-012-9782-5.

Huerta, R. R., and Saldaña, M. D. (2018). Pressurized fluid treatment of barley and canola straws to obtain carbohydrates and phenolics. *The Journal of Supercritical Fluids*, 141, 12-20. https://doi.org/10.1016/j.supflu.2017.11.029

Hunter, R. S. (1975). *The measurement of appearance*. Wiley, 348. ISBN: 978-0-471-83006-1. Accessed on April 5, 2023, at https://books.google.ca/books?hl=en&lr=&id=vK5DK9vqyCgC&oi=fnd&pg=PA1&dq=The+measurement+of+appearance&ots=kbn3r2KBLY&sig=TDrb3qKsfmSJz9KMy8XUYe-HbcM&redir_esc=y#v=onepage&q=The%20measurement%20of%20appearance&f=false.

Ibrahim, M., Ankwai, G. E., Gungshik, J. R., and Taave, P. (2021). Comparative extraction of essential oils of *Mentha piperita* (mint) by steam distillation and enfleurage. *Nigerian Journal of Chemical Research*, 26(2), 56-62. DOI:10.4314/njcr.v26i2.2.

Ilmi, A., Praseptiangga, D., and Muhammad, D. R. A. (2017). Sensory attributes and preliminary characterization of milk chocolate bar enriched with cinnamon essential oil. In *IOP conference series: Materials science and engineering*, 193(1), 012031. DOI 10.1088/1757-899X/193/1/012031.

Ivanović, J., Milovanović, S., Stamenić, M., Fanovich, M. A., Jaeger, P., and Žižović, I. (2014). Application of an integrated supercritical extraction and impregnation process for incorporation of thyme extracts into different carriers. *Handbook on Supercritical Fluids: Fundamentals, Properties and Applications*, 258-280. https://doi.org/10.3390/pr10040680.

Ixtaina, V.Y., Vega, A., Nolasco, S.M., Tomás, M.C., Gimeno, M., Bárzana, E. and Tecante, A. (2010). Supercritical carbon dioxide extraction of oil from Mexican chia seed (*Salvia hispanica* L.): Characterization and process optimization. *The Journal of Supercritical Fluids*, 55(1), 192-199. https://doi.org/10.1016/j.supflu.2010.06.003.

Jamshidi, F., Nouri, N., Sereshti, H. and Aliabadi, M. H. S. (2020). Synthesis of magnetic poly (acrylic acid-menthol deep eutectic solvent) hydrogel: Application for extraction of pesticides. *Journal of Molecular Liquids*, 318, 114073. https://doi.org/10.1016/j.molliq.2020.114073

Jiang, L., Han, Y., Xu, J. and Wang, T. (2022). Preparation and study of cellulose-based ZnO NPs@ HEC/C-β-CD/Menthol hydrogel as wound dressing. *Biochemical Engineering Journal*, 184, 108488. https://doi.org/10.1016/j.bej.2022.108488.

Jiao, Z., Cheng, J., Guo, M., and Han, S. (2019). Measurement and Correlation of Paeonol Solubility in Supercritical Carbon Dioxide. *Journal of Chemical & Engineering Data*, 64(10), 4424-4429. https://doi.org/10.1021/acs.jced.9b00483.

Jin, Y., Han, D., Tian, M., and Row, K. H. (2010). Supercritical CO_2 extraction of essential oils from *Chamaecyparis obtusa*. *Natural Product Communications*, 5(3), 461-464. https://doi.org/10.1177/1934578X1000500324.

Joglekar, M. M., Panaskar, S. N., Chougale, A. D., Kulkarni, M. J. and Arvindekar, A. U. (2013). A novel mechanism for antiglycative action of limonene through stabilization of protein conformation. *Molecular BioSystems*, 9(10), 2463-2472. DOI: 10.1039/c3mb00020f.

Juergens, U. R., Stöber, M. and Vetter, H. (1998). The anti-inflammatory activity of L-menthol compared to mint oil in human monocytes *in vitro*: a novel perspective for its therapeutic use in inflammatory diseases. *European Journal of Medical Research*, 3(12), 539-545. https://doi.org/10.1053/rmed.2003.1432.

Kaimoto, T., Hatakeyama, Y., Takahashi, K., Imagawa, T., Tominaga, M. and Ohta, T. (2016). Involvement of transient receptor potential A1 channel in algesic and analgesic actions of the organic compound limonene. *European Journal of Pain*, 20(7), 1155-1165. DOI: 10.1002/ejp.840.

Kamali, H., Aminimoghadamfarouj, N., Golmakani, E., and Nematollahi, A. (2015). The optimization of essential oils supercritical CO_2 extraction from *Lavandula hybrida* through static-dynamic steps procedure and semi-continuous technique using response surface method. *Pharmacognosy Research*, 7(1), 57. doi: 10.4103/0974-8490.147209.

Kamatou, G. P., Vermaak, I., Viljoen, A. M., and Lawrence, B. M. (2013). Menthol: a simple monoterpene with remarkable biological properties. *Phytochemistry*, 96, 15-25. https://doi.org/10.1016/j.phytochem.2013.08.005.

Kant, R., and Kumar, A. (2022). Process optimization of conventional steam distillation system for peppermint oil extraction. *Energy Sources, Part A: Recovery, Utilization, and Environmental Effects*, 44(2), 3960-3980. https://doi.org/10.1080/15567036.2022.2069886.

Katayama, S., Zhao, L., Yonezawa, S., and Iwai, Y. (2012). Modification of the surface of cotton with supercritical carbon dioxide and water to support nanoparticles. *The Journal of Supercritical Fluids*, 61, 199-205. https://doi.org/10.1016/j.supflu.2011.10.008.

Kazarian, S. G., Brantley, N. H., West, B. L., Vincent, M. F., and Eckert, C. A. (1997). In situ spectroscopy of polymers subjected to supercritical CO_2: plasticization and dye impregnation. *Applied Spectroscopy*, 51(4), 491-494. https://doi.org/10.1366/00037029719407.

Kemp, S. E., Hollowood, T., and Hort, J. (2009). Introduction. *Sensory evaluation. [electronic resource] : a practical handbook*. Ames, Iowa. DOI:10.1002/9781118688076.

Kim, S. H., Lee, S., Piccolo, S. R., Allen-Brady, K., Park, E. J., Chun, J. N., Kim, T. W., Cho, N. H., Kim, I. G., So, I. and Jeon, J. H. (2012). Menthol induces cell-cycle arrest in PC-3 cells

by down-regulating G2/M genes, including polo-like kinase 1. *Biochemical and Biophysical Research Communications*, 422(3), 436-441. https://doi.org/10.1016/j.bbrc.2012.05.010.

Kopcak, U., and Mohamed, R. S. (2005). Caffeine solubility in supercritical carbon dioxide/co-solvent mixtures. *The Journal of Supercritical Fluids*, 34(2), 209-214. https://doi.org/10.1016/j.supflu.2004.11.016.

Kotan, R., Kordali, S., and Cakir, A. (2007). Screening of antibacterial activities of twenty-one oxygenated monoterpenes. *Zeitschrift für Naturforschung C*, 62(7-8), 507-513. DOI: 10.1515/znc-2007-7-808.

Kumar, N., Nepali, K., Sapra, S., Bijjem, K. R. V., Kumar, R., Suri, O. P., and Dhar, K. L. (2012). Effect of nitrogen insertion on the antitussive properties of menthol and camphor. *Medicinal Chemistry Research*, 21, 531-537. DOI:10.1007/s00044-011-9560-1.

Kummer, R., Fachini-Queiroz, F. C., Estevão-Silva, C. F., Grespan, R., Silva, E. L., Bersani-Amado, C. A., and Cuman, R. K. N. (2013). Evaluation of anti-inflammatory activity of *Citrus latifolia Tanaka* essential oil and limonene in experimental mouse models. *Evidence-Based Complementary and Alternative Medicine*, 2013. https://doi.org/10.1155/2013/859083.

Lawrence, B. M. (2006). *Mint: the genus Mentha*. CRC press, 23-67. https://doi.org/10.1201/9780849307980.

Li, J. and Mooney, D. J. (2016). Designing hydrogels for controlled drug delivery. *Nature Reviews Materials*, 1(12), 1-17. https://doi.org/10.3390/books978-3-03928-357-6.

Li, J., Jia, X. and Yin, L. (2021). Hydrogel: Diversity of structures and applications in food science. *Food Reviews International*, 37(3), 313-372. https://doi.org/10.1080/87559129.2020.1858313.

Lis-Balchin, M. (2006). *Aromatherapy science: a guide for healthcare professionals*. Pharmaceutical press, 66-92. https://doi.org/10.1177/14664240060824.

Liu, J., Qu, S., Suo, Z. and Yang, W. (2021). Functional hydrogel coatings. *National Science Review*, 8(2), nwaa254. https://doi.org/10.1093/nsr/nwaa254.

Li, Y., Zhou, F., Wen, Y., Liu, K., Chen, L., Mao, Y., Yang, S. and Yi, T. (2014). (−)-Menthol based thixotropic hydrogel and its application as a universal antibacterial carrier. *Soft Matter*, 10(17), 3077-3085. https://doi.org/10.1039/C3SM52999A.

Lou, Z., Han, H., Zhou, M., Han, J., Cai, J., Huang, C., Zou, J., Zhou, X., Zhou, H. and Sun, Z. (2018). Synthesis of magnetic wood with excellent and tunable electromagnetic wave-absorbing properties by a facile vacuum/pressure impregnation method. *ACS Sustainable Chemistry & Engineering*, 6(1), 1000-1008. https://doi.org/10.1021/acssuschemeng.7b03332.

Lukic, I., Vulic, J., and Ivanovic, J. (2020). Antioxidant activity of PLA/PCL films loaded with thymol and/or carvacrol using scCO$_2$ for active food packaging. *Food Packaging and Shelf Life*, 26, 100578. https://doi.org/10.1016/j.fpsl.2020.100578.

Mainasara, M. M., Bakar, M. F. A., Waziri, A. H., and Musa, A. R. (2018). Comparison of phytochemical, proximate and mineral composition of fresh and dried peppermint (*Mentha piperita*) leaves. *Journal of Science and Technology*, 10(2), 85-91. DOI:10.30880/jst.2018.10.02.014.

Mai, T.C., Tran, N.T., Mai, D.T., Mai, T.T.N., Duyen, N.H.T., An, T.N.M., Alam, M., Dang, C.H. and Nguyen, T.D. (2022). Supercritical CO$_2$ assisted extraction of essential oil and naringin from *Citrus grandis* peel: in vitro antimicrobial activity and docking study. *RSC advances*, 12(40), 25962-25976. DOI: 10.1039/D2RA04068A.

Market study on essential oils: Citrus to remain most popular source. Persistence Market Research. (n.d.). Retrieved January 24, 2023, from https://www.persistencemarketresearch.com/market-research/essential-oils-market.asp

Markovic, D., Milovanovic, S., Radetic, M., Jokic, B., and Zizovic, I. (2015). Impregnation of corona modified polypropylene non-woven material with thymol in supercritical carbon dioxide for antimicrobial application. *The Journal of Supercritical Fluids*, 101, 215-221. https://doi.org/10.1016/j.supflu.2015.03.022.

Masmoudi, Y., Azzouk, L. B., Forzano, O., Andre, J. M., and Badens, E. (2011). Supercritical impregnation of intraocular lenses. *The Journal of Supercritical Fluids*, 60, 98-105. https://doi.org/10.1016/j.supflu.2011.08.014.

Masomeh, L., Narges, M., Hassan, R., and Hadi, A. (2017). Peppermint and its functionality: A review. *Archives of clinical microbiology*, 8(4). DOI: 10.4172/1989-8436.100053.

Mathur, A., Prasad, G. B. K. S., Rao, N., Babu, P., and Dua, V. K. (2011). Isolation and identification of antimicribial compound from *Mentha pipirita*. *Rasayan J*, 4(1), 36-42. doi: 10.1186/1476-0711-8-20.

Medeiros, G. R., Ferreira, S. R., and Carciofi, B. A. (2017). High pressure carbon dioxide for impregnation of clove essential oil in LLDPE films. *Innovative Food Science & Emerging Technologies*, 41, 206-215. https://doi.org/10.1016/j.ifset.2017.03.008.

Mekala, S., Silva, E. K., and Saldaña, M. D. (2022). Ultrasound-assisted production of emulsion-filled pectin hydrogels to encapsulate vitamin complex: Impact of the addition of xylooligosaccharides, ascorbic acid and supercritical CO$_2$ drying. *Innovative Food Science & Emerging Technologies*, 76, 102907. https://doi.org/10.1016/j.ifset.2021.102907.

Mezzomo, N., Martínez, J., and Ferreira, S. R. (2009). Supercritical fluid extraction of peach (*Prunus persica*) almond oil: kinetics, mathematical modeling and scale-up. *The Journal of Supercritical Fluids*, 51(1), 10-16. https://doi.org/10.1016/j.supflu.2009.07.008.

Milliporesigma. MilliporeSigma | Life Science Products & Service Solutions. (n.d.). https://www.sigmaaldrich.com/CA/en

Milovanovic, S., Hollermann, G., Errenst, C., Pajnik, J., Frerich, S., Kroll, S., Rezwan, K., and Ivanovic, J. (2018). Supercritical CO_2 impregnation of PLA/PCL films with natural substances for bacterial growth control in food packaging. *Food Research International*, 107, 486-495. https://doi.org/10.1016/j.foodres.2018.02.065.

Milovanovic, S., Markovic, D., Aksentijevic, K., Stojanovic, D. B., Ivanovic, J., and Zizovic, I. (2016). Application of cellulose acetate for controlled release of thymol. *Carbohydrate Polymers*, 147, 344-353. https://doi.org/10.1016/j.carbpol.2016.03.093.

Milovanovic, S., Stamenic, M., Markovic, D., Radetic, M., and Zizovic, I. (2013). Solubility of thymol in supercritical carbon dioxide and its impregnation on cotton gauze. *The Journal of Supercritical Fluids*, 84, 173-181. https://doi.org/10.1016/j.supflu.2013.10.003.

Mint essential oils market size, share: Industry Report, 2019-2025. (2018). *Mint Essential Oils Market Size, Share | Industry Report, 2019-2025*. Accessed on January 10, 2023, at https://www.grandviewresearch.com/industry-analysis/mint-essential-oils-market.

Mint flavour – Government of Canada. Accessed on March 15, 2023, at https://webprod.hc-sc.gc.ca/nhpid-bdipsn/ingredReq.do?id=12038&lang=eng#.

Miranda-Villa, P. P., Ganan, N. A., Martini, R. E., and Goni, M. L. (2022). Supercritical CO_2-assisted impregnation of polylactic acid films with R-carvone: Effect of processing on loading, mass transfer kinetics, and final properties. *Journal of CO_2 Utilization*, 61, 102029. https://doi.org/10.1016/j.jcou.2022.102029.

Moller, A.C., Parra, C., Said, B., Werner, E., Flores, S., Villena, J., Russo, A., Caro, N., Montenegro, I. and Madrid, A. (2020). Antioxidant and anti-proliferative activity of essential oil and main components from leaves of *Aloysia polystachya* harvested in Central Chile. *Molecules*, 26(1), 131. https://doi.org/10.3390/molecules26010131.

Musa, T.A., Sanagi, M.M., Wan Ibrahim, W.A., Ahmad, F. and Aboul-Enein, H.Y. (2014). Determination of 4-allyl resorcinol and chavibetol from piper betle leaves by subcritical water extraction combined with high-performance liquid chromatography. *Food Analytical Methods*, 7(4), 893-901. DOI:10.1007/s12161-013-9697-2.

Mustapa, A. N., Martin, A., Sanz-Moral, L. M., Rueda, M., and Cocero, M. J. (2016). Impregnation of medicinal plant phytochemical compounds into silica and alginate aerogels. *The Journal of Supercritical Fluids*, 116, 251-263. https://doi.org/10.1016/j.supflu.2016.06.002.

Nair, B. (2001). Final report on the safety assessment of *Mentha piperita* (Peppermint) oil, *Mentha piperita* (peppermint) leaf extract, *Mentha piperita* (peppermint) Leaf, and *Mentha piperita* (peppermint) leaf water. *International Journal of Toxicology*, 20, 61-73. https://doi.org/10.1080/10915810152902592.

Neethu, T. M., Dubey, P. K. and Kaswala, A. R. (2018). Prospects and applications of hydrogel technology in agriculture. *International Journal of Current Microbiology and Applied Sciences*, 7(5), 3155-3162. https://doi.org/10.1155/2022/4914836.

Nemoto, S., Sasaki, K., Toyoda, M., and Saito, Y. (1997). Effect of extraction conditions and modifiers on the supercritical fluid extraction of 88 pesticides. *Journal of Chromatographic Science*, 35(10), 467-477. https://doi.org/10.1093/chromsci/35.10.467.

Ngo, T. T., Liotta, C. L., Eckert, C. A., and Kazarian, S. G. (2003). Supercritical fluid impregnation of different azo-dyes into polymer: in situ UV/Vis spectroscopic study. *The Journal of Supercritical Fluids*, 27(2), 215-221. https://doi.org/10.1016/S0896-8446(02)00239-5.

Olmedo, R. H., Nepote, V., and Grosso, N. R. (2013). Preservation of sensory and chemical properties in flavoured cheese prepared with cream cheese base using oregano and rosemary essential oils. *LWT-Food Science and Technology*, 53(2), 409-417. https://doi.org/10.1016/j.lwt.2013.04.007.

Ozel, M.Z., Gogus, F. and Lewis, A.C. (2003). Subcritical water extraction of essential oils from *Thymbra spicata*. *Food Chemistry*, 82(3), 381-386. https://doi.org/10.1016/S0308-8146(02)00558-7.

Özel, M.Z., Göğüş, F. and Lewis, A.C. (2006). Comparison of direct thermal desorption with water distillation and superheated water extraction for the analysis of volatile components of *Rosa damascena* Mill. using GCxGC-TOF/MS. *Analytica Chimica Acta*, 566(2), 172-177. https://doi.org/10.1016/j.aca.2006.03.014.

Özer, E.Ö., İin, S.P., Akman, U. and Hortaçsu, Ö. (1996). Supercritical carbon dioxide extraction of spearmint oil from mint-plant leaves. *The Canadian Journal of Chemical Engineering*, 74(6), 920-928. https://doi.org/10.1002/cjce.5450740615.

Pajnik, J., Stamenić, M., Radetić, M., Tomanović, S., Sukara, R., Mihaljica, D., and Zizovic, I. (2017). Impregnation of cotton fabric with pyrethrum extract in supercritical carbon dioxide. *The Journal of Supercritical Fluids*, 128, 66-72. https://doi.org/10.1016/j.supflu.2017.05.006.

Pantić, M., Kotnik, P., Knez, Ž., and Novak, Z. (2016). High pressure impregnation of vitamin D3 into polysaccharide aerogels using moderate and low temperatures. *The Journal of Supercritical Fluids*, 118, 171-177. https://doi.org/10.1016/j.supflu.2016.08.008.

Pan, Z., and Tangratanavalee, W. (2003). Characteristics of soybeans as affected by soaking conditions. *LWT-Food Science and Technology*, 36(1), 143-151. https://doi.org/10.1016/S0023-6438(02)00202-5.

Park, J., Cho, W., Kang, H., Lee, B. B. J., Kim, T. S., and Hwang, S. J. (2014). Effect of operating parameters on PVP/tadalafil solid dispersions prepared using supercritical anti-solvent

process. *The Journal of Supercritical Fluids*, 90, 126-133. https://doi.org/10.1016/j.supflu.2014.04.001.

Patel, T., Ishiuji, Y. and Yosipovitch, G. (2007). Menthol: a refreshing look at this ancient compound. *Journal of the American Academy of Dermatology*, 57(5), 873-878. https://doi.org/10.1016/j.jaad.2007.04.008.

Patrick, H. R., Griffith, K., Liotta, C. L., Eckert, C. A. and Gläser, R. (2001). Near-critical water: A benign medium for catalytic reactions. *Industrial & Engineering Chemistry Research*, 40(26), 6063-6067. https://doi.org/10.1021/ie010178+.

Pavlić, B., Vidović, S., Vladić, J., Radosavljević, R. and Zeković, Z. (2015). Isolation of coriander (*Coriandrum sativum* L.) essential oil by green extractions versus traditional techniques. *The Journal of Supercritical Fluids*, 99, 23-28. https://doi.org/10.1016/j.supflu.2015.01.029.

Pergolizzi Jr, J. V., Taylor Jr, R., LeQuang, J. A., Raffa, R. B., and NEMA Research Group. (2018). The role and mechanism of action of menthol in topical analgesic products. *Journal of Clinical Pharmacy and Therapeutics*, 43(3), 313-319. https://doi.org/10.1111/jcpt.12679.

Pina, L.T., Serafini, M.R., Oliveira, M.A., Sampaio, L.A., Guimarães, J.O. and Guimarães, A.G. (2022). Carvone and its pharmacological activities: A systematic review. *Phytochemistry*, 196, 113080. https://doi.org/10.1016/j.phytochem.2021.113080.

Porter, N. G., and Lammerink, J. P. (1994). Effect of temperature on the relative densities of essential oils and water. *Journal of Essential Oil Research*, 6(3), 269-277. https://doi.org/10.1080/10412905.1994.9698375.

Pourmortazavi, S. M., Sefidkon, F., and Hosseini, S. G. (2003). Supercritical carbon dioxide extraction of essential oils from *Perovskia atriplicifolia* Benth. *Journal of Agricultural and Food Chemistry*, 51(18), 5414-5419. DOI: 10.1021/jf0341619.

Prado, J.M., Dalmolin, I., Carareto, N.D., Basso, R.C., Meirelles, A.J., Oliveira, J.V., Batista, E.A. and Meireles, M.A.A. (2012). Supercritical fluid extraction of grape seed: Process scale-up, extract chemical composition and economic evaluation. *Journal of Food Engineering*, 109(2), 249-257. https://doi.org/10.1016/j.jfoodeng.2011.10.007.

Prado, J. M., Prado, G. H., and Meireles, M. A. A. (2011). Scale-up study of supercritical fluid extraction process for clove and sugarcane residue. *The Journal of Supercritical Fluids*, 56(3), 231-237. https://doi.org/10.1016/j.supflu.2010.10.036.

Q3C — Tables and list guidance for industry – Food and Drug Administration (2017). Accessed April 4, 2023, at https://www.fda.gov/media/71737/download

Quitain, A. T., Oro, K., Katoh, S., and Moriyoshi, T. (2006). Recovery of oil components of okara by ethanol-modified supercritical carbon dioxide extraction. *Bioresource Technology*, 97(13), 1509-1514. https://doi.org/10.1016/j.biortech.2005.06.010.

Qu, X., Wirsén, A., Olander, B., and Albertsson, A. C. (2001). Surface modification of high density polyethylene tubes by coating chitosan, chitosan hydrogel and heparin. *Polymer Bulletin*, 46, 223-229. DOI:10.1007/s002890170078.

Rashmi, Rimpy, and Ahuja, M. (2020). Iodine impregnated poly (N-Vinylpyrrolidone) grafted antibacterial cotton gauze for wound dressing applications. *Fibers and Polymers*, 21, 1411-1421. DOI: 10.1007/s12221-020-9856-1.

Ravber, M., Knez, Ž. and Škerget, M. (2015). Simultaneous extraction of oil-and water-soluble phase from sunflower seeds with subcritical water. *Food Chemistry*, 166, 316-323. https://doi.org/10.1016/j.foodchem.2014.06.025.

Reverchon, E., Ambruosi, A. and Senatore, F. (1994). Isolation of peppermint oil using supercritical CO_2 extraction. *Flavour and Fragrance Journal*, 9(1), 19-23. https://doi.org/10.1002/ffj.2730090105.

Roberto, D., Micucci, P., Sebastian, T., Graciela, F., and Anesini, C. (2010). Antioxidant activity of limonene on normal murine lymphocytes: relation to H_2O_2 modulation and cell proliferation. *Basic & Clinical Pharmacology & Toxicology*, 106(1), 38-44. DOI: 10.1111/j.1742-7843.2009.00467.x.

Rojas, A., Torres, A., Añazco, A., Villegas, C., Galotto, M. J., Guarda, A., and Romero, J. (2018). Effect of pressure and time on scCO2-assisted incorporation of thymol into LDPE-based nanocomposites for active food packaging. *Journal of CO2 Utilization*, 26, 434-444. https://doi.org/10.1016/j.jcou.2018.05.031.

Rojas, A., Torres, A., José Galotto, M., Guarda, A., and Julio, R. (2020). Supercritical impregnation for food applications: A review of the effect of the operational variables on the active compound loading. *Critical Reviews in Food Science and Nutrition*, 60(8), 1290-1301. DOI: 10.1080/10408398.2019.1567459.

Romero-Fierro, D. A., Camacho-Cruz, L. A., Bustamante-Torres, M. R., Hidalgo-Bonilla, S. P., and Bucio, E. (2022). Modification of cotton gauzes with poly (acrylic acid) and poly (methacrylic acid) using gamma radiation for drug loading studies. *Radiation Physics and Chemistry*, 190, 109787. https://doi.org/10.1016/j.radphyschem.2021.109787.

Rosa, M. T. M., Alvarez, V. H., Albarelli, J. Q., Santos, D. T., Meireles, M. A. A., and Saldana, M. D. (2020). Supercritical anti-solvent process as an alternative technology for vitamin complex encapsulation using zein as wall material: Technical-economic evaluation. *The Journal of Supercritical Fluids*, 159, 104499. https://doi.org/10.1016/j.supflu.2019.03.011.

Rossmann, M., Braeuer, A., Leipertz, A., and Schluecker, E. (2013). Manipulating the size, the morphology and the polymorphism of acetaminophen using supercritical antisolvent (SAS) precipitation. *The Journal of Supercritical Fluids*, 82, 230-237. https://doi.org/10.1016/j.supflu.2013.07.015.

Roy, B.C., Goto, M., Kodama, A. and Hirose, T. (1996). Supercritical CO_2 extraction of essential oils and cuticular waxes from peppermint leaves. *Journal of Chemical Technology & Biotechnology: International Research in Process*, *Environmental and Clean Technology*, 67(1), 21-26. https://doi.org/10.1002/(SICI)1097-4660(199609)67:1<21::AID-JCTB522>3.0.CO;2-0.

Sahraoui, N. and Boutekedjiret, C. (2015). Innovative process of essential oil extraction: steam distillation assisted by microwave. *In Progress in Clean Energy,* 1, 831-841. Springer, Cham. DOI:10.1007/978-3-319-16709-1_61.

Sajadian, S. A., Amani, M., Ardestani, N. S., and Shirazian, S. (2022). Experimental analysis and thermodynamic modelling of lenalidomide solubility in supercritical carbon dioxide. *Arabian Journal of Chemistry*, 15(6), 103821. https://doi.org/10.1016/j.arabjc.2022.103821.

Saldaña, M. D. A., Mohamed, R. S., Baer, M. G., and Mazzafera, P. (1999). Extraction of purine alkaloids from mate (*Ilex paraguariensis*) using supercritical CO_2. *Journal of Agricultural and Food Chemistry*, 47(9), 3804-3808. DOI: 10.1021/jf981369z.

Saldaña, M. D. A., Sun, L., Guigard, S. E., and Temelli, F. (2006). Comparison of the solubility of β-carotene in supercritical CO_2 based on a binary and a multicomponent complex system. *The Journal of Supercritical Fluids*, 37(3), 342-349. https://doi.org/10.1016/j.supflu.2006.01.010.

Saldaña, M. D. A., and Valdivieso-Ramirez, C. S. (2015). Pressurized fluid systems: Phytochemical production from biomass. *The Journal of Supercritical Fluids*, 96, 228-244. https://doi.org/10.1016/j.supflu.2014.09.037.

Salea, R., Veriansyah, B., and Tjandrawinata, R. R. (2017). Optimization and scale-up process for supercritical fluids extraction of ginger oil from *Zingiber officinale* var. Amarum. *The Journal of Supercritical Fluids*, 120, 285-294. https://doi.org/10.1016/j.supflu.2016.05.035.

Samadi, M., Zainal Abidin, Z., Yoshida, H., Yunus, R. and Awang Biak, D.R. (2020). Towards higher oil yield and quality of essential oil extracted from *Aquilaria Malaccensis* wood via the subcritical technique. *Molecules*, 25(17), 3872. https://doi.org/10.3390/molecules25173872.

Sanchez-Sanchez, J., Fernández-Ponce, M. T., Casas, L., Mantell, C., and de la Ossa, E. M. (2017). Impregnation of mango leaf extract into a polyester textile using supercritical carbon dioxide. *The Journal of Supercritical Fluids*, 128, 208-217. https://doi.org/10.1016/j.supflu.2017.05.033.

Santiago, J. V. A., Jayachitra, J., Shenbagam, M. and Nalini, N. (2012). Dietary d-limonene alleviates insulin resistance and oxidative stress-induced liver injury in high-fat diet and L-NAME-treated rats. *European Journal of Nutrition*, 51(1), 57. DOI: 10.1007/s00394-011-0182-7.

Santos, D.T., Santana, Á.L., Meireles, M.A.A., Gomes, M.T.M., Torres, R.A.D.C., Albarelli, J.Q., Bakatselou, A., Ensinas, A.V., Maréchal, F., Santos, D.T. and Santana, Á.L. (2020). Supercritical Fluid Biorefining Using Supercritical CO_2 as an Antisolvent for Micronization, Coprecipitation, and Fractionation: Fundamentals, Processing, and Effect of Process Conditions. *Supercritical Fluid Biorefining: Fundamentals, Applications and Perspectives*, 1-12. DOI:10.1007/978-3-030-47055-5_1.

Schmidt, E. (2020). Production of essential oils. *In Handbook of Essential Oils*, 125-160. CRC Press. https://doi.org/10.1201/9781351246460.

Singh, A., Ahmad, A. and Bushra, R. (2016). Supercritical carbon dioxide extraction of essential oils from leaves of *Eucalyptus globulus* L., their analysis and application. *Analytical Methods*, 8(6), 1339-1350. https://doi.org/10.1039/C5AY02009C.

Shahsavarpour, M., Lashkarbolooki, M., Eftekhari, M.J. and Esmaeilzadeh, F. (2017). Extraction of essential oils from *Mentha spicata L.*(Labiatae) via optimized supercritical carbon dioxide process. *The Journal of Supercritical Fluids*, 130, 253-260. https://doi.org/10.1016/j.supflu.2017.02.004.

Skerget, M., Knez, Z., and Knez-Hrncic, M. (2011). Solubility of solids in sub-and supercritical fluids: a review. *Journal of Chemical & Engineering Data*, 56(4), 694-719. https://doi.org/10.1021/acs.jced.7b00778.

Sodeifian, G., Garlapati, C., Razmimanesh, F., and Ghanaat-Ghamsari, M. (2021). Measurement and modeling of clemastine fumarate (antihistamine drug) solubility in supercritical carbon dioxide. *Scientific Reports*, 11(1), 24344. DOI: 10.1038/s41598-021-03596-y.

Sodeifian, G., Sajadian, S. A., and Derakhsheshpour, R. (2020). Experimental measurement and thermodynamic modeling of Lansoprazole solubility in supercritical carbon dioxide: Application of SAFT-VR EoS. *Fluid Phase Equilibria*, 507, 112422. https://doi.org/10.1016/j.fluid.2019.112422.

Sorour, H. K., Hosny, R. A., and Elmasry, D. M. (2021). Effect of peppermint oil and its microemulsion on necrotic enteritis in broiler chickens. *Veterinary World*, 14(2), 483. doi: 10.14202/vetworld.2021.483-491.

Souza, J. M., Henriques, M., Teixeira, P., Fernandes, M. M., Fangueiro, R., and Zille, A. (2019). Comfort and infection control of chitosan-impregnated cotton gauze as wound dressing. *Fibers and Polymers*, 20, 922-932. DOI 10.1007/s12221-019-9053-2.

Sovová, H., and Jež, J. (1994). Solubility of menthol in supercritical carbon dioxide. *Journal of Chemical and Engineering Data*, 39(4), 840-841. https://doi.org/10.1021/je00016a045.

Sulieman, A.M.E., Abdelrahman, S.E. and Abdel Rahim, A.M. (2011). Phytochemical analysis of local spearmint (*Mentha spicata*) leaves and detection of the antimicrobial activity of its oil. *Journal of Microbiology Research*, 1(1), 1-4. doi: 10.5923/j.microbiology.20110101.01.

Sun, J. (2007). D-Limonene: safety and clinical applications. *Alternative medicine review*, 12(3).

Tisserand, R., and Balacs, T. (1996). Essential oil safety. *Churchill Livingstone*, 7(3), 28-32. https://doi.org/10.1016/B978-0-443-06241-4.00003-5.

Torres, A., Ilabaca, E., Rojas, A., Rodríguez, F., Galotto, M. J., Guarda, A., Villegas, C. and Romero, J. (2017). Effect of processing conditions on the physical, chemical and transport properties of polylactic acid films containing thymol incorporated by supercritical impregnation. *European Polymer Journal*, 89, 195-210. https://doi.org/10.1016/j.eurpolymj.2017.01.019.

Ubeyitogullari, A., and Ciftci, O. N. (2017). Generating phytosterol nanoparticles in nanoporous bioaerogels via supercritical carbon dioxide impregnation: Effect of impregnation conditions. *Journal of Food Engineering*, 207, 99-107. https://doi.org/10.1016/j.jfoodeng.2017.03.022.

U.S. National Library of Medicine. PubChem. National Center for Biotechnology Information. PubChem Compound Database. Accessed September 18, 2023, at https://pubchem.ncbi.nlm.nih.gov.

Varona, S., Rodríguez-Rojo, S., Martín, Á., Cocero, M. J., and Duarte, C. M. (2011). Supercritical impregnation of lavandin (*Lavandula hybrida*) essential oil in modified starch. *The Journal of Supercritical Fluids*, 58(2), 313-319. https://doi.org/10.1016/j.supflu.2011.06.003.

Vatankhah, H., and Ramaswamy, H. S. (2019). High pressure impregnation (HPI) of apple cubes: Effect of pressure variables and carrier medium. *Food Research International*, 116, 320-328. https://doi.org/10.1016/j.foodres.2018.08.042.

Venkateshappa, S. M., and Sreenath, K. P. (2013). Potential medicinal plants of Lamiaceae. American International Journal of Research in Formal, *Applied & Natural Sciences*, 3(1), 82-87.

Vieira, A.J., Beserra, F.P., Souza, M.C., Totti, B.M. and Rozza, A.L. (2018). Limonene: Aroma of innovation in health and disease. *Chemico-Biological Interactions*, 283, 97-106. https://doi.org/10.1016/j.cbi.2018.02.007.

Wang, D., Meng, Y., Zhao, X., Fan, W., Yi, T., and Wang, X. (2019). Sunflower oil flavored by essential oil from *Punica granatum cv. Heyinshiliu* peels improved its oxidative stability and sensory properties. *LWT*, 111, 55-61. https://doi.org/10.1016/j.lwt.2019.05.005.

Wees, D. (2013). Mint. The Canadian Encyclopedia. Accessed January 9, 2023, at https://www.thecanadianencyclopedia.ca/en/article/mint.

Wu, H., Li, J., Jia, Y., Xiao, Z., Li, P., Xie, Y., Zhang, A., Liu, R., Ren, Z., Zhao, M. and Zeng, C. (2019). Essential oil extracted from *Cymbopogon citronella* leaves by supercritical carbon dioxide: antioxidant and antimicrobial activities. *Journal of Analytical Methods in Chemistry*, 2019, 1-10. https://doi.org/10.1155/2019/8192439.

Wu, Z., Tan, B., Liu, Y., Dunn, J., Martorell Guerola, P., Tortajada, M., Cao, Z. and Ji, P. (2019). Chemical composition and antioxidant properties of essential oils from peppermint, native spearmint and scotch spearmint. *Molecules*, 24(15), 2825. https://doi.org/10.3390/molecules24152825.

Yang, J., Shen, M., Luo, Y., Wu, T., Chen, X., Wang, Y. and Xie, J. (2021). Advanced applications of chitosan-based hydrogels: From biosensors to intelligent food packaging system. *Trends in Food Science & Technology*, 110, 822-832. https://doi.org/10.1016/j.tifs.2021.02.032.

Yilmaztekin, M., Lević, S., Kalušević, A., Cam, M., Bugarski, B., Rakić, V., Pavlović, V. and Nedović, V. (2019). Characterisation of peppermint (*Mentha piperita* L.) essential oil encapsulates. *Journal of Microencapsulation*, 36(2), 109-119. https://doi.org/10.1080/02652048.2019.1607596.

Yosipovitch, G., Szolar, C., Hui, X. Y., and Maibach, H. (1996). Effect of topically applied menthol on thermal, pain and itch sensations and biophysical properties of the skin. *Archives of Dermatological Research*, 288, 245-248. DOI: 10.1007/BF02530092.

Yu, J. P., Guan, Y. X., Yao, S. J., and Zhu, Z. Q. (2011). Preparation of roxithromycin-loaded poly (l-lactic acid) films with supercritical solution impregnation. *Industrial & Engineering Chemistry Research*, 50(24), 13813-13818. https://doi.org/10.1021/ie201294u.

Zabihi, S., Esmaeili-Faraj, S. H., Borousan, F., Hezave, A. Z., and Shirazian, S. (2020). Loxoprofen solubility in supercritical carbon dioxide: experimental and modeling approaches. *Journal of Chemical & Engineering Data*, 65(9), 4613-4620. https://doi.org/10.1021/acs.jced.0c00470.

Zakaria, S. M., and Kamal, S. M. M. (2016). Subcritical water extraction of bioactive compounds from plants and algae: applications in pharmaceutical and food ingredients. *Food Engineering Reviews*, 8(1), 23-34. DOI:10.1007/s12393-015-9119-x.

Zarrinpashne, S., and Gorji Kandi, S. (2019). A study on the extraction of essential oil of Persian black cumin using static supercritical CO_2 extraction, and comparison with hydro-distillation extraction method. *Separation Science and Technology*, 54(11), 1778-1786. https://doi.org/10.1080/01496395.2018.1541907.

Zeković, Z., Kaplan, M., Pavlić, B., Olgun, E.O., Vladić, J., Canlı, O. and Vidović, S. (2016). Chemical characterization of polyphenols and volatile fraction of coriander (*Coriandrum sativum* L.) extracts obtained by subcritical water extraction. *Industrial Crops and Products*, 87, 54-63. https://doi.org/10.1016/j.indcrop.2016.04.024.

Zhang, W., Shi, R., Gao, T., Hu, Y., Zhou, J., Li, C., Wang, P., Yang, H., Xing, W., Dong, L. and Gao, F. (2023). Repeated Inhalation of Peppermint Essential Oil Improves Exercise Performance in Endurance-Trained Rats. *Nutrients*, 15(11), 2480. doi: 10.3390/nu15112480.

Zhang, X. Z., Wang, L., Liu, D. W., Tang, G. Y. and Zhang, H. Y. (2014). Synergistic inhibitory effect of berberine and d-limonene on human gastric carcinoma cell line MGC803. *Journal of Medicinal Food*, 17(9), 955-962. doi: 10.1089/jmf.2013.2967.

Zhao, H., Ren, S., Yang, H., Tang, S., Guo, C., Liu, M., Tao, Q., Ming, T. and Xu, H. (2022). Peppermint essential oil: Its phytochemistry, biological activity, pharmacological effect and application. *Biomedicine & Pharmacotherapy*, 154, 113559. https://doi.org/10.1016/j.biopha.2022.113559.

Zhao, Y., Chen, Y., Gao, M., Wu, L., and Wang, Y. (2023). Comparative investigation of key aroma terpenoids of *Litsea cubeba* essential oil by sensory, chromatographic, spectral and molecular studies. *LWT*, 176, 114519. https://doi.org/10.1016/j.lwt.2023.114519.

Zhao, Y., and Saldaña, M. D. A. (2019). Hydrolysis of cassava starch, chitosan and their mixtures in pressurized hot water media. *The Journal of Supercritical Fluids*, 147, 293-301. https://doi.org/10.1016/j.supflu.2018.11.013.

Zhao, Y., and Xie, J. (2004). Practical applications of vacuum impregnation in fruit and vegetable processing. *Trends in Food Science & Technology*, 15(9), 434-451. https://doi.org/10.1016/j.tifs.2004.01.008.

Zhou, H. C., Lin, Y. M., Wei, S. D., and Tam, N. F. Y. (2011). Structural diversity and antioxidant activity of condensed tannins fractionated from mangosteen pericarp. *Food Chemistry*, 129(4), 1710-1720. https://doi.org/10.1016/j.foodchem.2011.06.036.

Zhu, L., Lan, H., He, B., Hong, W. and Li, J. (2010). Encapsulation of menthol in beeswax by a supercritical fluid technique. *International Journal of Chemical Engineering*, 2010. https://doi.org/10.1155/2010/608680.

APPENDIX

Appendix A. SC-CO$_2$ + co-solvent extraction of essential oil from *Mentha × piperita*
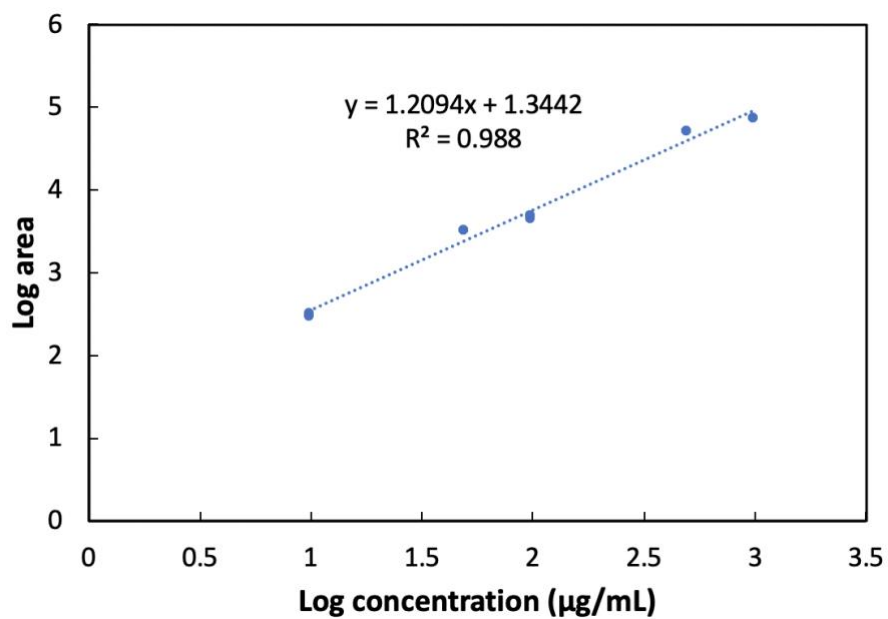
Fig. A1. Standard curve of menthone for GC analysis.
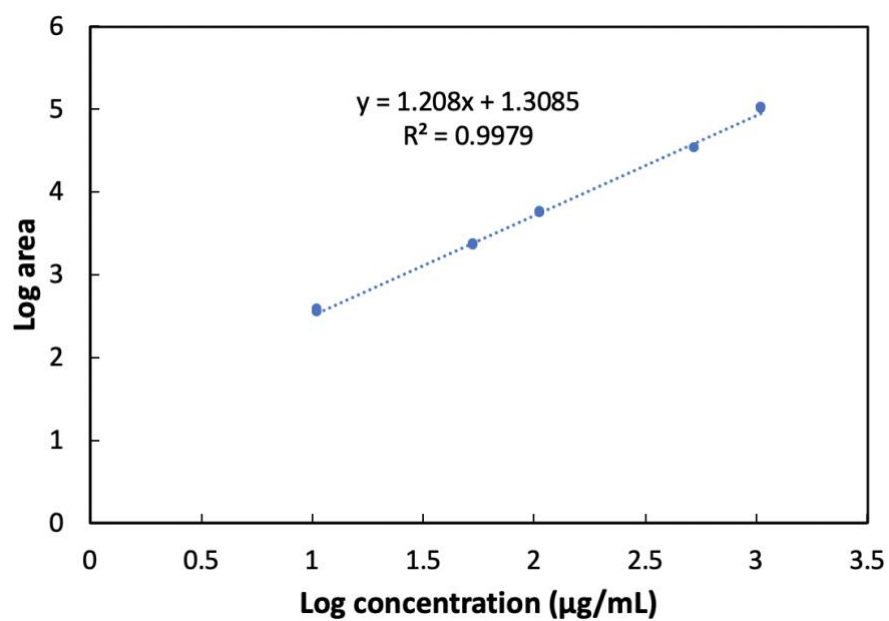
Fig. A2. Standard curve of menthol for GC analysis.
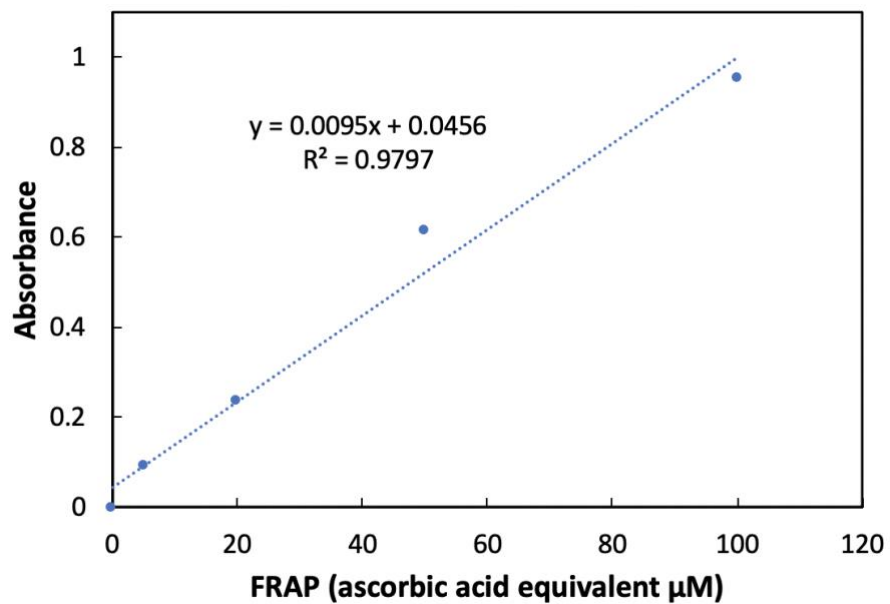
Fig. A3. Standard curve of ascorbic acid for FRAP assay.

Table A1. Ferric reducing antioxidant power of peppermint essential oil obtained at 110 bar and 50 °C at different concentrations in methanol(50 mg/mL, 100 mg/mL, 200 mg/mL, and 500 mg/mL).

Concentration (mg/mL)	FRAP (μM ascorbic acid equivalent)
50	15.621 ± 1.042^د
100	56.253 ± 3.424^c
200	72.989 ± 1.935^a
500	82.253 ± 2.084^a

[a-c] Different letters in the same column indicate significant differences ($p < 0.05$).

Table A2. Yield and menthol and menthone contents of SC-CO$_2$ extraction of essential oil from peppermint.

Temperature (°C)	Pressure (bar)	Mint Loaded (g)	Vial (g)	Vial+oil (g)	Oil collected (g)	Yield (%)	Menthol content (%)	Menthone content (%)
		Equipment 1 (0.5 mL CO$_2$/min at pump condition)						
45	100	4.5270	7.2359	7.2381	0.0022	0.0485[ef]	26.4323[bcd]	0.0362[bc]
		4.5115	7.0437	7.0465	0.0028	0.0621[ef]	23.2445[bcd]	0.0233[bc]
	110	4.5188	7.0983	7.1014	0.0031	0.0686[ef]	32.9621[ab]	0.0061[c]
		4.5253	7.1084	7.1114	0.003	0.0662[ef]	32.6297[ab]	0.0102[c]
	120	4.5065	7.0993	7.1026	0.0033	0.0732[ef]	10.5502[f]	0.0449[bc]
		4.5626	7.0906	7.0948	0.0042	0.0920[ef]	5.3565[f]	0.0209[bc]
50	100	4.5572	7.0820	7.0845	0.0025	0.0548[ef]	30.1628[bc]	0.0365[bc]
		4.5480	7.2729	7.2759	0.003	0.0659[ef]	27.5360[bc]	0.0407[bc]
	105	4.7050	7.1117	7.1139	0.0022	0.0467[ef]	NA	NA
		4.6054	7.1064	7.1079	0.0015	0.0325[ef]	NA	NA
	110	4.5261	7.1167	7.1233	0.0066	0.1458[cd]	40.7117[a]	0.0703[bc]
		4.5189	7.0904	7.0981	0.0077	0.1703[cd]	36.9938[a]	0.0525[bc]
	115	4.5570	7.1564	7.1598	0.0034	0.0746[ef]	NA	NA
		4.5463	7.1084	7.1115	0.0031	0.0681[ef]	NA	NA
	120	4.5972	7.1254	7.1294	0.004	0.0870[def]	26.3366[bc]	0.0494[bc]
		5.0197	7.0412	7.0469	0.0057	0.1135[def]	24.8386[bc]	0.0364[bc]
	200	4.0812	7.1693	7.1781	0.0088	0.2156[bc]	14.6345[de]	0.3125[a]
		4.1531	7.1625	7.1710	0.0085	0.2046[bc]	18.7623[de]	0.2604[a]
	300	4.0129	7.1245	7.1356	0.0111	0.2765[b]	10.8474[ef]	0.2427[a]
		4.0096	7.1551	7.1656	0.0105	0.2618[b]	8.5702[ef]	0.1550[a]
	400	4.1145	7.0205	7.0349	0.0144	0.3510[a]	4.6174[f]	0.1130[b]
		4.0193	7.0811	7.0940	0.0129	0.3209[a]	4.3434[f]	0.0948[b]

Table A2. Continued.

Temperature (°C)	Pressure (bar)	Mint Loaded (g)	Vial (g)	Vial+oil (g)	Oil collected (g)	Yield (%)	Menthol content (%)	Menthone content (%)
		Equipment 1 (0.5 mL CO_2/min at pump condition)						
55	100	4.5023	7.1023	7.1037	0.0014	0.0310^f	22.2861^{cd}	0.0561^{bc}
		4.5216	7.0959	7.0981	0.0022	0.0486^f	24.4285^{cd}	0.0428^{bs}
	110	4.6111	7.0598	7.0658	0.006	0.1301^{de}	29.0222^{bc}	0.0327^{bc}
		4.5382	7.1133	7.1175	0.0042	0.0925^{de}	23.6881^{bc}	0.0236^{bc}
	120	4.5398	7.1008	7.1043	0.0035	0.0770^{ef}	3.9818^f	0.0079^c
		4.5154	7.0952	7.097	0.0018	0.0398^{ef}	4.0511^f	0.0121^c
		Equipment 2 (3 mL CO_2/min at pump condition)						
50	110	3.0012	5.1486	5.1715	0.0229	0.7630^b	48.3567^a	2.3405^a
		3.1521	5.1099	5.1304	0.0205	0.6503^b	46.7221^a	2.2328^a
	200	3.2213	5.1660	5.1921	0.0261	0.8102^b	42.0880^a	1.8377^{ab}
		3.2500	5.2866	5.3229	0.0363	1.1169^b	35.5301^a	1.2681^{ab}
	300	3.0320	8.8123	8.8414	0.0291	0.9597^b	17.0997^b	0.5352^c
		3.1003	5.1360	5.1785	0.0425	1.3708^b	19.9717^b	0.5565^c
	400	3.0620	5.2921	5.3501	0.0580	1.8941^a	21.1111^b	0.8404^{bc}
		3.1770	5.3610	5.4260	0.0650	2.0459^a	24.2235^b	0.7257^{bc}

[a-e] Different letters in the same column and same flow rate indicate significant differences ($p < 0.05$). NA: Not analyzed due to low yields.

$$Yield\ (\%) = \left(\frac{Extracted\ essential\ oil\ (g)}{Total\ feed\ (g)}\right) \times 100 \qquad \textbf{Eq. A1}$$

Table A3. Yield, menthol and menthone content of SC-CO_2 + co-solvent extraction of essential oil from peppermint at 110 bar and 50 °C with a CO_2 flow rate of 0.5 mL/min

Co-solvent	mass of co-solvent (g)	Mint Loaded (g)	Vial (g)	Vial+oil (g)	Oil collected (g)	Yield (%)	Menthol content (%)	Menthone content (%)
Ethanol	1	4.6086	7.1068	7.1144	0.0076	0.1649[b]	24.2766[a]	0.4700[a]
	1.1	4.5071	7.1548	7.17	0.0152	0.3372[b]	28.8634[a]	0.5335[a]
Acetone	1.3	4.7409	7.1146	7.1591	0.0445	0.9386[a]	20.2248[b]	0.3849[a]
	1.3	4.4579	7.1378	7.1678	0.03	0.6729[a]	17.0141[b]	0.3736[a]
Isopropyl acetate	2.4	4.0198	7.16	7.1712	0.0112	0.2786[b]	29.6364[a]	0.4077[a]
	2.4	4.0885	7.1639	7.1801	0.0162	0.3962[b]	23.0222[a]	0.3323[a]

[a-b] Different letters in the same column indicate significant differences ($p < 0.05$).

Appendix B. Solubility of menthol in supercritical carbon dioxide and its impregnation on cotton gauze

Table B1. Solubility of menthol in SC-CO_2.

T (°C)	P (bar)	CO_2 density (g/mL)	V (mL)	Mass of CO_2 (g)	Empty vial (g)	Vial+ menthol (g)	Menthol collected (g)	Solubility (mg menthol/g CO_2)	Mole of menthol	Mole of CO_2	Solubility (mole fraction)
45	100	0.50655	39.7	20.1100	7.1520	7.8245	0.6725	33.4410	2.14×10^{-4}	0.0227	9.33×10^{-3b}
			40.2	20.3633	7.1398	7.8013	0.6615	32.4848	2.08×10^{-4}	0.0227	9.07×10^{-3b}
45	110	0.55325	43.2	23.9004	7.1341	8.0972	0.9631	40.2963	2.58×10^{-4}	0.0227	1.12×10^{-2ab}
			44.7	24.7302	7.1795	8.1901	1.0106	40.8648	2.62×10^{-4}	0.0227	1.14×10^{-2ab}
45	120	0.59995	39.5	23.6980	7.1364	8.1231	0.9867	41.6363	2.66×10^{-4}	0.0227	1.16×10^{-2a}
			37.1	22.2581	7.1665	8.2398	1.0733	48.2205	3.09×10^{-4}	0.0227	1.34×10^{-2a}
45	200	0.81215	20	16.2430	7.1038	7.8589	0.7551	46.4877	2.97×10^{-4}	0.0227	1.29×10^{-2a}
			25.3	20.5473	7.1064	8.0032	0.8968	43.6454	2.79×10^{-4}	0.0227	1.21×10^{-2a}
45	300	0.8903	24.8	22.0794	7.1648	7.9471	0.7823	35.4311	2.27×10^{-4}	0.0227	9.88×10^{-3b}
			23.94	21.3137	7.1707	7.9312	0.7605	35.6811	2.28×10^{-4}	0.0227	9.95×10^{-3b}
50	100	0.3844	27.5	10.5710	7.1625	7.3046	0.1421	13.4424	8.60×10^{-5}	0.0227	3.77×10^{-3cd}
			29.4	11.3013	7.1411	7.2995	0.1584	14.0160	8.97×10^{-5}	0.0227	3.93×10^{-3cd}
50	110	0.44748	36.5	16.3330	7.1456	7.7102	0.5646	34.5680	2.21×10^{-4}	0.0227	9.64×10^{-3b}
			35.4	15.8407	7.1582	7.7035	0.5453	34.4237	2.20×10^{-4}	0.0227	9.60×10^{-3b}
50	120	0.51056	30.3	15.4699	7.1762	7.734	0.5578	36.0569	2.31×10^{-4}	0.0227	1.01×10^{-2ab}
			31.6	16.1336	7.1697	7.7693	0.5996	37.1644	2.38×10^{-4}	0.0227	1.04×10^{-2ab}
50	200	0.7844	28.5	22.3554	7.1726	8.0645	0.8919	39.8964	2.55×10^{-4}	0.0227	1.11×10^{-2d}
			29.4	23.0613	7.1894	8.0765	0.8871	38.4669	2.46×10^{-4}	0.0227	1.07×10^{-2d}
50	300	0.8706	30.4	26.4662	7.1515	8.0907	0.9392	35.4867	2.27×10^{-4}	0.0227	9.90×10^{-3c}
			29.2	25.4215	7.1498	8.2013	1.0515	41.3625	2.65×10^{-4}	0.0227	1.15×10^{-2c}

Table B1. Continued.

T (°C)	P (bar)	CO_2 density (g/mL)	V (mL)	Mass of CO_2 (g)	Empty vial (g)	Vial+ menthol (g)	Menthol collected (g)	Solubility (mg menthol/g CO_2)	Mole of menthol	Mole of CO_2	Solubility (mole fraction)
55	100	0.3372	33.9	11.4310	7.1662	7.2456	0.0794	6.9459	4.44×10^{-5}	0.0227	1.95×10^{-3d}
			32.6	10.9927	7.1318	7.2198	0.088	8.0053	5.12×10^{-5}	0.0227	2.25×10^{-3d}
55	110	0.40013	37.6	15.0448	7.1464	7.4401	0.2937	19.5215	1.25×10^{-4}	0.0227	5.47×10^{-3c}
			35.9	14.3646	7.1601	7.3941	0.234	16.2899	1.04×10^{-4}	0.0227	4.57×10^{-3c}
55	120	0.46306	36.5	16.9016	7.1471	7.6948	0.5477	32.4050	2.07×10^{-4}	0.0227	9.04×10^{-3b}
			34.9	16.1607	7.18	7.7373	0.5573	34.4846	2.21×10^{-4}	0.0227	9.62×10^{-3b}
55	200	0.7541	35.3	26.6197	7.1462	8.1012	0.955	35.8756	2.30×10^{-4}	0.0227	1.00×10^{-2b}
			36.1	27.2230	7.1438	8.1326	0.9888	36.3222	2.32×10^{-4}	0.0227	1.01×10^{-2b}
55	300	0.8503	13.5	11.4790	7.1493	7.5602	0.4109	35.7956	2.29×10^{-4}	0.0227	9.98×10^{-3ab}
			14.8	12.5844	7.1038	7.6241	0.5203	41.3447	2.65×10^{-4}	0.0227	1.15×10^{-2ab}

[a-c] Different letters in the solubility column indicate significant differences ($p < 0.05$). P: pressure, T: temperature, V: volume of CO_2.

$$\text{Solubility} = \frac{\dfrac{\text{mass of menthol (g)}}{\text{molecular weight of menthol (g/mole)}}}{\dfrac{\text{mass of } CO_2 \text{ (g)}}{\text{molecular weight of } CO_2 \text{ (g/mole)}} + \dfrac{\text{mass of menthol (g)}}{\text{molecular weight of menthol (g/mole)}}} \qquad \textbf{Eq. B1}$$

$$\text{Mass of } CO_2 = \text{Flow rate (L/min)} \times \text{density of } CO_2 \text{ (g/L)} \times \text{time (min)} \qquad \textbf{Eq. B2}$$

Table B2. Effect of temperature and pressure on CO_2 properties and solubility of menthol in SC-CO_2.

Run	Temperature (°C)	Pressure (bar)	CO_2 density (kg/m^3)	CO_2 dynamic viscosity (10^{-6} Pa S)	Solubility (Mole fraction)
1	45	100	506.55	38.09	$9.20 \pm 0.19 \times 10^{-3}$ [b]
2	45	110	553.25	42.91	$1.13 \pm 0.01 \times 10^{-2}$ [ab]
3	45	120	599.95	47.72	$1.25 \pm 0.13 \times 10^{-2}$ [a]
4	45	200	812.15	73.76	$1.25 \pm 0.05 \times 10^{-2}$ [a]
5	45	300	890.30	89.95	$9.91 \pm 0.05 \times 10^{-3}$ [b]
6	50	100	384.40	28.34	$3.85 \pm 0.11 \times 10^{-3}$ [cd]
7	50	110	447.48	33.98	$9.62 \pm 0.03 \times 10^{-3}$ [b]
8	50	120	510.56	39.62	$1.02 \pm 0.02 \times 10^{-2}$ [ab]
9	50	200	784.40	68.93	$1.09 \pm 0.03 \times 10^{-2}$ [ab]
10	50	300	870.60	85.5	$1.07 \pm 0.12 \times 10^{-2}$ [ab]
11	55	100	337.20	26.04	$2.10 \pm 0.21 \times 10^{-3}$ [d]
12	55	110	400.13	31.09	$5.02 \pm 0.64 \times 10^{-3}$ [c]
13	55	120	463.06	36.15	$9.33 \pm 0.41 \times 10^{-3}$ [b]
14	55	200	754.10	64.56	$1.01 \pm 0.01 \times 10^{-2}$ [b]
15	55	300	850.30	81.53	$1.07 \pm 0.11 \times 10^{-2}$ [ab]

Table B3. Impregnation yield of menthol into cotton gauze at different SC-CO_2 processing conditions.

No.	Time (min)	Depressurization rate (bar/min)	Menthol loaded (g)	Cotton gauze (g)	Impregnated cotton gauze (g)	Entrapment efficiency (%)	Impregnation yield (%)
1		6	0.1021	0.2523	0.2831	30.1665	12.2076[c]
2	30		0.1045	0.2645	0.2912	25.5502	10.0945[c]
3		60	0.098	0.2423	0.2565	14.4897	5.8605[d]
4			0.1052	0.2642	0.2804	15.3992	6.1317[d]
5		6	0.104	0.2566	0.3371	77.4038	31.3717[a]
6	300		0.0994	0.249	0.3235	74.9497	29.9196[a]
7		60	0.1003	0.2477	0.3012	53.3399	21.5987[b]
8			0.101	0.2566	0.3152	58.0198	22.8371[b]

[a-d] Different letters in the same column indicate significant differences ($p < 0.05$).

$$\text{Impregnation yield (\%)} = \frac{m_f - m_i}{m_i} \times 100 \qquad \textbf{Eq. B3}$$

Where, m_i and m_f are the masses of cotton gauze before and after the impregnation process, respectively.

$$\text{Entrapment efficiency (\%)} = \frac{m_{\text{menthol loaded}}\ (g) - m_{\text{menthol impregnated}}\ (g)}{m_{\text{menthol loaded}}\ (g)} \times 100 \qquad \textbf{Eq. B4}$$

Table B4. Colour measurement of cotton gauze at different SC-CO$_2$ menthol impregnation processing conditions.

No.	30 min				300 min			
	6 bar/min		60 bar/min		6 bar/min		60 bar/min	
L	83.11	83.54	83.45	83.53	83.46	84.04	83.47	83.32
a	-0.58	-0.32	-0.40	-0.50	-0.42	-0.43	-0.47	-0.41
b	3.07	2.74	3.09	3.04	3.55	3.03	3.70	3.30
ΔE	0.4202	0.1886	0.2387	0.2624	0.6952	0.6659	0.8500	0.4501
Average ΔE	0.30±0.16[a]		0.25±0.02[a]		0.68±0.02[a]		0.65±0.28[a]	

[a] Same letter in the same row indicates no significant difference (p>0.05).

$$\Delta E = \sqrt{(L^* - L)^2 + (a^* - a)^2 + (b^* - b)^2}$$ **Eq. B5**

where, L^*, a^*, and b^* represent the color parameters of the control cotton gauze, while L, a, and b represent the color parameters of the menthol-impregnated cotton gauze. *L* represents darkness to lightness (0-100), *a* represents greenness to redness (-128 to +127), and *b* represents blueness to yellowness (-128 to +127).

Table B5. Visual documentation of SC-CO$_2$ menthol impregnated cotton gauzes under different experimental conditions.

Experimental condition	Impregnated cotton gauze
30 min and 6 bar/min	
30 min and 60 bar/min	
300 min and 6 bar/min	
300 min and 60 bar/min	